

UNITED STATES AIR FORCE
SUMMER RESEARCH PROGRAM -- 1997
HIGH SCHOOL APPRENTICESHIP FINAL REPORTS

VOLUME 13
PHILLIPS LABORATORY

RESEARCH & DEVELOPMENT LABORATORIES
5800 Uplander Way
Culver City, CA 90230-6608

Program Director, RDL
Gary Moore

Program Manager, AFOSR
Major Linda Steel-Goodwin

Program Manager, RDL
Scott Licoscos

Program Administrator, RDL
Johnetta Thompson

Program Administrator
Rebecca Kelly-Clemons

Submitted to:

AIR FORCE OFFICE OF SCIENTIFIC RESEARCH
Bolling Air Force Base
Washington, D.C.

December 1997

20010321 082

Am 01-06-12 40

REPORT DOCUMENTATION PAGE

Form Approved

reviewing
formation

Public reporting burden for this collection of information is estimated to average 1 hour per response, including the time for reviewing instructions, see the collection of information. Send comments regarding this burden estimate or any other aspect of this collection of information, including suggested Operations and Reports, 1215 Jefferson Davis Highway, Suite 1204, Arlington, VA 22202-4302, and to the Office of Management and Budget, Paper

AFRL-SR-BL-TR-00-

077D

1. AGENCY USE ONLY (Leave blank)	2. REPORT DATE	3. REPO	5. FUNDING NUMBERS
	December, 1997		F49620-93-C-0063
4. TITLE AND SUBTITLE 1997 Summer Research Program (SRP), High School Apprenticeship Program (HSAP), Final Reports, Volume 13, Phillips Laboratory			6. AUTHOR(S) Gary Moore
7. PERFORMING ORGANIZATION NAME(S) AND ADDRESS(ES) Research & Development Laboratories (RDL) 5800 Uplander Way Culver City, CA 90230-6608			8. PERFORMING ORGANIZATION REPORT NUMBER
9. SPONSORING/MONITORING AGENCY NAME(S) AND ADDRESS(ES) Air Force Office of Scientific Research (AFOSR) 801 N. Randolph St. Arlington, VA 22203-1977			10. SPONSORING/MONITORING AGENCY REPORT NUMBER
11. SUPPLEMENTARY NOTES			
12a. DISTRIBUTION AVAILABILITY STATEMENT Approved for Public Release		12b. DISTRIBUTION CODE	
13. ABSTRACT (Maximum 200 words) The United States Air Force Summer Research Program (USAF-SRP) is designed to introduce university, college, and technical institute faculty members, graduate students, and high school students to Air Force research. This is accomplished by the faculty members (Summer Faculty Research Program, (SFRP)), graduate students (Graduate Student Research Program (GSRP)), and high school students (High School Apprenticeship Program (HSAP)) being selected on a nationally advertised competitive basis during the summer intersession period to perform research at Air Force Research Laboratory (AFRL) Technical Directorates, Air Force Air Logistics Centers (ALC), and other AF Laboratories. This volume consists of a program overview, program management statistics, and the final technical reports from the HSAP participants at the Phillips Laboratory.			
14. SUBJECT TERMS Air Force Research, Air Force, Engineering, Laboratories, Reports, Summer, Universities, Faculty, Graduate Student, High School Student			15. NUMBER OF PAGES
			16. PRICE CODE
17. SECURITY CLASSIFICATION OF REPORT Unclassified	18. SECURITY CLASSIFICATION OF THIS PAGE Unclassified	19. SECURITY CLASSIFICATION OF ABSTRACT Unclassified	20. LIMITATION OF ABSTRACT UL

PREFACE

Reports in this volume are numbered consecutively beginning with number 1. Each report is paginated with the report number followed by consecutive page numbers, e.g., 1-1, 1-2, 1-3; 2-1, 2-2, 2-3.

This document is one of a set of 16 volumes describing the 1997 AFOSR Summer Research Program. The following volumes comprise the set:

<u>VOLUME</u>	<u>TITLE</u>
1	Program Management Report <i>Summer Faculty Research Program (SFRP) Reports</i>
2A & 2B	Armstrong Laboratory
3A & 3B	Phillips Laboratory
4A & 4B	Rome Laboratory
5A , 5B & 5C	Wright Laboratory
6	Arnold Engineering Development Center, United States Air Force Academy and Air Logistics Centers <i>Graduate Student Research Program (GSRP) Reports</i>
7A & 7B	Armstrong Laboratory
8	Phillips Laboratory
9	Rome Laboratory
10A & 10B	Wright Laboratory
11	Arnold Engineering Development Center, United States Air Force Academy, Wilford Hall Medical Center and Air Logistics Centers <i>High School Apprenticeship Program (HSAP) Reports</i>
12A & 12B	Armstrong Laboratory
13	Phillips Laboratory
14	Rome Laboratory
15A, 15B & 15C	Wright Laboratory
16	Arnold Engineering Development Center

HSAP FINAL REPORT TABLE OF CONTENTS**i-xiv**

1. INTRODUCTION	1
2. PARTICIPATION IN THE SUMMER RESEARCH PROGRAM	2
3. RECRUITING AND SELECTION	3
4. SITE VISITS	4
5. HBCU/MI PARTICIPATION	4
6. SRP FUNDING SOURCES	5
7. COMPENSATION FOR PARTICIPATIONS	5
8. CONTENTS OF THE 1995 REPORT	6

APPENDICIES:

A. PROGRAM STATISTICAL SUMMARY	A-1
B. SRP EVALUATION RESPONSES	B-1

HSAP FINAL REPORTS

SRP Final Report Table of Contents

Author	University/Institution Report Title	Armstrong Laboratory Directorate	Vol-Page
Andrea L Black	Red Mountain High School , Mesa , AZ	AL/HRA	12 - 1
Kimberly K Blazer	Oakwood High School , Dayton , OH Repeatability Evaluation of Night Vision Goggles for Geometric Measurements	AL/CFHV	12 - 2
Kristen R Bonnema	Wayne High School , Huber Heights , OH The Effects of Individual Differences and team processes on Team Member schema similarity and task P	AL/CFHI	12 - 3
David M Brogan	Robert E. Lee High School , San Antonio , TX The use of 3-Dimensional modeling in the widespread Dissemination of complex scientific data	AL/OERS	12 - 4
Matthew S Caspers	MacArthur High School , San Antonio , TX A Study of the 39-40 Hz Signal to determine an index of Gravitational induced loss of Consciousness	AL/CFTF	12 - 5
Elizabeth M Cobb	Belmont High School , Dayton , OH A Study fo Pitch and Contact Associated with the Opening and Closing of Vaocal Cords	AL/CFBA	12 - 6
Indra E Cortina	Theodore Roosevelt High School , San Antonio , TX The Effect of Hyperbaric Oxygenation on the Mitotic Div of Prostate Cancer Cells	AL/AOH	12 - 7
Maria A Evans	John Jay High School , San Antonio , TX Mercury Analysis By Cold Vapor By Atomic Absortion	AL/OEAO	12 - 8
Daniel L Hardmeyer	James Madison High School , San Antonio , TX Neuropsychological Examinations For Pilots	AL/AOC	12 - 9
Nafisa Islam	Centerville High School . Centerville , OH Effects of timed exposure to Dibromobenzene on /arachidonic acid levels in skin using a methyl Este	AL/OET	12 - 10
Kathleen S Kao	Keystone School , San Antonio , TX Effects of Brain Temperature ofn Fatigue in Rats Due to Maziaml Exercise and Radio Frequency Radiati	ALOERB	12 - 11

SRP Final Report Table of Contents

Author	University/Institution Report Title	Armstrong Laboratory Directorate	Vol-Page
Lauren M Lamm		AL/OEAO	12 - 12
	Keystone School , San Antonio , TX Analyses of Metal Concentrations By Flame Atomic Absorption Spectroscopy		
Evan D Large		AL/HRGO	12 - 13
	Northwestern High School , Springfield , OH ABDAR Remote Engineering		
Jason L Law		AL/CFT	12 - 14
	Oliver Wendell Holmes High , San Antonio , TX		
Shaun M Little		AL/HRCC	12 - 15
	Floresville High School , Floresville , TX The role of Microsoft's directx 3 software development Kit in the rapid development of high fidelity		
Katie E Lorenz		AL/CFHP	12 - 16
	Chaminade-Julienne High School , Dayton , OH Visual Acuity between 6 and 60 Meters		
Darby M Mahan		AL/CF	12 - 17
	Tippecanoe High School , Tipp City , OH		
Priscilla M Medina		AL/EQP	12 - 18
	PSJ High School , Port Saint Joe , FL A Look into the Air Force's Computer Department		
Mark T Meiners		AL/HRA	12 - 19
	Dobson High , Mesa , AZ A Study of Accuracy and Response Time in Tests of Spatial Ability		
David J Miller		AL/OERS	12 - 20
	Texas Academy of Mathematics , Denton , TX An Analysis of Radiofrequency Radiation Induced Temperature gradients in the Rat Brain		
Joseph R Moate		AL/EQM	12 - 21
	Rutherford High School , PANAMA CITY , FL		
Shannon J Murphy		AL/CFTF	12 - 22
	Keystone School , San Antonio , TX An Investigation of The Precision of the El-Mar Fixation Analysis Software Technology		

SRP Final Report Table of Contents

Author	University/Institution Report Title	Armstrong Laboratory Directorate	Vol-Page
Christina A Navalta	Health Careers High School , San Antonio , TX Metals Analysis by Atomic Absorption Using A Graphite Furnace	AL/OEAO	12 - 23
Christine P Pan	Health Careers High School , San Antonio , TX Spinning a Web	AL/HRCC	12 - 24
Savitha K Reddy	Miami Valley School , Dayton , OH Study of factors Influencing Injury Potential Associated with Emergency Egress	AL/CFBE	12 - 25
Nitha K Reddy	Miami Valley School , Dayton , OH A Study of the Methodology Used In An Experiment Testing The Effect of Localizing Auditory Signals O	AL/CFBA	12 - 26
Master I Resendiz	William Howard Taft High School , San Antonio , TX A study of the shifts in scene perception memory	AL/CFTF	12 - 27
Leandra M Scheidt	Wayne High School , Huber Heights , OH	AL/OET	12 - 28
Lachel A Sharp	William Howard Taft High School , San Antonio , TX A study of the Analysis of Urinary Benzodiazepines Using Enzyme Hydrolysis	AL/AOEL	12 - 29
James E Sovel	Rutherford High School , PANAMA CITY , FL	AL/EQA	12 - 30
Curtis J Sparks	Xenia High School , Xenia , OH ABDR:Remote Engineering Requests	AL/HRGO	12 - 31
Lauren M Spencer	Rutherford High School , PANAMA CITY , FL Alternative Training Agents Laboratory-Scale Work	AL/EQL	12 - 32
Tyler W Standage	Gilbert High School , Gilbert , AZ A Study of Accuracy and Response time in tests of Spatial Ability	AL/HRA	12 - 33

SRP Final Report Table of Contents

Author	University/Institution Report Title	Armstrong Laboratory Directorate	Vol-Page
Rachel J Strickland		AL/EQP	12 - 34
	A. Crawford Mosely High School , Lynn Haven , FL the Process ofd Technical Publication/Documentation Via Electronic Media For the Armstrong Laborato		
Lydia R Strickland		AL/EQL	12 - 35
	A. Crawford Mosely High School , Lynn Haven , FL Anaerobic Degradatin Products of Toluene and Laboratory MSDS Management		
Kelly C Todd		AL/AOH	12 - 36
	Theodore Roosevelt High School , San Antonio , TX The Effect of Hyperbaric Oxygenation on the Mitotic Div of Prostate Cancer Cells		
Tammy L Venema		AL/CFBS	12 - 37
	Stebbins High School , Dayton , OH Cerebral hemodynamic Response to a Squat-Stand at IG		
Max P Vilimpoc		AL/CFHP	12 - 38
	Beavercreek High School , Dayton , OH A Study of Psycho-Physiological Effects on Brainwave Activity During Varying levels of Activity		
Elizabeth A Walker		AL/AOH	12 - 39
	Theodore Roosevelt High School , San Antonio , TX The Effect of Hyperbaric Oxygenation on the Mitotic Div of Prostate Cancer Cells		
Nathan L Wright		AL/CFBV	12 - 40
	Dayton Christian High School , Dayton , OH CG and MOI Study of Human and Manikin Segments		
Muchieh A Yu		AL/AOE	12 - 41
	Theodore Roosevelt High School , San Antonio , TX Detection of Clostridium Difficile Toxins by Polymerase Chain Reaction		

SRP Final Report Table of Contents

Author	University/Institution Report Title	Phillips Laboratory Directorate	Vol-Page
Marilyn R Blundell	Rosamond High School , Rosamond , CA Engineering Assistant	PL/RKO	13 - 1
Aureen A Ferguson	Moriarity High School , Moriarity , NM Experimental Validation of Three-Dimensional Reconstruction of Inhomogeneity Images in turbid Media	PL/LIMI	13 - 2
Erica S Gerken	Manzano High School , Albuquerque , NM Chaotic Dynamics in a Nd:YAG laser	PL/LIDD	13 - 3
Paulan B Kha	Chelmsford High School , North Chelmsford , MA	PL/GPOS	13 - 4
Paul G Loftsgard	Quartz Hill High School , Quartz Hill . CA A Study on Optical Paternation	PL/RKS	13 - 5
Tawn R Miller	Manzano High School , Albuquerque . NM A Study of Space Structure's Isolation	PL/VTV	13 - 6
Amy W Mok	Newton North High School , Newtonville , MA A study of the Effect of fuel Sulfur Content on the Production of Aerosols in Aircraft Exhaust Plum	PL/GPID	13 - 7
Martin P Morales	Palmdale High School , Palmdale , CA the Separations and Reactions of Cyclohexyl Poss Compounds	PL/RKS	13 - 8
David D Parker	Boron High School , Boron , CA Intranet Web Page, Design and Development	PL/RKD	13 - 9
Kimberly A Robinson	Sandia High School , Albuquerque , NM Scientific Visualization methods at the Center for Plasma Theory and Computation	PL/WSQA	13 - 10
Michael P Schoenfeld	NewMexico Military Ins. , Roswell , NM Study of the Effect of Heat Flow on the Performance of an Alkali Metal Thermal-to-Electric Converter	PL/VTV	13 - 11

SRP Final Report Table of Contents

<u>Author</u>	<u>University/Institution Report Title</u>	<u>Phillips Laboratory Directorate</u>	<u>Vol-Page</u>
Thomas J Shea	Tehachapi High School , Tehachapi , CA A study of the Characterization of reduced Toxicity Monopropellants	PL/RKS	13 - 12
Carl W Steinbach	Lincoln-Sudbury Regional High , Sudbury , MA A Study of the Interrelation of Cloud Thickness and Cloud Liquid Water Content in Maritime Stratocum	PL/GPAB	13 - 13
Nhi T Tran	Manzano High School , Albuquerque , NM Optically Addressed Spatial Light Modulators as real-time Holographic Media	PL/LIMS	13 - 14
Jeremy L White	Sandia High School , Albuquerque , NM Constructing a Computer Model of the Space Shuttle and The Effects of Lasers on Materials in Space	PL/WSAT	13 - 15
Joanne Wu	Newton North High School , Newtonville , MA Development of Algorithms to Objectively Forecast Present Weather and Surface Visibility By Means fo	PL/GPAB	13 - 16
Aaron Zimmerman	Sandia High School , Albuquerque , NM IDASS ADDITIONS	PL/WSAT	13 - 17

SRP Final Report Table of Contents

Author	University/Institution Report Title	Rome Laboratory Directorate	Vol-Page
Christine A Angell	Camden High School , Camden , NY HTML Computer Language	RL/C3CA	14 - 1
efan M Enjem	Whitesboro Senior High School , Marcy , NY Writing World-Wide Web (WWW) Pages	RL/IRAE	14 - 2
ared S Feldman	Rome Free Academy , Rome , NY AFOSR SUMMER 1997 INTERNSHIP	RL/ERDR	14 - 3
ouglas M Feldmann	Oneida Senior High School , Oneida , NY Examination of the nearest-neighbor rule in voice pattern Classification	RL/OCSS	14 - 4
atrick X Fitzgerald	Holland Patent High School , Holland Patent , NY The Multi-Temporal Trainable Delay(MTTD) neural Network Architecture	RL/IRDS	14 - 5
aniel E Grabski	Holland Patent High School , Holland Patent , NY RF Module Life Test System Design	RL/ERDA	14 - 6
andra L Jablonka	Oneida Senior High School , Oneida , NY Antenna Pattern Measurements Using Infrared Imaging Techniques	RL/ERST	14 - 7
Colin M Kinsella	Oneida Senior High School , Oneida , NY A Study of Genetic Algorithms	RL/C3CA	14 - 8
Matthew A Miling	VVS Senior High School , Verona , NY A Study of Hostile Electromagnetic Environments within Multichip Modules	RL/ERST	14 - 9
Francis P Ruiz	Rome Free Academy , Rome , NY	RL/ERDD	14 - 10
Roshan P Shah	Camden High School , Camden , NY Multi-Paradigmatic Programming: Integrating Prolog and Visual Basic	RL/C3CA	14 - 11

SRP Final Report Table of Contents

<u>Author</u>	<u>University/Institution</u>	<u>Rome Laboratory</u>	<u>Vol-Page</u>
	<u>Report Title</u>	<u>Directorate</u>	
		<u>RL/IRAA</u>	<u>14 - 12</u>
Brian B Tuch	New Hartford Senior High School , New Hartford , NY A Study of the Application, Uses, and Performance of Spread Spectrum Technology in Digital Signal Pr	RL/IRDS	14 - 13
Brian S Walsh	Whitesboro High School , Whitesboro , NY Web based Computer Programming	RLERDR	14 - 14
David A Young	Rome Free Academy , Rome , NY Reproducing the Copper/Gold Eutectic Curve Using Computer Simulations		

SRP Final Report Table of Contents

Author	University/Institution Report Title	Wright Laboratory Directorate	Vol-Page
Michael C Austin	Fairborn High School , Fairborn , OH System Administration	WL/AASE	15 - 1
Surav K Bedi	Wayne High School , Huber Heights , OH Synthesis & Characterization of Melt Intercalated Nanocomposites	WL/MLBP	15 - 2
Kristal W Bhagat	Dayton Christian High School , Dayton , OH A Study of the Effects of Varying Pulse Width and Duty Cycle On Polymer Dispersed	WL/MLPJ	15 - 3
Margaret A Bruns	Dixie High School , New Lebanon , OH Surface Structure and Optical Properties of a Sensitive Snake Infared Detector	WL/DOR	15 - 4
Monica M Campbell	Carroll High School , Dayton , OH Window Design for Laser Velocimetere Data Aquisition	WL/POTF	15 - 5
Mericio B Castro	Belmont High School , Dayton , OH	WL/AACF	15 - 6
John R Caudill	Fairborn High School , Fairborn , OH 2 PhotonIonization and Disassociative Attachment of Eletrons To Excited Molcules	WL/POOX	15 - 7
Bernardo V Cavour	Fairmont High School , Kettering , OH High School Appentice Program Accomplishments	WL/FIBT	15 - 8
Christopher R Clark	Niceville Senior High School , Niceville , FL Neural Networks & Digital Image Processing	WL/MNGA	15 - 9
Aaron Davis	Niceville Senior High School , Niceville , FL Electronic Studies of Polypyrrole Films Grown on Semiconductor Wafers	WL/MNMF	15 - 10
Debbie L Dressler	Centerville High School , Centerville , OH Traction Models	WL/POS1	15 - 11

SRP Final Report Table of Contents

Author	University/Institution Report Title	Wright Laboratory Directorate	Vol-Page
Molly M Flanagan	Chaminade-Julienne High School , Dayton , OH	WL/POTF	15 - 12
Landon W Frymire	Laurel Hill High School , Laurel Hill , FL Technical Report Library User's Manual	WL/MNAV	15 - 13
Allison D Gadd	Carroll High School , Dayton , OH	WL/FIVS	15 - 14
Matthew A Gerding	Fairborn High School , Fairborn , OH The Study of the Electro-Optic Coefficients of DR-1 and Dans	WL/MLPO	15 - 15
Jon M Graham	Carroll High School , Riverside , OH The Flight Dynamics Lab	WL/DOR	15 - 16
Trenton Hamilton	Rocky Bayou Christian School , Niceville , FL Cast Ductile Iron (CDI) (A Controlled Fragmentation Study)	WL/MNM	15 - 17
Neil Harrison	Ft Walton Beach High SC , Ft Walton BEACH , FL Comparison of Experimental Penetration Data with Various Penetration Prediction Methodologies	WL/MNM	15 - 18
Angela C Helm	Carroll High School , Dayton , OH	WL/AACT	15 - 19
Anna S Hill	Carroll High School , Dayton , OH Window design for Laser velocimeter Data Aquisition	WL/POTF	15 - 20
Erek A Kasse	Bellbrook High School , Bellbrook , OH Friction and Solid Lubricants	WL/MLBT	15 - 21
Maria Lee	Wayne High School , Huber Heights , OH the Database Design for a Configuration Mnagement Library	WL/AAST	15 - 22

SRP Final Report Table of Contents

Author	University/Institution Report Title	Wright Laboratory Directorate	Vol-Page
Colleen A Lefevre	Lehman High School , Sidney , OH the Effect of Chain Lengths on Bond Orders and Geometry in Simple Cyanines0	WL/DOR	15 - 23
John P Lightle	Tippecanoe High School , Tipp City , OH A Study of two methods for Predicting fin Center of Pressure position	WL/FIGC	15 - 24
Alexander R Lippert	Choctawhatchee High School , Ft Walton BEACH , FL Nanoparticle Doped Organic Electronic Junction Devices	WL/MNMF	15 - 25
Jackson W Mac Nealy	Chaminade-Julienne High School , Dayton , OH Web Page Design to Display Infrared Imagery	WL/AACA	15 - 26
Jonathan S Mah	Centerville High School , Centerville , OH The Integration of Circuit synthesis and Schematic Programs Using Prolog, ad Evaluatation of a Graph	WL/AASH	15 - 27
David Mandel	Niceville Senior High School , Niceville , FL Terminal Ballistics Data Acquisition & Analysis	WL/MNM	15 - 28
Michele V Manuel	Crestview High School , Crestview , FL The Mechanical & Metallurgical Characterization of Liquid Phase Sintered Tungsten Alloyw	WL/MNM	15 - 29
Lori M Marshall	Carroll High School , Dayton , OH A Study of Chemical Vapor Depositiion and Pulse Laser Deposition	WL/DOR	15 - 30
Terrence J McGregor	Fairborn High School , Fairborn , OH Chain Armor Ballistic Testing : Establishing the Ballistic Limit	WL/FIVS	15 - 31
Deborah S Mills	West Liberty-Dalem Jr./Sr. High School , West Liberty , OH A Summer at Wright Patterson Air Force Base	WL/DOR	15 - 32
Ryan M Moore	Centerville High School . Centerville , OH Studies in Computational Chemistry and Biomimetics	WL/MLPJ	15 - 33

SRP Final Report Table of Contents

Author	University/Institution Report Title	Wright Laboratory Directorate	Vol-Page
Jeremy M Mount	Bellbrook High School , Bellbrook , OH	WL/FIIB	15 - 34
John D Murchison	Ft Walton Beach High SC , Ft Walton BEACH , FL Methodology for the Creation of a Randomized Shot-Line Generator	WL/MNSA	15 - 35
Disha J Patel	Fairmont High School , Kettering , OH	WL/AACT	15 - 36
Neill W Perry	Crestview High School , Crestview , FL Empirical Characterization of Mid-Infrared Photodetectors for a Dual-Wavelength Ladar System	WL/MNGS	15 - 37
Kathleen A Pirog	Niceville Senior High School , Niceville , FL The Implications of Photomodeler on the Generation of 3D Models	WL/MNGA	15 - 38
Nathan A Power	Heritage Christian School , Xenia , OH The World Wide Web and Hyper Text Markup Language	WL/AAOP	15 - 39
Shaun G Power	Heritage Christian School , Xenia , OH	WL/AACI	15 - 40
Josh J Pressnell	Fairmont High School , Kettering , OH A Study n Internet Programming and World Wide Web Publishing	WL/AACN	15 - 41
Stephanie M Puterbaugh	Beavercreek High School , Dayton , OH Initial Experimental evaluation of an Axial Groove Heat Pipe for Aircraft Applications	WL/POOS	15 - 42
Matthew R Rabe	Carroll High School , Dayton , OH	WL/POSC	15 - 43
Kristan M Raymond	Ft Walton Beach High SC , Ft Walton BEACH , FL Immersion Corrosion Testing of Tungsten Heavy-Metal Alloys	WL/MNSE	15 - 44

SRP Final Report Table of Contents

Author	University/Institution Report Title	Wright Laboratory Directorate	Vol-Page
David S Revill		WL/MNGA	15 - 45
	Choctawhatchee High School , Ft Walton BEACH , FL Verification of State of Chemical Equations & Generation of Textures for Phenomenology Modeling		
Harris T Schneiderman		WL/FIMC	15 - 46
	Miami Valley School , Dayton , OH A Study of the capabilities of computational fluid dynamics technology to simulate the flight perfor		
Nicole L Speelman		WL/MLIM	15 - 47
	Stebbins High School , Dayton , OH Development and Application of Materials Characterization web Site		
Kari D Sutherland		WL/MLPJ	15 - 48
	Dayton Christian High School , Dayton , OH A Study of the Effects of the Performance of Polymer Dispersed Liquid Crystal Holographic Gratings w		
Christine M Task		WL/MLIM	15 - 49
	Stebbins High School , Dayton , OH		
Rebecca M Thien		WL/DOR	15 - 50
	Chaminade-Julienne High School , Dayton , OH A Study of the Corrosion Resistance of Sol-Gels		
Jonathan D Tidwell		WL/MNM	15 - 51
	Rocky Bayou Christian School , Niceville , FL Data Reduction for Blast Arena Lethality Enhancement		
Robert L Todd		WL/MLLI	15 - 52
	Carroll High School , Dayton , OH The Characterization of A Scud Fragment		
Elizabeth A Walker		WL/MNA	15 - 53
	Niceville Senior High School , Niceville , FL Concept vs Reality:Developing a Theoretical Sequencing Program for Shock Induced Combustion		
Darren C Wells		WL/DOR	15 - 54
	Bellbrook High School , Bellbrook , OH A Study of the Tension and Shear Strength of Bidirectional Epoxy-Resin Composites		
Tuan P Yang		WL/MNM	15 - 56
	Choctawhatchee High School , Ft Walton BEACH , FL Thermal Characterization of the 1,3,3-Trinitroazetidine (ADNAZ) Binary Mixture		

SRP Final Report Table of Contents

Author	University/Institution Report Title	Arnold Engineering Development Center Directorate	Vol-Page
Karllee R Barton	Coffee County Central High , Manchester , TN A Math Model of the Flow Characteristics of The J4 gaseous Nitrogen Repress Systems	AEDC	16 - 1
Jason G Bradford	Franklin County Senior High School , Winchester , TN Design of A Serachable Data Retreving Web Based Page	AEDC	16 - 2
James R Brandon	Coffee County Central High , Manchester , TN	AEDC	16 - 3
Barbara E King	Franklin County Senior High School , Winchester , TN Assessment of Microwave Horn Antenna Radiation Pattern	AEDC	16 - 4
Kaitrin T Maher	Coffee County Central High , Manchester , TN Analysis of DWSG Characterizations	AEDC	16 - 5
Steven W Marlowe	Franklin County Senior High School , Winchester , TN Writing a Cost Estimate Program Using The Java Programming Language	AEDC	16 - 6
Michael R Munn	Coffee County Central High , Manchester . TN Construction of a Graphical User Interface for the Thermally Perfect Gas Code	AEDC	16 - 7
Jason A Myers	Coffee County Central High , Manchester . TN Intranet Development Problem with Powerpoint	AEDC	16 - 8
James P Nichols	Tullahoma High School , Tullahoma , TN Assessment of Reflecting Microwave Horn Data Within A Plasma	AEDC	16 - 9
James M Perryman	Shelbyville Central High School , Shelbyville , TN Computer Manipulation of Raman Spectroscopy Test	AEDC	16 - 10
Kristin A Pierce	Coffee County Central High , Manchester . TN Evaluation of Arc Heater Performance and Operational Stability	AEDC	16 - 11

SRP Final Report Table of Contents

<u>Author</u>	<u>University/Institution Report Title</u>	<u>Arnold Engineering Development Center Directorate</u>	<u>Vol-Page</u>
Daniel M Thompson	Shelbyville Central High School , Shelbyville , TN Maintenance of Facilities	AEDC	16 - 12
James R Williamson	Franklin County Senior High School , Winchester , TN Access Conversions	AEDC	16 - 13

1. INTRODUCTION

The Summer Research Program (SRP), sponsored by the Air Force Office of Scientific Research (AFOSR), offers paid opportunities for university faculty, graduate students, and high school students to conduct research in U.S. Air Force research laboratories nationwide during the summer.

Introduced by AFOSR in 1978, this innovative program is based on the concept of teaming academic researchers with Air Force scientists in the same disciplines using laboratory facilities and equipment not often available at associates' institutions.

The Summer Faculty Research Program (SFRP) is open annually to approximately 150 faculty members with at least two years of teaching and/or research experience in accredited U.S. colleges, universities, or technical institutions. SFRP associates must be either U.S. citizens or permanent residents.

The Graduate Student Research Program (GSRP) is open annually to approximately 100 graduate students holding a bachelor's or a master's degree; GSRP associates must be U.S. citizens enrolled full time at an accredited institution.

The High School Apprentice Program (HSAP) annually selects about 125 high school students located within a twenty mile commuting distance of participating Air Force laboratories.

AFOSR also offers its research associates an opportunity, under the Summer Research Extension Program (SREP), to continue their AFOSR-sponsored research at their home institutions through the award of research grants. In 1994 the maximum amount of each grant was increased from \$20,000 to \$25,000, and the number of AFOSR-sponsored grants decreased from 75 to 60. A separate annual report is compiled on the SREP.

The numbers of projected summer research participants in each of the three categories and SREP "grants" are usually increased through direct sponsorship by participating laboratories.

AFOSR's SRP has well served its objectives of building critical links between Air Force research laboratories and the academic community, opening avenues of communications and forging new research relationships between Air Force and academic technical experts in areas of national interest, and strengthening the nation's efforts to sustain careers in science and engineering. The success of the SRP can be gauged from its growth from inception (see Table 1) and from the favorable responses the 1997 participants expressed in end-of-tour SRP evaluations (Appendix B).

AFOSR contracts for administration of the SRP by civilian contractors. The contract was first awarded to Research & Development Laboratories (RDL) in September 1990. After completion of the

1990 contract, RDL (in 1993) won the recompetition for the basic year and four 1-year options.

2. PARTICIPATION IN THE SUMMER RESEARCH PROGRAM

The SRP began with faculty associates in 1979; graduate students were added in 1982 and high school students in 1986. The following table shows the number of associates in the program each year.

YEAR	SRP Participation, by Year			TOTAL
	SFRP	GSRP	HSAP	
1979	70			70
1980	87			87
1981	87			87
1982	91	17		108
1983	101	53		154
1984	152	84		236
1985	154	92		246
1986	158	100	42	300
1987	159	101	73	333
1988	153	107	101	361
1989	168	102	103	373
1990	165	121	132	418
1991	170	142	132	444
1992	185	121	159	464
1993	187	117	136	440
1994	192	117	133	442
1995	190	115	137	442
1996	188	109	138	435
1997	148	98	140	427

Beginning in 1993, due to budget cuts, some of the laboratories weren't able to afford to fund as many associates as in previous years. Since then, the number of funded positions has remained fairly constant at a slightly lower level.

3. RECRUITING AND SELECTION

The SRP is conducted on a nationally advertised and competitive-selection basis. The advertising for faculty and graduate students consisted primarily of the mailing of 8,000 52-page SRP brochures to chairpersons of departments relevant to AFOSR research and to administrators of grants in accredited universities, colleges, and technical institutions. Historically Black Colleges and Universities (HBCUs) and Minority Institutions (MIs) were included. Brochures also went to all participating USAF laboratories, the previous year's participants, and numerous individual requesters (over 1000 annually).

RDL placed advertisements in the following publications: *Black Issues in Higher Education*, *Winds of Change*, and *IEEE Spectrum*. Because no participants list either *Physics Today* or *Chemical & Engineering News* as being their source of learning about the program for the past several years, advertisements in these magazines were dropped, and the funds were used to cover increases in brochure printing costs.

High school applicants can participate only in laboratories located no more than 20 miles from their residence. Tailored brochures on the HSAP were sent to the head counselors of 180 high schools in the vicinity of participating laboratories, with instructions for publicizing the program in their schools. High school students selected to serve at Wright Laboratory's Armament Directorate (Eglin Air Force Base, Florida) serve eleven weeks as opposed to the eight weeks normally worked by high school students at all other participating laboratories.

Each SFRP or GSRP applicant is given a first, second, and third choice of laboratory. High school students who have more than one laboratory or directorate near their homes are also given first, second, and third choices.

Laboratories make their selections and prioritize their nominees. AFOSR then determines the number to be funded at each laboratory and approves laboratories' selections.

Subsequently, laboratories use their own funds to sponsor additional candidates. Some selectees do not accept the appointment, so alternate candidates are chosen. This multi-step selection procedure results in some candidates being notified of their acceptance after scheduled deadlines. The total applicants and participants for 1997 are shown in this table.

1997 Applicants and Participants			
PARTICIPANT CATEGORY	TOTAL APPLICANTS	SELECTEES	DECLINING SELECTEES
SFRP	490	188	32
(HBCU/MI)	(0)	(0)	(0)
GSRP	202	98	9
(HBCU/MI)	(0)	(0)	(0)
HSAP	433	140	14
TOTAL	1125	426	55

4. SITE VISITS

During June and July of 1997, representatives of both AFOSR/NI and RDL visited each participating laboratory to provide briefings, answer questions, and resolve problems for both laboratory personnel and participants. The objective was to ensure that the SRP would be as constructive as possible for all participants. Both SRP participants and RDL representatives found these visits beneficial. At many of the laboratories, this was the only opportunity for all participants to meet at one time to share their experiences and exchange ideas.

5. HISTORICALLY BLACK COLLEGES AND UNIVERSITIES AND MINORITY INSTITUTIONS (HBCU/MIs)

Before 1993, an RDL program representative visited from seven to ten different HBCU/MIs annually to promote interest in the SRP among the faculty and graduate students. These efforts were marginally effective, yielding a doubling of HBCI/MI applicants. In an effort to achieve AFOSR's goal of 10% of all applicants and selectees being HBCU/MI qualified, the RDL team decided to try other avenues of approach to increase the number of qualified applicants. Through the combined efforts of the AFOSR Program Office at Bolling AFB and RDL, two very active minority groups were found, HACU (Hispanic American Colleges and Universities) and AISES (American Indian Science and Engineering Society). RDL is in communication with representatives of each of these organizations on a monthly basis to keep up with their activities and special events. Both organizations have widely-distributed magazines/quarterlies in which RDL placed ads.

Since 1994 the number of both SFRP and GSRP HBCU/MI applicants and participants has increased ten-fold, from about two dozen SFRP applicants and a half dozen selectees to over 100 applicants and two dozen selectees, and a half-dozen GSRP applicants and two or three selectees to 18 applicants and 7 or 8 selectees. Since 1993, the SFRP had a two-fold applicant increase and a two-fold selectee increase. Since 1993, the GSRP had a three-fold applicant increase and a three to four-fold increase in selectees.

In addition to RDL's special recruiting efforts, AFOSR attempts each year to obtain additional funding or use leftover funding from cancellations the past year to fund HBCU/MI associates. This year, 5 HBCU/MI SFRPs declined after they were selected (and there was no one qualified to replace them with). The following table records HBCU/MI participation in this program.

YEAR	SFRP		GSRP	
	Applicants	Participants	Applicants	Participants
1985	76	23	15	11
1986	70	18	20	10
1987	82	32	32	10
1988	53	17	23	14
1989	39	15	13	4
1990	43	14	17	3
1991	42	13	8	5
1992	70	13	9	5
1993	60	13	6	2
1994	90	16	11	6
1995	90	21	20	8
1996	119	27	18	7

6. SRP FUNDING SOURCES

Funding sources for the 1997 SRP were the AFOSR-provided slots for the basic contract and laboratory funds. Funding sources by category for the 1997 SRP selected participants are shown here.

1997 SRP FUNDING CATEGORY	SFRP	GSRP	HSAP
AFOSR Basic Allocation Funds	141	89	123
USAF Laboratory Funds	48	9	17
HBCU/MI By AFOSR (Using Procured Addn'l Funds)	0	0	N/A
TOTAL	9	98	140

SFRP - 188 were selected, but thirty two canceled too late to be replaced.

GSRP - 98 were selected, but nine canceled too late to be replaced.

HSAP - 140 were selected, but fourteen canceled too late to be replaced.

7. COMPENSATION FOR PARTICIPANTS

Compensation for SRP participants, per five-day work week, is shown in this table.

1997 SRP Associate Compensation

PARTICIPANT CATEGORY	1991	1992	1993	1994	1995	1996	1997
Faculty Members	\$690	\$718	\$740	\$740	\$740	\$770	\$770
Graduate Student (Master's Degree)	\$425	\$442	\$455	\$455	\$455	\$470	\$470
Graduate Student (Bachelor's Degree)	\$365	\$380	\$391	\$391	\$391	\$400	\$400
High School Student (First Year)	\$200	\$200	\$200	\$200	\$200	\$200	\$200
High School Student (Subsequent Years)	\$240	\$240	\$240	\$240	\$240	\$240	\$240

The program also offered associates whose homes were more than 50 miles from the laboratory an expense allowance (seven days per week) of \$50/day for faculty and \$40/day for graduate students. Transportation to the laboratory at the beginning of their tour and back to their home destinations at the end was also reimbursed for these participants. Of the combined SFRP and GSRP associates, 65 % (194 out of 286) claimed travel reimbursements at an average round-trip cost of \$776.

Faculty members were encouraged to visit their laboratories before their summer tour began. All costs of these orientation visits were reimbursed. Forty-three percent (85 out of 188) of faculty associates took orientation trips at an average cost of \$388. By contrast, in 1993, 58 % of SFRP associates took

orientation visits at an average cost of \$685; that was the highest percentage of associates opting to take an orientation trip since RDL has administered the SRP, and the highest average cost of an orientation trip. These 1993 numbers are included to show the fluctuation which can occur in these numbers for planning purposes.

Program participants submitted biweekly vouchers countersigned by their laboratory research focal point, and RDL issued paychecks so as to arrive in associates' hands two weeks later.

This is the second year of using direct deposit for the SFRP and GSRP associates. The process went much more smoothly with respect to obtaining required information from the associates, only 7% of the associates' information needed clarification in order for direct deposit to properly function as opposed to 10% from last year. The remaining associates received their stipend and expense payments via checks sent in the US mail.

HSAP program participants were considered actual RDL employees, and their respective state and federal income tax and Social Security were withheld from their paychecks. By the nature of their independent research, SFRP and GSRP program participants were considered to be consultants or independent contractors. As such, SFRP and GSRP associates were responsible for their own income taxes, Social Security, and insurance.

8. CONTENTS OF THE 1997 REPORT

The complete set of reports for the 1997 SRP includes this program management report (Volume 1) augmented by fifteen volumes of final research reports by the 1997 associates, as indicated below:

1997 SRP Final Report Volume Assignments

LABORATORY	SFRP	GSRP	HSAP
Armstrong	2	7	12
Phillips	3	8	13
Rome	4	9	14
Wright	5A, 5B	10	15
AEDC, ALCs, WHMC	6	11	16

APPENDIX A -- PROGRAM STATISTICAL SUMMARY

A. Colleges/Universities Represented

Selected SFRP associates represented 169 different colleges, universities, and institutions,
GSRP associates represented 95 different colleges, universities, and institutions.

B. States Represented

SFRP -Applicants came from 47 states plus Washington D.C. Selectees represent 44 states.

GSRP - Applicants came from 44 states. Selectees represent 32 states.

HSAP - Applicants came from thirteen states. Selectees represent nine states.

Total Number of Participants	
SFRP	189
GSRP	97
HSAP	140
TOTAL	426

Degrees Represented			
	SFRP	GSRP	TOTAL
Doctoral	184	0	184
Master's	2	41	43
Bachelor's	0	56	56
TOTAL	186	97	298

SFRP Academic Titles	
Assistant Professor	64
Associate Professor	70
Professor	40
Instructor	0
Chairman	1
Visiting Professor	1
Visiting Assoc. Prof.	1
Research Associate	9
TOTAL	186

Source of Learning About the SRP		
Category	Applicants	Selectees
Applied/participated in prior years	28%	34%
Colleague familiar with SRP	19%	16%
Brochure mailed to institution	23%	17%
Contact with Air Force laboratory	17%	23%
<i>IEEE Spectrum</i>	2%	1%
<i>BIIHE</i>	1%	1%
Other source	10%	8%
TOTAL	100%	100%

APPENDIX B – SRP EVALUATION RESPONSES

1. OVERVIEW

Evaluations were completed and returned to RDL by four groups at the completion of the SRP. The number of respondents in each group is shown below.

Table B-1. Total SRP Evaluations Received

Evaluation Group	Responses
SFRP & GSRPs	275
HSAPs	113
USAF Laboratory Focal Points	84
USAF Laboratory HSAP Mentors	6

All groups indicate unanimous enthusiasm for the SRP experience.

The summarized recommendations for program improvement from both associates and laboratory personnel are listed below:

- A. Better preparation on the labs' part prior to associates' arrival (i.e., office space, computer assets, clearly defined scope of work).
- B. Faculty Associates suggest higher stipends for SFRP associates.
- C. Both HSAP Air Force laboratory mentors and associates would like the summer tour extended from the current 8 weeks to either 10 or 11 weeks; the groups state it takes 4-6 weeks just to get high school students up-to-speed on what's going on at laboratory. (Note: this same argument was used to raise the faculty and graduate student participation time a few years ago.)

2. 1997 USAF LABORATORY FOCAL POINT (LFP) EVALUATION RESPONSES

The summarized results listed below are from the 84 LFP evaluations received.

1. LFP evaluations received and associate preferences:

Table B-2. Air Force LFP Evaluation Responses (By Type)

Lab	Evals Recv'd	How Many Associates Would You Prefer To Get ?				(% Response)					
		SFRP			GSRP (w/Univ Professor)			GSRP (w/o Univ Professor)			
		0	1	2	3+	0	1	2	3+	0	1
AEDC	0	-	-	-	-	-	-	-	-	-	-
WHMIC	0	-	-	-	-	-	-	-	-	-	-
AL	7	28	28	28	14	54	14	28	0	86	0
USAFA	1	0	100	0	0	100	0	0	0	0	100
PL	25	40	40	16	4	88	12	0	0	84	12
RL	5	60	40	0	0	80	10	0	0	100	0
WL	46	30	43	20	6	78	17	4	0	93	4
Total	84	32%	50%	13%	5%	80%	11%	6%	0%	73%	23%

LFP Evaluation Summary. The summarized responses, by laboratory, are listed on the following page. LFPs were asked to rate the following questions on a scale from 1 (below average) to 5 (above average).

2. LFPs involved in SRP associate application evaluation process:

- a. Time available for evaluation of applications:
- b. Adequacy of applications for selection process:

3. Value of orientation trips:

4. Length of research tour:

- 5. a. Benefits of associate's work to laboratory:
b. Benefits of associate's work to Air Force:
- 6. a. Enhancement of research qualifications for LFP and staff:
b. Enhancement of research qualifications for SFRP associate:
c. Enhancement of research qualifications for GSRP associate:
- 7. a. Enhancement of knowledge for LFP and staff:
b. Enhancement of knowledge for SFRP associate:
c. Enhancement of knowledge for GSRP associate:

8. Value of Air Force and university links:

9. Potential for future collaboration:

- 10. a. Your working relationship with SFRP:
b. Your working relationship with GSRP:

11. Expenditure of your time worthwhile:

(Continued on next page)

12. Quality of program literature for associate:
 13. a. Quality of RDL's communications with you:
 b. Quality of RDL's communications with associates:
 14. Overall assessment of SRP:

Table B-3. Laboratory Focal Point Reponses to above questions

	<i>AEDC</i>	<i>AL</i>	<i>USAFA</i>	<i>PL</i>	<i>RL</i>	<i>WHMC</i>	<i>WL</i>
<i># Evals Recv'd</i>	0	7	1	14	5	0	46
<i>Question #</i>							
2	-	86 %	0 %	88 %	80 %	-	85 %
2a	-	4.3	n/a	3.8	4.0	-	3.6
2b	-	4.0	n/a	3.9	4.5	-	4.1
3	-	4.5	n/a	4.3	4.3	-	3.7
4	-	4.1	4.0	4.1	4.2	-	3.9
5a	-	4.3	5.0	4.3	4.6	-	4.4
5b	-	4.5	n/a	4.2	4.6	-	4.3
6a	-	4.5	5.0	4.0	4.4	-	4.3
6b	-	4.3	n/a	4.1	5.0	-	4.4
6c	-	3.7	5.0	3.5	5.0	-	4.3
7a	-	4.7	5.0	4.0	4.4	-	4.3
7b	-	4.3	n/a	4.2	5.0	-	4.4
7c	-	4.0	5.0	3.9	5.0	-	4.3
8	-	4.6	4.0	4.5	4.6	-	4.3
9	-	4.9	5.0	4.4	4.8	-	4.2
10a	-	5.0	n/a	4.6	4.6	-	4.6
10b	-	4.7	5.0	3.9	5.0	-	4.4
11	-	4.6	5.0	4.4	4.8	-	4.4
12	-	4.0	4.0	4.0	4.2	-	3.8
13a	-	3.2	4.0	3.5	3.8	-	3.4
13b	-	3.4	4.0	3.6	4.5	-	3.6
14	-	4.4	5.0	4.4	4.8	-	4.4

3. 1997 SFRP & GSRP EVALUATION RESPONSES

The summarized results listed below are from the 257 SFRP/GSRP evaluations received.

Associates were asked to rate the following questions on a scale from 1 (below average) to 5 (above average) - by Air Force base results and over-all results of the 1997 evaluations are listed after the questions.

1. The match between the laboratories research and your field:
2. Your working relationship with your LFP:
3. Enhancement of your academic qualifications:
4. Enhancement of your research qualifications:
5. Lab readiness for you: LFP, task, plan:
6. Lab readiness for you: equipment, supplies, facilities:
7. Lab resources:
8. Lab research and administrative support:
9. Adequacy of brochure and associate handbook:
10. RDL communications with you:
11. Overall payment procedures:
12. Overall assessment of the SRP:
13. a. Would you apply again?
b. Will you continue this or related research?
14. Was length of your tour satisfactory?
15. Percentage of associates who experienced difficulties in finding housing:
16. Where did you stay during your SRP tour?
 - a. At Home:
 - b. With Friend:
 - c. On Local Economy:
 - d. Base Quarters:
17. Value of orientation visit:
 - a. Essential:
 - b. Convenient:
 - c. Not Worth Cost:
 - d. Not Used:

SFRP and GSRP associate's responses are listed in tabular format on the following page.

Table B-4. 1997 SFRP & GSRP Associate Responses to SRP Evaluation

# res	Arnold	Brooks	Edwards	Eglin	Griffis	Hanscom	Kelly	Kirtland	Lackland	Robins	Tyndall	WPAFB	average
1	4.8	4.4	4.6	4.7	4.4	4.9	4.6	4.6	5.0	5.0	4.0	4.7	4.6
2	5.0	4.6	4.1	4.9	4.7	4.7	5.0	4.7	5.0	5.0	4.6	4.8	4.7
3	4.5	4.4	4.0	4.6	4.3	4.2	4.3	4.4	5.0	5.0	4.5	4.3	4.4
4	4.3	4.5	3.8	4.6	4.4	4.4	4.3	4.6	5.0	4.0	4.4	4.5	4.5
5	4.5	4.3	3.3	4.8	4.4	4.5	4.3	4.2	5.0	5.0	3.9	4.4	4.4
6	4.3	4.3	3.7	4.7	4.4	4.5	4.0	3.8	5.0	5.0	3.8	4.2	4.2
7	4.5	4.4	4.2	4.8	4.5	4.3	4.3	4.1	5.0	5.0	4.3	4.3	4.4
8	4.5	4.6	3.0	4.9	4.4	4.3	4.3	4.5	5.0	5.0	4.7	4.5	4.5
9	4.7	4.5	4.7	4.5	4.3	4.5	4.7	4.3	5.0	5.0	4.1	4.5	4.5
10	4.2	4.4	4.7	4.4	4.1	4.1	4.0	4.2	5.0	4.5	3.6	4.4	4.3
11	3.8	4.1	4.5	4.0	3.9	4.1	4.0	4.0	3.0	4.0	3.7	4.0	4.0
12	5.7	4.7	4.3	4.9	4.5	4.9	4.7	4.6	5.0	4.5	4.6	4.5	4.6

Numbers below are percentages

13a	83	90	83	93	87	75	100	81	100	100	100	86	87
13b	100	89	83	100	94	98	100	94	100	100	100	94	93
14	83	96	100	90	87	80	100	92	100	100	70	84	88
15	17	6	0	33	20	76	33	25	0	100	20	8	39
16a	-	26	17	9	38	23	33	4	-	-	-	30	
16b	100	33	-	40	-	8	-	-	-	-	36	2	
16c	-	41	83	40	62	69	67	96	100	100	64	68	
16d	-	-	-	-	-	-	-	-	-	-	-	0	
17a	-	33	100	17	50	14	67	39	-	50	40	31	35
17b	-	21	-	17	10	14	-	24	-	50	20	16	16
17c	-	-	-	-	10	7	-	-	-	-	-	2	3
17d	100	46	-	66	30	69	33	37	100	-	40	51	46

4. 1997 USAF LABORATORY HSAP MENTOR EVALUATION RESPONSES

Not enough evaluations received (5 total) from Mentors to do useful summary.

5. 1997 HSAP EVALUATION RESPONSES

The summarized results listed below are from the 113 HSAP evaluations received.

HSAP apprentices were asked to rate the following questions on a scale from 1 (below average) to 5 (above average)

1. Your influence on selection of topic/type of work.
2. Working relationship with mentor, other lab scientists.
3. Enhancement of your academic qualifications.
4. Technically challenging work.
5. Lab readiness for you: mentor, task, work plan, equipment.
6. Influence on your career.
7. Increased interest in math/science.
8. Lab research & administrative support.
9. Adequacy of RDL's Apprentice Handbook and administrative materials.
10. Responsiveness of RDL communications.
11. Overall payment procedures.
12. Overall assessment of SRP value to you.
13. Would you apply again next year? Yes (92 %)
14. Will you pursue future studies related to this research? Yes (68 %)
15. Was Tour length satisfactory? Yes (82 %)

	Arnold	Brooks	Edwards	Eglin	Griffiss	Hanscom	Kirtland	Tyndall	WPAFB	Totals
# resp	5	19	7	15	13	2	7	5	40	113
1	2.8	3.3	3.4	3.5	3.4	4.0	3.2	3.6	3.6	3.4
2	4.4	4.6	4.5	4.8	4.6	4.0	4.4	4.0	4.6	4.6
3	4.0	4.2	4.1	4.3	4.5	5.0	4.3	4.6	4.4	4.4
4	3.6	3.9	4.0	4.5	4.2	5.0	4.6	3.8	4.3	4.2
5	4.4	4.1	3.7	4.5	4.1	3.0	3.9	3.6	3.9	4.0
6	3.2	3.6	3.6	4.1	3.8	5.0	3.3	3.8	3.6	3.7
7	2.8	4.1	4.0	3.9	3.9	5.0	3.6	4.0	4.0	3.9
8	3.8	4.1	4.0	4.3	4.0	4.0	4.3	3.8	4.3	4.2
9	4.4	3.6	4.1	4.1	3.5	4.0	3.9	4.0	3.7	3.8
10	4.0	3.8	4.1	3.7	4.1	4.0	3.9	2.4	3.8	3.8
11	4.2	4.2	3.7	3.9	3.8	3.0	3.7	2.6	3.7	3.8
12	4.0	4.5	4.9	4.6	4.6	5.0	4.6	4.2	4.3	4.5
Numbers below are percentages										
13	60%	95%	100%	100%	85%	100%	100%	100%	90%	92%
14	20%	80%	71%	80%	54%	100%	71%	80%	65%	68%
15	100%	70%	71%	100%	100%	50%	86%	60%	80%	82%

ENGINEERING ASSISTANT

Emily Blundell

**Rosamond High School
2925 Rosamond Blvd.
Rosamond, CA 93560**

**Final Report for:
High School Office of Scientific Research
Bolling Air Force Base, DC**

and

Phillips Laboratory

August 1997

ENGINEERING ASSISTANT

Emily Blundell
Rosamond High School

Abstract

As an Engineering Assistant, I did three types of work. All involved working with drawings. I revised two drawings for an Engineer at the Satellite Engine Operations Complex, designed drawings for a Technical Library, and made an excel spreadsheet of data collected from drawings at the Space Environmental Propulsion Complex.

ENGINEERING ASSISTANT

Emily Blundell

As an Engineering Assistant, I worked with drawings done by or needed by Engineers. I worked in different parts of Phillips Laboratory, such as Experimental Support Division, Satellite Engine Operations Complex, and Space Environmental Propulsion Complex. Working in different areas gave me an opportunity to learn new things.

When working at the Experimental Support Division, I designed floor plans for three different room that are going to be part of a Technical Library. I measured and mapped out the rooms. I also needed to find exactly how many filing cabinets and bookcases would fit into each room. Bookcases and filing cabinets needed to be found to be put into the rooms. So I went over to the supply building and found bookcases.

I took the bookcases from supply and put them in one of the rooms and started to fill them up with book and binders. These books and binders will eventually be looked through by another Engineer.

At the Satellite Engine Operations Complex, I revised two drawings of an engine that is going to be tested. I did this by using Claris Cad Drafting. Drafting is something new to me, so I had to learn by watching a video about the basics of Claris Cad. Using Cad is a more accurate way of drawing.

After revising the drawings, I took the drawings out to the test cell, where the engine will eventually be tested, and followed each different system, such as liquid oxygen, gaseous nitrogen, water, and propane systems. I checked each individual valve, filter, gage, etc., for part numbers, manufacturer name, and other details. This was quite exciting, because I was able to climb all over different areas to find what I needed.

Next, after I was done searching, I put all the information into a spreadsheet and found which valves, filters, etc. did not have any information besides a manufacturer's name. So I looked in the Thomas Register Catalogs to find other information about the parts, but if there was not any information, I copied down the manufacturer's name and number, so that a catalog can be ordered.

My job at the Space Environmental Propulsion Complex was to figure out which drawings were there and were needed at the complex. There were three different buildings that contained drawings I needed to look at. I went through drawings and made a rough list of drawing titles, numbers, and dates. Using this information, I went over to General Physics, which is an on-site contractor hired to maintain area drawings, and looked in the Drawing Archives to see what drawings are there from the Space Environmental Propulsion Complex.

I found which drawings are at General Physics which are not at the Space Environmental Propulsion Complex and vice versa. Then, using Microsoft Excel, I made up a more complete list of all drawings that are at the Space Environmental Propulsion Complex. Drawings that have neither titles nor drawing numbers were put on two

separate spreadsheet so that titles or drawing numbers can be found later on.

I also printed out a copy of the drawing list and saved all the information on a disk so that, in the future, more drawings can be added to the list. General Physics and the Space Environmental Propulsion Complex will have to get together and print out which drawings that they each need.

I conclude that as an Engineering Assistant, I have learned what to expect when becoming an Engineer and different things I can do as an Engineer. As an Engineer, I would like to design things and what I have done this year at Phillips Laboratory has helped to give me a head start.

**EXPERIMENTAL VALIDATION OF THREE-DIMENSIONAL RECONSTRUCTION
OF INHOMOGENEITY IMAGES IN TURBID MEDIA**

**Lauren Ferguson
Moriarty High School
Moriarty, New Mexico 87035**

**Hanli Liu
Assistant Professor
Joint Program in Biomedical Engineering**

**Kelly Lau
Graduate Student
Joint Program in Biomedical Engineering**

**University of Texas at Arlington
P.O. Box 19138
Arlington, TX 76019**

**Final Report for:
High School Summer Research Program**

**Sponsored by:
Phillips Laboratory
Kirtland AFB, NM
and
Air Force Office of Scientific Research
Bolling AFB, Washington D.C.**

August 1997

EXPERIMENTAL VALIDATION OF THREE-DIMENSIONAL RECONSTRUCTION
OF INHOMOGENEITY IMAGES IN TURBID MEDIA

Lauren Ferguson
Moriarty High School
Moriarty, New Mexico

Abstract

Near infrared radiation for imaging tumors in tissue has been recently explored and investigated. In particular, to validate a novel FFT imaging reconstruction algorithm, we have performed experiments on tissue phantoms using a frequency-domain photon migration system. The system includes an amplitude-modulated laser diode, two radio frequency (RF) signal generators, an avalanche photo detector, and a lock-in amplifier. The tissue phantoms were made with inhomogeneities imbedded and were then scanned with the system at various RF frequencies. The data from the amplitude and phase measurements were analyzed using the FFT reconstruction algorithm. The reconstructed data show clear validation of the FFT algorithm and afford to localize inhomogeneities hidden in turbid media in three dimensions. In addition, based on the results, we present preliminary analysis on optimization of experimental parameters to obtain good-quality, reconstructed images with best experimental efficiency.

EXPERIMENTAL VALIDATION OF THREE-DIMENSIONAL RECONSTRUCTION OF INHOMOGENEITY IMAGES IN TURBID MEDIA

Lauren Ferguson

1. Introduction

In the last few years, numerous research efforts and technology developments have been made towards using near infrared (NIR) radiation for human tissue quantification and imaging. Three forms of light used in the field include short-pulsed light in time-domain (TD), intensity-modulated light in frequency-domain(FD), and a continuous wave form (CW). Among them, the frequency-domain system has its advantages over the other two: a FD system can acquire data almost in real time in an order of ms, much faster than a TD system, which utilizes a single photon counting method and requires much longer data acquisition time (in multi seconds). In addition, with the help of diffusion theory, the FD system allows us to extract the optical properties of tissues/organs under study and to image inhomogeneities hidden in tissues/organs. In comparison, CW method is in lack of quantification unless close-distanced (2-5 mm) measurements are performed.

The light source used for a FD system is intensity modulated at a radio frequency (RF) ranging from several MHz up to GHz at the wavelength range from 650 nm to 900 nm. In principle, NIR light illuminating tissues becomes very much scattered about 1 mm after the light travels in tissue. In the FD case, the intensity-modulated light travelling in tissue will form diffuse photon density waves (DPDW's), and the amplitude and phase of DPDW's carry information on the optical properties of the tissue. By extracting amplitude, phase, or optical properties of thick tissue, we can reconstruct tissue images that show inhomogeneities imbedded inside the thick tissue. This provides a new methodology for tumor imaging in medical applications.

Over last few years, common geometries used for imaging studies are 1) source(s)-detector pairs scanning horizontally or 2) circularly.¹ In both cases, mechanical movement is required, and it provides only two-dimensional images. Recently, Matson et al proposed a new approach to three-dimensional tumor localization in turbid media with the use of FD measurements in a single plane.² The theoretical basis of this novel reconstruction algorithm stems from Fourier Optics: applying Fast Fourier Transform (FFT) to the diffusion equation that DPDW's obey, and then extending the solution of Fourier Optics to DPDW's. This FFT reconstruction algorithm has several advantages, such as, 1) the light source does not need to move mechanically, 2) it has a potential to avoid mechanical movement, which has been shown to produce significant errors in imaging reconstruction. The theory has yet to be verified by experiments, although it was supported by computer simulations at one RF frequency of 1 GHz with selected scanning parameters.

The goal of this summer research project is to experimentally validate and optimize this three-dimensional reconstruction algorithm to image inhomogeneities in turbid media. In this report, we will first introduce the theoretical foundation for the FFT reconstruction algorithm, followed by a brief description on experimental setups, materials and methods. Then we will show experimental results and reconstructed images, and then investigate the correlation among experimental parameters that affect the quality of the reconstructed images. Furthermore, computer simulations are performed to confirm the findings that a larger scanning area is more crucial than smaller scanning pixels to obtain a higher resolution image. Finally, we will draw conclusions from this study and indicate future work.

2. Theoretical Background

Based on Fourier Optics³, we define the following relations:

$$A_z(f_x, f_y) = \iint U(x, y, z) e^{-i2\pi(f_x x + f_y y)} dx dy, \quad (1)$$

$$U(x, y, z) = \iint A_z(f_x, f_y) e^{i2\pi(f_x x + f_y y)} df_x df_y, \quad (2)$$

where $U(x, y, z)$ is the complex field of a monochromatic wave across the plane at z , and A_z is a two-dimensional Fourier transform of the function $U(x, y, z)$. It can be shown that a free-space solution to the source-free Helmholtz equation exists in the form of spatial frequency spectrum across a plane parallel to the xy plane but at a distance z from it.³

In addition, it has been proved⁴ that the diffusion equation adequately represents photon propagation in tissue, and the source-free diffusion equation in FD can be written as

$$\nabla^2 U(x, y, z) + k^2 U(x, y, z) = 0, \quad (3)$$

where $U(x, y, z)$ is the spatial distribution of a DPDW in a scattering medium, and $k^2 = (-v\mu_a + i\omega)/D = 3\mu_s'(-\mu_a + i\omega/v)$, v is the speed of light travelling in tissue, ω is the modulation frequency of the light multiplied by 2π , and μ_a and μ_s' are absorption and reduced scattering coefficients of the scattering medium, respectively.

Now inserting the inverse Fourier transform definition, eq. (2), into the diffusion equation, eq. (3), results in:

$$\frac{d^2}{dz^2} A_z(f_x, f_y) + \left[k^2 - (2\pi f_x)^2 - (2\pi f_y)^2 \right] A_z(f_x, f_y) = 0. \quad (4)$$

In analogy to the solution obtained in Fourier Optics for regular plane waves, we can find a solution to eq. (4) using the Fourier transform definition:

$$A_{z_l}(f_x, f_y) = A_{Z_0}(f_x, f_y) e^{i\Delta z \sqrt{k^2 - (2\pi f_x)^2 - (2\pi f_y)^2}}, \quad (5)$$

where $\Delta z = z_0 - z_1$, is the distance between the detection plane at z_0 and the reconstruction plane z_1 . Furthermore, we can define a transfer function, $H_{\Delta z}(f_x, f_y)$, describing how a DPDW propagates in a homogeneous medium,

$$H_{\Delta z}(f_x, f_y) = \frac{A_{z_1}(f_x, f_y)}{A_{z_0}(f_x, f_y)} = \exp \left\{ i \Delta z \sqrt{\left(\frac{-\nu \mu_a + i \omega}{D} \right) - (2\pi f_x)^2 - (2\pi f_y)^2} \right\}. \quad (6)$$

It is worthwhile to notice several important points:

- 1) in using diffusion theory, we neglect boundary effects and assume the medium to be homogeneous with spherical inhomogeneities;
- 2) in applying Fourier Optics to obtain equation (5), we extend the wave vector, k , from a real number to a complex number to include scattering effects, as the diffusion equation does;
- 3) eq. (6) describes the change in the Fourier transform of the photon density wave as it propagates, and thus eq. (6) can be used to invert the propagation and to reconstruct the photon density wave behind the detection plane.

3. Necessity of Experiments

The primary goal of this summer research project is to experimentally validate the FFT reconstruction algorithm, as introduced above. Taking experiments is necessary because

- 1) experiments permit studying boundary effects on the reconstructed images by using finite sizes of tissue phantoms;
- 2) we can study instrument detectability and sensitivity in locating hidden objects with different sizes and optical properties;
- 3) we can optimize scan parameters by performing experiments with various scan dimensions, pixel sizes, and modulation frequencies;
- 4) measurement on homogeneous samples provide feasibility of obtaining correct background information for the reconstruction and demonstrate the importance of such information.

4. Experimental Setup

As shown in Figure 1, the electronic components of our FD system include two RF signal generators, (Rhode & Schwarz, SMY01) ranging from 9 kHz to 1.04 GHz, two 50% power splitters (Mini-Circuits, ZFSC-2-1), two RF amplifiers (Mini-Circuits, ZFL-1000H), a NIR laser diode (LaserMax Inc, LSX-3500) modulatable up to 100 MHz at 780 nm and 680 nm with laser powers of 3 mW (at 116 mA) at 9 mW, an Avalanche Photo Diode (APD) (Hamamatsu, C5331), two frequency mixers (Mini-Circuits, ZLW-2), two low pass filters with the corner frequency at 1 MHz (Mini-Circuits, SLP-1.9), a lock-in amplifier (Stanford Research Systems, SR850), and a computer-controlled, two-dimensional positioning stage (Aerotech, Inc. ATS100).

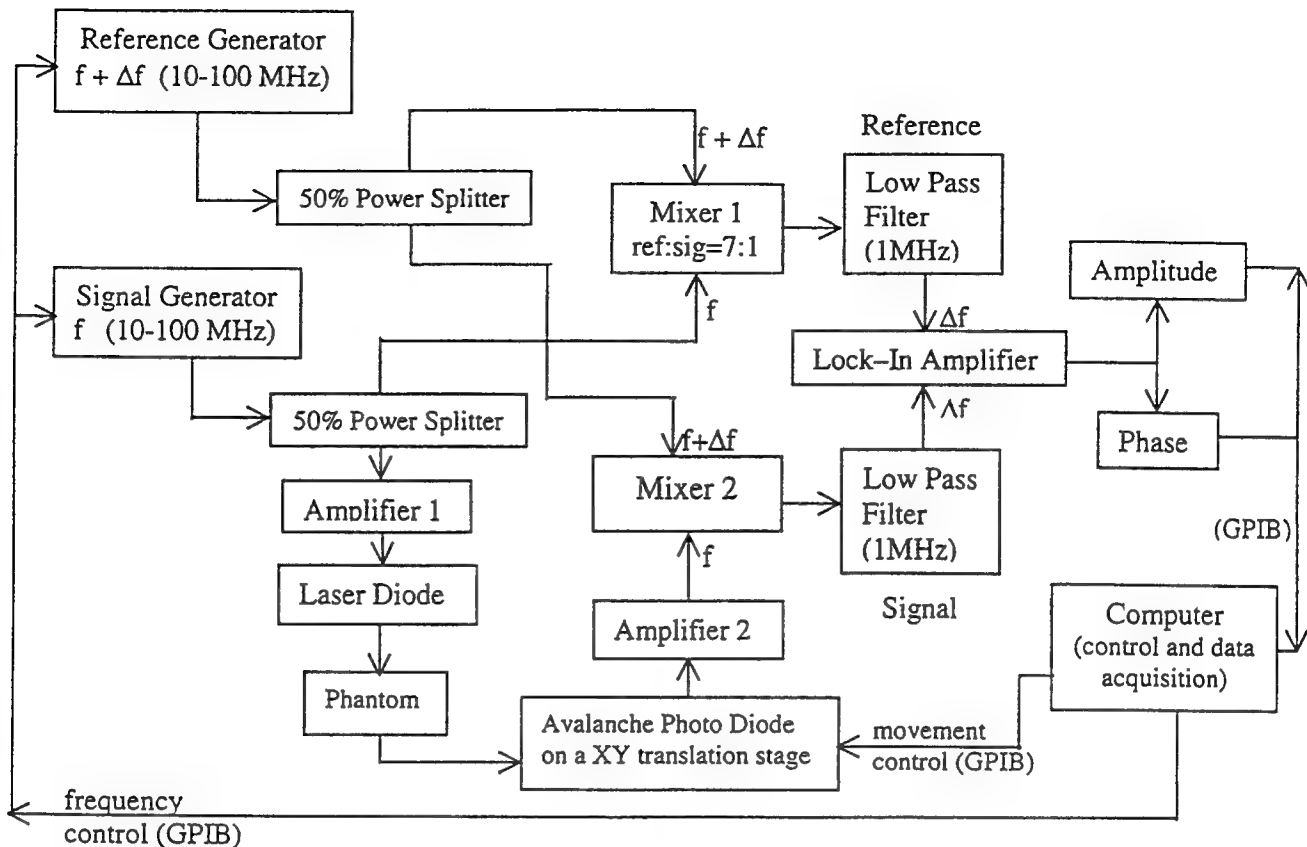


Figure 1. Experimental Setup of a FD system

The frequencies of the two signal generators were chosen from 10 to 100 MHz with an offset $\Delta f = 25$ kHz for the reference signal with respect to the measurement signal in order to achieve a heterodyne system. Both RF signals for the reference at $f + \Delta f$ and for the measurement at f were 50% power split, and a branch from each the two RF signal generator was mixed by Mixer 1 to generate a reference signal for a lock-in amplifier. The output levels of the two signal generators were set up with a ratio of 7 to 1 between the reference and measurement signals to optimize the mixing efficiency. The second branch of the measurement signal at f was amplified to gain enough power to modulate the intensity of a NIR laser diode at 780 nm. Then the intensity-modulated, manufacture-collimated laser light illuminated a tissue phantom and then was detected by a movable APD to convert the optical signal to electrical signal. A second amplifier amplified the output of APD before the electrical signal was mixed with the second branch of the reference signal at $f + \Delta f$ using Mixer 2. The output frequencies of Mixer 1 and Mixer 2 consisted of $2f + \Delta f$, $f + \Delta f$, f , Δf , and higher harmonic components. By utilizing two low pass filters with a corner frequency of 1 MHz, only the signal with frequency of Δf at 25 kHz passes to the lock-in amplifier. The corresponding readings for amplitude and phase were recorded

automatically by a computer; in turn, feedback from the computer controlled the sensitivity and time constant settings for the lock-in amplifier based on the readings. In addition, through a GPIB interface, the computer set the RF frequencies for the two signal generators and controlled a XY positioning stage, which held the APD for 2-dimensional imaging scans.

5. Materials and Methods

Tissue phantoms were made out of plastic resin that hardens in molds by adding catalyst. The resin is combined with TiO_2 powder for scattering property and sometimes with NIR dye for absorption property.⁵ The optical properties of homogeneous phantoms were determined using the slope algorithm⁶ in transmission geometry. Since the algorithm requires the information on the homogeneous background medium that contains an object/objects, multiple samples were made as a set at the same time to ensure that the samples of the set have the same background optical properties. In general, a set of phantoms included a homogeneous sample, and two others with different objects implanted inside. The phantom sizes were typically 14cm x 14cm x 5cm, and absorption and scattering coefficients of background media were within a range of 0.01 to 0.1 cm^{-1} and 3 to 17 cm^{-1} , respectively. The objects used as inhomogeneities were plastic black, white, and clear beads with various diameters and shapes, as shown and listed in Figure 2.

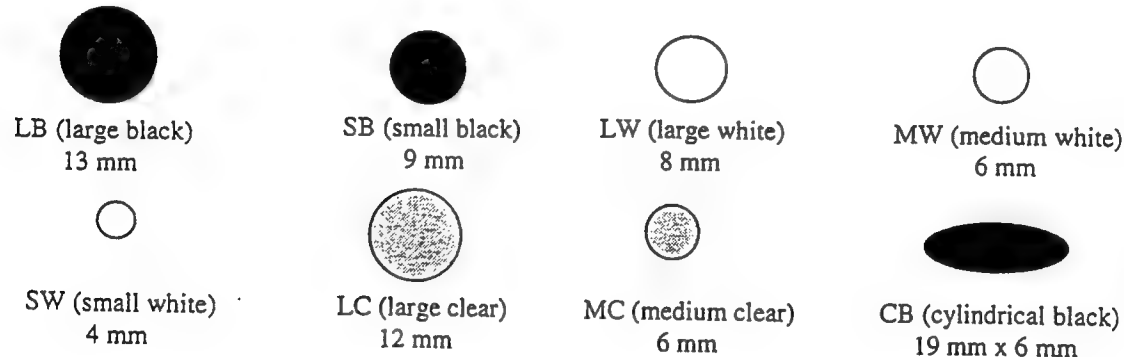
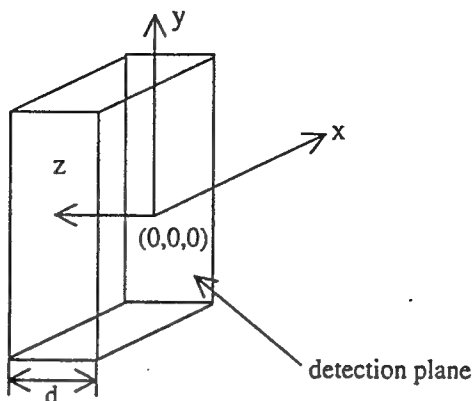


Figure 2. Beads used as tumor objects imbedded in tissue phantoms

We will use a XYZ coordinate system, shown in Figure 3, in this report to refer to the positions of hidden objects in the phantoms. The XY plane is in parallel with the detection plane, the origin is at the center of the detection plane, and the Z axis is pointing from the detection plane into the phantom. Normally, a bead was placed at the center of a phantom with a coordinate of $(0, 0, d/2 \text{ cm})$, where d is the thickness of the phantom. For multiple hidden tumors, two beads (the same or different kinds) were placed at $(0, -2 \text{ cm}, -d/2 \text{ cm})$ and $(0, 2 \text{ cm}, -d/2 \text{ cm})$ inside of a phantom. In making inhomogeneous phantoms, we positioned the object(s) on top of a semi-dried, background material which has been cast earlier, and then added equal amount of ready-to-cast resin on top of the first part to complete the

phantom. In this way, we implanted the objects inside the phantoms with good 3-dimensional coordinate references, and X-ray measurements have confirmed the positions of imbedded objects.

Figure 3. the xyz coordinate system used to label locations of hidden objects inside a phantom.



All of the scans used for this report were performed on areas of 8 cm x 8 cm having 64x64, 32x32, or 16x16 pixels with pixel spacing of 0.125 cm, 0.25 cm, and 0.5 cm, respectively. The modulation frequencies were scanned from 10 MHz to 100 MHz in various steps in actual experiments, but all the data shown in this report were taken mainly at 20 or 40 MHz. An average measurement time was about 2.5 hours for a 32x32 scan with two modulation frequencies (20 and 40 MHz). The experiments were performed in transmission geometry with the light source fixed at one side of the sample and the movable detector located on the other side of the sample. The software package Interactive Data Language (IDL) was used to process the measured data and to perform the reconstruction algorithm. In addition, the PMI⁷ simulation code was used to predict and confirm the experimental data.

Because the transfer function contains an exponential decay term, the reconstructed DPDW's are not stable, containing ringing patterns. A better understanding for this artifact is under investigation. However, at present stage, to stabilize the reconstructed data or eliminate ringing patterns, we utilized a low-pass filter (pillbox) to cut off high spatial frequency components. Specifically, the cutoff frequency was ranged from only a few pixels, such as 1-4, in the spatial frequency domain. We multiplied the Fourier spectra by this cutoff filter before inverse Fourier transforming the spatial frequency spectra to reconstruct the DPDW's. For convenience, in the rest of the report, we will use "filter" as a short notation to represent the pixel number in Fourier domain of cutoff spatial frequencies.

After the amplitude, A, and phase, θ , were measured as a function of positions in a XY plane at $z=z_0$, we followed the procedures given below to reconstruct three-dimensional images:

- 1) based on A and θ , calculate complex photon density waves $U_h(x,y,z_0)$ and $U_{inh}(x,y,z_0)$, respectively, for both homogeneous sample and the sample containing objects;
- 2) subtract the homogeneous wave from the inhomogeneous wave, $U(x,y,z_0)=U_{in}(x,y,z_0)-U_h(x,y,z_0)$;

- 3) FFT $U(x,y,z_0)$ to obtain its Fourier transform $A(f_x, f_y, z_0)$;
- 4) multiply $A(f_x, f_y, z_0)$ by the transfer function to execute the reconstruction process at z_1 ;
- 5) multiply $A(f_x, f_y, z_1)$ by a low-pass filter with a selected filter number (cutoff pixels);
- 6) inverse FFT $A(f_x, f_y, z_1)$ to the spatial domain for the reconstructed image at z_1 ;
- 7) repeat steps 4) to 6) for different values of z_1 to back propagate the reconstruction;
- 8) determine the x, y coordinates of the hidden object at the detection plane, and then plot amplitude versus z to localize the tumor in Z direction.

6. Experimental Results and Image Reconstructions

Figure 4 shows an example of amplitude images of DPDW's measured at the detection plane using a 680 nm laser scanned with 32x32 pixels on a 8 cm x 8 cm area of a phantom containing one black object. The phantom was 4.7 cm thick, and the black bead had a diameter of 9 mm imbedded at (0, 0, 2.3 cm). The illumination spot on the phantom was located at (-1.5 cm, 0, 2.3 cm), 1.5 cm off-centered in x axis with respect to the center of the phantom. The modulation frequency used for this set of measurements was 20 MHz, and the filter used for the reconstruction was 2. The absorption and reduced scattering coefficients of the background medium were 0.14 ± 0.06 and $3.1 \pm 1.4 \text{ cm}^{-1}$, respectively, which were determined using a homogeneous sample. Three amplitude plots of the complex DPDW's in Figure 4 are obtained at the detection plane for a homogeneous field [4(a)] measured from the homogeneous sample, perturbed field [4(b)] from the inhomogeneous sample, and the deviation between the two fields [4(c)], i.e., perturbed field (pfield) - homogeneous field (hfield). Notice that in obtaining the image of 4(c), we first subtracted the two complex fields (pfield-hfield), which were calculated from amplitude and phase measurements of the two samples, and then plotted the amplitude of the subtracted field.

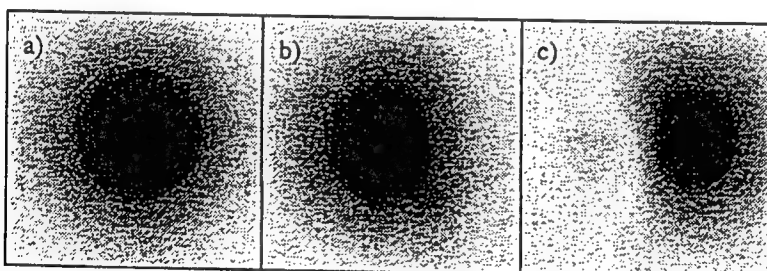


Figure 4. Amplitude images of the DPDW's measured at the detection plane from a phantom with one hidden high-absorbing object, scanned at 20 MHz with an array size of 32 x 32. a) homogeneous field=hfield, b) perturbed field=pfield, c) pfield-hfield.

Figure 5 uses the same set of data as those for Figure 4. In the case of Figure 5, the FFT reconstruction algorithm was utilized to obtain the images at different depths behind the detection plane. The filter used here was 2. Let's first look at Figures 5(c) to 5(e), which are amplitude images at the

detection plane, 1.25 cm, and 2.5 cm behind the detection plane, respectively. The center of the actual black object is 2.3 cm behind the detection surface and 1.5 cm off from the center of the scanned area in X direction. These three images clearly and consistently show the location of the center of a hidden inhomogeneity in the XY plane at different depths, indicating that the object is a few centimeters deep behind the detection plane. For more quantitative localization of the object in Z direction, we need to have a XZ/YZ image or a plot in Z direction at the selected x and y coordinates of the detected object determined from the previous XY images. Figures 5(a) and 5(b) are cross-section images at XZ and YZ planes passing through the center of the scanned area. The top of Figure 5(a) corresponds to the detection plane along x axis, and the bottom represents the illumination plane. In this case, this XZ plane goes through the center of the object horizontally at $y=0$, and one can see that the imaged object is 1.4 cm off from the center in x direction. A plot of amplitude versus Z at the corresponding x coordinate provides the location of the object in Z direction (not shown). Same principle applies to Figure 5(b), in which case the YZ plane is at $x=0$, 1.5 cm apart from the plane passing through the center of the object. Because of this, this image does not give accurate location of the object in Z direction.

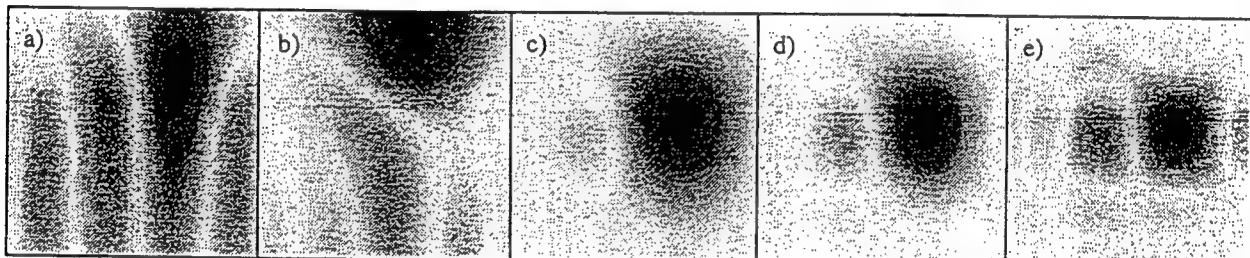


Figure 5. Reconstructed images for a phantom with one object, scanned at 20 MHz with an array size of 32×32 . a) x-z plane: the plane through the center of the measured volume horizontally, b) y-z plane: the plane through the center of the measured volume vertically, c) x-y plane: the detection plane, d) x-y plane: 1.25 cm behind the detection plane, e) x-y plane: plane near the object's center, 2.5 cm behind the detection plane.

Figure 6 is obtained from another set of two phantoms, one of which is homogeneous and the other having two high-absorbing objects with diameters of 9 mm. With the use of a 780 nm laser modulated at 20 MHz, the absorption and reduced scattering coefficients of the background medium are found to be 0.015 ± 0.001 cm and 15.1 ± 0.3 cm, respectively. The thickness of the inhomogeneous phantom is 4.2 cm. The two objects were imbedded inside the phantom with a separation of 4 cm apart at $(0, -2 \text{ cm}, 2.1 \text{ cm})$ and $(0, 2 \text{ cm}, 2.1 \text{ cm})$. The phantom was set 0.5 cm off centered with respect to the laser and the scanning plane along x axis. Similarly to Figure 5, Figures 6(a) and 6(b) are amplitude images measured from the homogeneous and inhomogeneous phantoms, and subtraction of the two complex fields of the two samples gives Figure 6(c). These three images are obtained at the detection

plane and show clearly two hidden objects after the simple subtraction. Furthermore, if the FFT reconstruction algorithm is applied, we can obtain the reconstructed amplitude images of DPDW's at different depths behind the detection plane. Figures 7(c) to 7(f) show such amplitude images reconstructed at the detection plane, 1 cm, and 2 cm behind the detection plane, respectively. All three images indicate consistently and unambiguously two hidden objects at about (0.5 cm, 2cm) and (0.5 cm, -2 cm) in the XY plane at different depths. As the reconstructed plane goes deeper and closer to the center of the hidden objects, the resolution for the imaged objects becomes better. In this case, a YZ image, shown in Figure 7(b), supports the findings from the XY images, and it also provides locations of the two objects in depth, which occur at the peaks of the two dark, cylindrical spots. Since the image plane for Figure 7(a) is in between the two objects, not passing through either center of the hidden objects, this XZ image does not give us very useful information in locating objects.

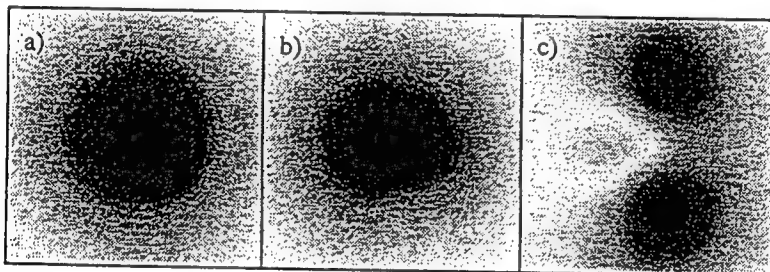


Figure 6. Amplitude images of the DPDW's measured from a phantom with two high-absorbing objects, scanned at 20 MHz with an array size of 32 x 32. a) hfield, b) pfield, and c) pfield-hfield.

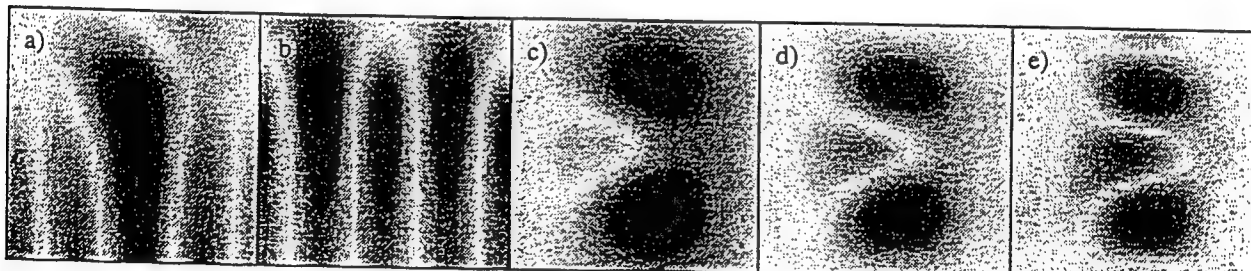


Figure 7. Reconstructed images for a phantom with two objects, scanned at 20 MHz with an array size of 32 x 32 for a scan area of 8 cm x 8cm with Filter 2 used for the reconstruction. a) x-z plane: the plane through the center of the measured volume horizontally, b) y-z plane: the plane through the center of the measured volume vertically, c) x-y plane: at the detection plane, d) x-y plane: 1 cm behind the detection plane, and e) x-y plane: plane near the object's center, 2 cm behind the detection plane.

Notice that there are multiple bright, ringing patterns/loops in Figure 7(b); they are artifacts due to Fourier transform. Higher filters used in the Fourier domain for the reconstruction algorithm give more ringing patterns. This limits the bandwidth of the spatial frequency components in the reconstruction and

thus limits the spatial resolution of the reconstructed images. If higher spatial frequency components are included, we have to be careful to differentiate the real hidden objects from FFT reconstruction artifacts. In the next section, we will discuss how to select filter numbers, or cutoff spatial frequencies, to optimize the reconstructed images. Further studies and understanding of the cause of ringing patterns are underway.

The phantom used to obtain Figure 8 contains two objects, one black marble having 13 mm diameter and one white bead of 8 mm diameter. They were implanted at the middle of a 4.5 cm thick phantom in Z direction and about 2.5 cm apart vertically (or horizontally) symmetric to the center of the phantom. Similarly, 32x32 pixels were chosen to scan a 8cm x 8cm area with a modulation frequency of 20 MHz. The absorption and reduced scattering coefficients of the background are $0.017 \pm 0.001 \text{ cm}^{-1}$ and $15.9 \pm 0.6 \text{ cm}^{-1}$, respectively. Figures 8(a) and 8(b) are amplitude plots, respectively, at the detection plane and 2 cm behind the detection plane near the centers of the objects. It is seen that at the detection plane, the image for the white object does not appear very well, whereas the image for the black object is very obvious and clear. The reconstructed image on the XY plane near the centers of the objects (Figure 8(b)), however, displays two clear imaging spots with different magnitudes. The big, dark spot is corresponding to the black marble, and the small, light spot stems from the white bead. We can easily obtain the separation distance of 2.7 cm between the spots from Figure 8(b). To confirm the result, we turned the phantom 90° around the Z axis (the axis perpendicular to the detection plane) and rescanned the phantom. The reconstructed images for this case are shown in Figures 8(c) and 8(d), and the results are very consistent with those observed in Figures 8(a) and 8(b).

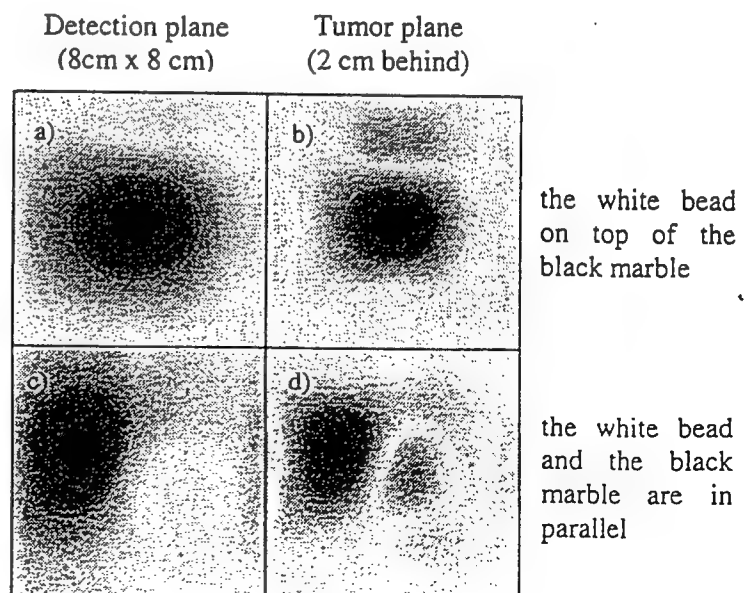


Figure 8. Amplitude images of a phantom with two objects, a 13 mm black marble and a 8 mm white bead, scanned at 20 MHz with an array size of 32 x 32. a) and c): at the detection (x-y) plane, b) and d): near the center of the samples, 2 cm behind the detection plane. Filter of 2 was used for this reconstruction.

In order to know how different wavelengths and powers of the laser affect the quality of the reconstructed images, we performed two measurements on the same phantom using a 780 nm, 3 mW and a 680 nm, 9 mW laser diode. In this case, the phantom contained two objects, one 12 mm black marble and 12 mm clear bead. These two objects were imbedded in the middle of a 5 cm thick phantom, and other parameters were the same as those used for Figure 8. The background medium has absorption and reduced scattering coefficients of $0.016 \pm 0.00 \text{ cm}^{-1}$ and $10.0 \pm 0.7 \text{ cm}^{-1}$ at 780 nm, and $0.015 \pm 0.001 \text{ cm}^{-1}$ and $13.7 \pm 0.3 \text{ cm}^{-1}$ at 680 nm. With a 3 mW laser at 780 nm, we reconstructed amplitude images of the phantom, shown in Figures 9(a) and 9(b), at the detection plane and at the plane passing the centers of the objects, 2.5 cm behind the detection plane. It is seen that the clear bead does not give a very distinguished, resolvable feature in either case. Furthermore, after we switched to a higher (9 mW) power laser at 680 nm, the reconstructed images (Figures 9(c) and 9(d)) look similar to those with the 780 nm laser, except that the 680 nm, higher power laser gives a little better spatial resolution than the other case. This may be because a higher power laser gives a better signal-to-noise ratio. But overall, there is no significant difference between these two lasers in imaging large-mismatched objects in our phantoms.

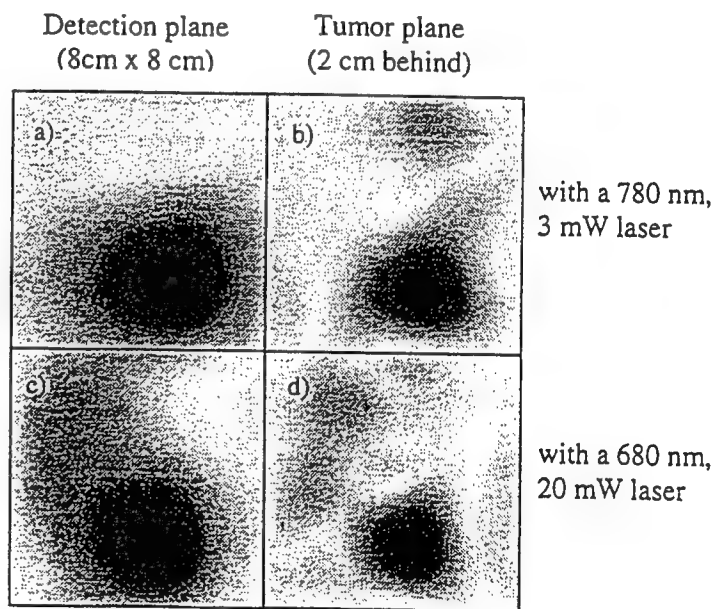


Figure 9. Amplitude images of a phantom with two objects, scanned at 20 MHz with an array size of 32×32 . Filter is 2. a) and c): at the detection (x-y) plane; b) and d): at the plane passing through the center of the objects.

To study the relationship between the quality of the reconstructed images and pixel spacing, we also performed a series of scans on the same phantom with array sizes of 64×64 , 32×32 , and 16×16 having pixel spacing of 0.125 cm/pixel, 0.25 cm/pixel, and 0.5 cm/pixel, respectively. In this case, the phantom was 4.4 cm thick and contained a 8 mm black and a 9 mm white bead. They were located at the middle depth of the sample and about 4 cm apart along Y axis with the white bead on top of the black bead. Figure 10 presents a set of reconstructed amplitude images at both the detection plane and at the

plane near the centers of the objects, 2 cm below the detection plane. The filter used here was 1, and the laser was at 780 nm. Figure 10 shows clearly that there is not much difference in image quality among the reconstructed images using either smaller (0.125 cm/pixel) or larger (0.5 cm/pixel) pixel spacing.

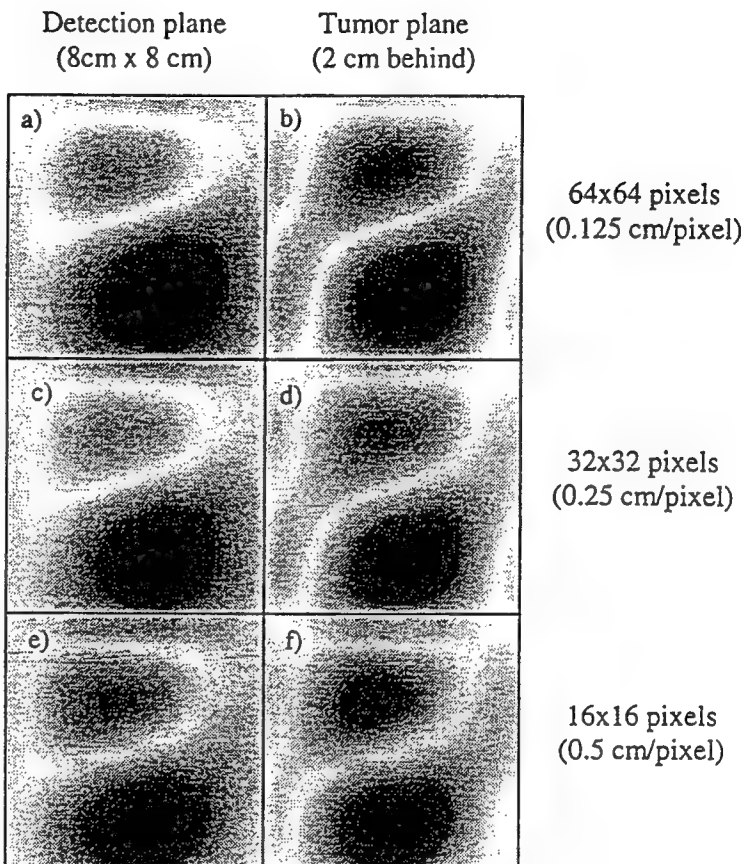


Figure 10. Image comparisons for three different pixel spacing. a), c), e): Images reconstructed at the detection plane; b), d), f): near the tumor plane, 2 cm behind the detection plane. Filter used here was 1.

To obtain the object location in Z direction, we first determine the x and y coordinates of the detected object(s) based on XY images, such as those shown in Figure 10, and then plot the amplitude versus Z to obtain the peak position. The z coordinate at the peak of the amplitude will be the location of the hidden object in Z direction. To show this strategy, we plot a z plot in Figure 11(a) based on Figure 10(d) at $X_{pixel}=20$, $Y_{pixel}=6$, which are the pixel coordinates of the observed, dark spot for the hidden black bead. In this case, the pixel step in Z direction is the same as that used in X and Y directions, i.e., 0.25 cm/pixel. Figure 11(a) displays a peak at pixel number=8 behind the detection plane, implying that this peak is at $8 \times 0.25 \text{ cm} = 2 \text{ cm}$ behind the detection plane. Similarly, Figure 11(b) plots the amplitude versus Z pixels at $X_{pixel}=20$, $Y_{pixel}=22$, for the other observed spot resulting from the hidden white bead. This figure shows a dip at $Z_{pixel}=8$ behind the detection plane, giving the consistent location of the hidden

object in Z direction. A dip, rather than a peak, in amplitude might stem from a possible fact that the absorption of the white bead is lower than the background material.

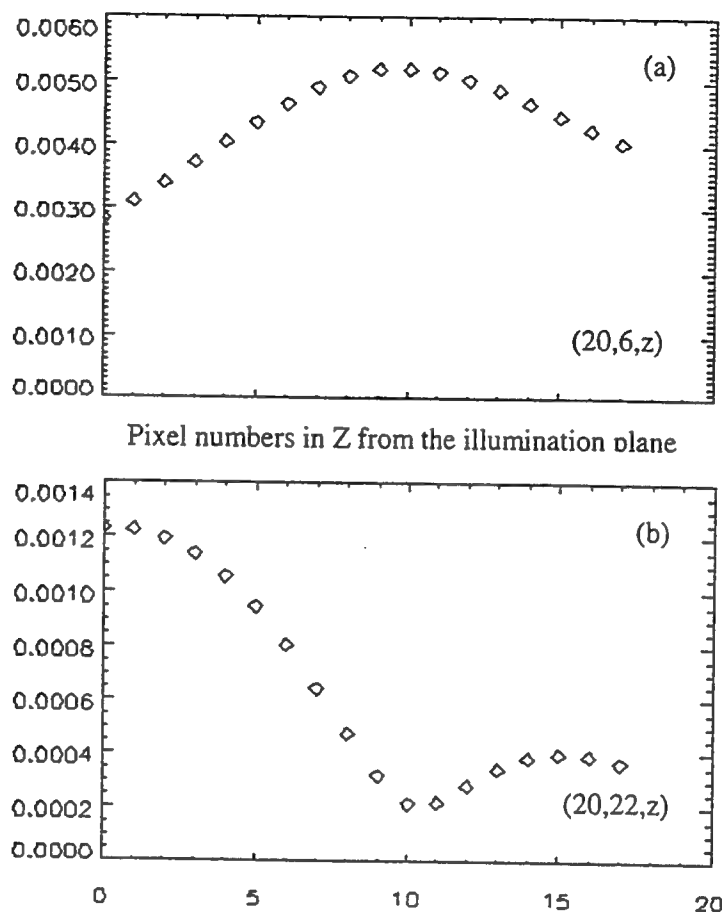


Figure 11. Z plots along the lines perpendicular to the detection plane and containing the black bead (a) and white bead (b). The pixel spacing in Z direction is 0.25 cm/pixel, corresponding to that shown in Figures 10(c) and 10(d). The filter used here was 2.

To confirm the object location in depth obtained from Figure 11, we plot two Z plots for the data with 16×16 array sizes, as shown in Figures 10(e) and 10(f), at the corresponding x and y coordinates of the two implanted objects. These two Z plots are given in Figures 12(a) and 12(b), respectively, for the black and white bead. In this case, the pixel spacing in Z is 0.5 cm/pixel. One can see that a peak and a dip appear at Z pixel number=4 behind the detection plane, i.e., $4 \times 0.5 \text{ cm} = 2 \text{ cm}$ behind the detection plane. Thus, the object location in Z direction given in figure 11 is in good agreement with that in figure 11.

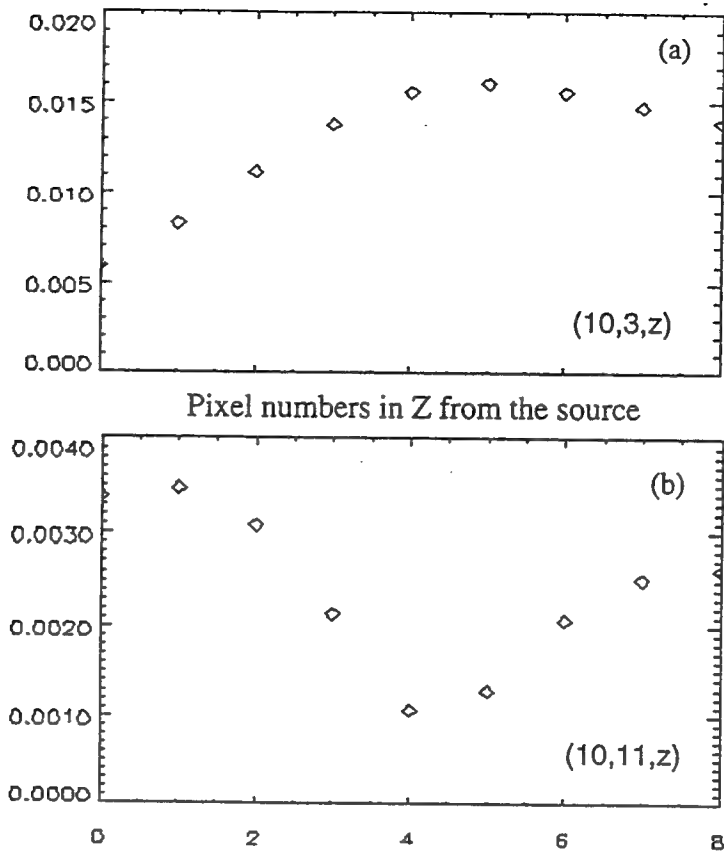


Figure 12. Z plots along the lines perpendicular to the detection plane and containing the black bead (a) and white bead (b). The pixel size in Z direction is 0.5 cm/pixel, corresponding to that shown in Figures 9(e) and 9(f). The filter used here was 2.

7. Data Analysis

Parameters used to scan and reconstruct images are as follows: 1) scanning dimensions/areas, such as 8x8 or 4x4 cm², 2) pixel spacing, such as 0.125, 0.25, or 0.5 cm/pixel, 3) modulation frequencies at 20, 40, or 100 MHz, and 4) filters numbers or cutoff spatial frequencies. What is the relationship among those parameters, and how do they affect the resolution of the reconstructed images? The answer to these questions may be helpful to optimize the scanning and reconstruction parameters for good-quality reconstructed images with best efficiency.

When a FFT of a 2-dimensional spatial domain function is performed, the number of pixels (or elements) in the spatial frequency domain is equal to the same number of pixels in the spatial domain. The 2-d spatial frequencies, f_x and f_y , will be multiple increments of Δf_x and Δf_y . Thus, we can rewrite the transfer function (TF) as follows:

$$H_z(f_x, f_y) = \frac{A_z(f_x, f_y)}{A_0(f_x, f_y)} = \exp \left\{ i \Delta z \sqrt{\left(\frac{-v\mu_a + i\omega}{D} \right) - (2\pi f_x)^2 - (2\pi f_y)^2} \right\}$$

$$= \exp \left\{ -\Delta z \sqrt{\left(\frac{\nu \mu_a}{D}\right) + (2\pi n \Delta f_x)^2 + (2\pi n \Delta f_y)^2} - i \frac{\omega}{D} \right\}, \quad (7)$$

where Δz is the distance from the detection plane to the reconstructed plane behind the detection plane, and Δz is a positive number. n is an integer, ranging from 0 to n_{max} , where n_{max} is equal to one half of the number of pixels in a row in the spatial domain. In the reconstruction algorithm, n corresponds to the filter number for the cutoff spatial frequency. It is known that the increments in the 2-d spatial frequency domain, Δf_x and Δf_y , are related to the dimension of the spatial domain as:

$$\Delta f_x = \frac{1}{L_x} = \frac{1}{\text{dimension}(x)}, \Delta f_y = \frac{1}{L_y} = \frac{1}{\text{dimension}(y)}. \quad (8)$$

Therefore, the TF becomes

$$H_z(f_x, f_y) = \exp \left\{ -\Delta z B [\cos(\frac{\theta}{2}) + i \sin(\frac{\theta}{2})] \right\} = e^{-\Delta z B \cos(\frac{\theta}{2})} e^{i \Delta z B \sin(\frac{\theta}{2})}, \quad (9)$$

where B is a real number and $B = \left[[3\mu_a \mu_s' + (\frac{2\pi n}{L_x})^2 + (\frac{2\pi n}{L_y})^2]^2 + (\frac{\omega}{D})^2 \right]^{\frac{1}{4}}, \quad (10)$

$$\theta = \tan^{-1} \left[\frac{\omega/D}{3\mu_a \mu_s' + (\frac{2\pi n}{L_x})^2 + (\frac{2\pi n}{L_y})^2} \right]. \quad (11)$$

Eqs. (9) to (11) show quantitative dependence of the TF on the spatial dimension, L_x and L_y , modulation frequency, ω , and cutoff pixels, n , for spatial frequencies. It is seen from eq. (9) that the TF, H_z , has an decaying amplitude of $e^{-\Delta z B \cos(\frac{\theta}{2})}$ with a phasor of $e^{i \Delta z B \sin(\frac{\theta}{2})}$. For a given phantom or tissue with fixed values of absorption and reduced scattering coefficients, μ_a and μ_s' having typical values of 0.1 and 10 cm^{-1} , B and θ , and thus H_z , are functions of ω and n , if the scan dimensions, L_x and L_y , are selected. Figure 13 demonstrates that $\theta/2$ is relatively small with a range of modulation frequencies less than 100 MHz. This means that the transfer function is approximately a pure attenuation function with the phasor equal to 1 when the modulation frequencies are within 100 MHz. Using the same parameters as those for

Figure 13, we plot the amplitude of $e^{-\Delta z B \cos(\frac{\theta}{2})}$ with $\theta=0$, as shown in Figure 14. It is seen that at lower modulation frequencies, such as 20 MHz, the amplitude of the transfer function decays much faster than that at higher modulation frequencies, such as 1 GHz. This plot also shows that to obtain the same

magnitude of the normalized amplitude of TF, the number of pixels for Δf would be much smaller at 20 MHz than that at 1GHz. This makes the cutoff filter in the spatial frequency domain to be more limited at lower modulation frequencies than at higher modulation frequencies, i.e., only to be 1 or 2 pixels at 20 MHz but to be up to 5 more pixels at 1GHz. In addition, based on eq. (10), the cutoff filters can be equivalently improved by increasing the scanning dimensions, L_x and L_y .

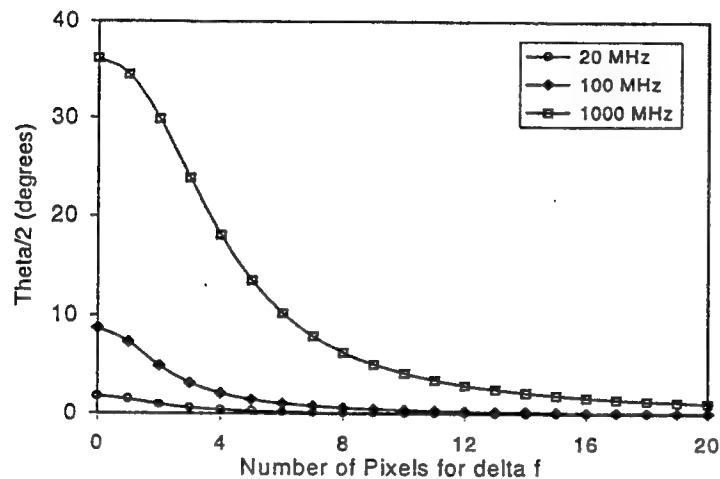


Figure 13. Dependence of $\theta/2$ in degrees on the number of pixels for Δf in the spatial frequency domain. The parameters used for this plot are: $\mu_a=0.1 \text{ cm}^{-1}$, $\mu_s'=10 \text{ cm}^{-1}$, $L_x=L_y=8 \text{ cm}$.

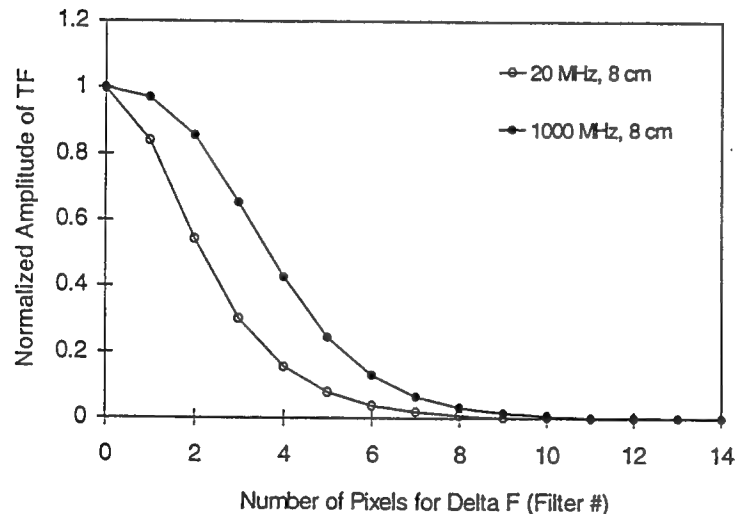


Figure 14. Dependence of normalized amplitude of transfer function on the number of pixels for Δf in the spatial frequency domain. The parameters used for this plot are: $\mu_a=0.1 \text{ cm}^{-1}$, $\mu_s'=10 \text{ cm}^{-1}$, $L_x=L_y=8 \text{ cm}$.

Thus, to improve the resolution of the reconstructed images, we can use higher modulation frequencies or increase the sizes (dimensions) of the detection plane. Decrease in pixel spacing would not be a crucial factor at this point, as long as the sampling frequency (number of pixels per unit length) is larger than the spatial frequency of the imbedded object, i.e., $1/(2*\text{diameter of the object})$, according to Nyquist's law.

To confirm the findings mentioned above, we have also conducted theoretical simulations using similar parameters. The results are very consistent with the experimental data.

In the case of biomedical imaging, let us discuss two extreme cases as follows: the first case is where the medium is highly absorbing in comparison to the modulation frequency. For example, at 20 MHz, we have μ_a (typically $0.1\text{--}0.3 \text{ cm}^{-1}$) $\gg \omega/v$ ($=0.006 \text{ cm}^{-1}$ for 20 MHz signal), and the TF becomes a purely exponential decay function. We can approximately use the following relationship to optimize the parameters for the cutoff filter and the scanning dimension, n , L_x and L_y .

$$(2\pi n/L_x)^2 + (2\pi n/L_y)^2 = 3\mu_a\mu_s' \sim 3 \text{ cm}^{-2}, \text{ or } n/L_x \sim 0.2 \text{ cm}^{-1}.$$

In the second case, where the modulation frequency is comparable to or higher than the absorption factor of the medium, we will have μ_a (typically $0.04\text{--}0.1 \text{ cm}^{-1}$) $\ll \omega/v$ ($=0.3 \text{ cm}^{-1}$ for 1 GHz signal). The TF has an exponential decay term and phase shift. In this case, we will use the following relationship to estimate the parameters for the cutoff filter and the scanning dimension, n , L_x and L_y .

$$(2\pi n\Delta f_x)^2 + (2\pi n\Delta f_y)^2 = 3\mu_s'\omega \sim 3\pi \text{ cm}^{-2}, \text{ or } n\Delta f_x \sim 0.6 \text{ cm}^{-1}.$$

8. Conclusions and Future Work

What we have learned from this summer research project is as follows:

- 1) the FFT reconstruction algorithm works in imaging and positioning inhomogeneities 3-dimensionally with good accuracy;
- 2) background information is necessary and important for accurate reconstruction;
- 3) At present stage, for high sensitivity, the imbedded object should be off-centered with respect to the light source and the detection plane. Further studies are underway to improve the reconstruction algorithm in order to eliminate this requirement.
- 4) large scanning dimension/area is more important than small scanning pixel size to achieve better resolution;
- 5) high modulation frequencies ($>500 \text{ MHz}$) may be helpful to achieve better resolution; low modulation frequencies can provide adequate information for tumor screening;
- 6) this summer project has demonstrated that the experimental set-up works and the results generated from it are in good agreement with the theoretical simulations. Inhomogeneities can be detected and located in three-dimensions. However, we are not able to characterize the optical properties of the inhomogeneities at this point. This remains for further study.

Our future work includes:

- 1) make phantoms containing objects which are small, purely absorptive, perturbations from the background medium;
- 2) take measurements on the new phantoms;

- 3) complete a diffraction tomographic model for quantitative reconstruction of optical property imaging;
- 4) apply the diffraction tomographic model to the data taken from the new phantoms for μ_a , μ_s' image reconstruction;
- 5) extend the modulation frequencies to KHz range, and explore the possibility at using CCD cameras for image capture;
- 6) extend the system to clinical tests.

9. Acknowledgement

The authors are grateful to Dr. Chuck Matson for providing adequate laboratory equipment and the bulk of the reconstruction programs, as well as for his theoretical insight and useful discussions. In addition, the authors also wish to thank Grant Denton and Scott Newey for all of their helpful technical support. Without all of them, this research project would not have been possible.

10. References

¹ M. A. O'Leary, D. A. Boas, B. Chance, and A. G. Yodh, "Simultaneous Scattering and Absorption Images of Heterogeneous Media Using Diffusive Waves within the Rytov Approximation," SPIE, 2389, p.328-339 (1995).

Brain W. Pogue, Michael S. Patterson, and Tom J. Farrell, "Forward and Inverse Calculations for 3-D Frequency-Domain Diffuse Optical Tomography," SPIE, 2389, p.328-339 (1995).

² C. L. Matson, N. Clark, L. McMackin, and J. S. Fender, "Three-dimensional tumor localization in thick tissue with the use of diffuse photon-density waves," Appl. Opt. 36, 214-220 (1997).

³ Joseph W. Goodman, Introduction to Fourier Optics, (San Francisco, McGraw-Hill Book Company, 1968).

⁴ M. S. Patterson, B. Chance, and B. C. Wilson, "Time resolved reflectance and transmittance for the non-invasive measurement of tissue optical properties," Appl. Opt. 28, 2331-2336 (1989).

⁵ M. Firbank, M. Hiraoka, and D. T. Delpy, "Development of a stable and reproducible tissue equivalent phantom for use in infrared spectroscopy and imaging," SPIE, 1888, 264-274 (1993).

⁶ J. B. Fishkin and E. Gratton, "Propagation of photon-density waves in strongly scattering media containing an absorbing semi-infinite plane bounded by a straight edge," J. Opt. Soc. Am. A 10, 127-140 (1993).

⁷ See the PMI (Photon Migration Imaging) Code Home Page: <http://www.osa.org/homes/BIOOPTIC/Resource/softwar.htm>

Chaotic Dynamics in a Nd:YAG laser

Erica S. Gerken

**Manzano High School
12200 Lomas Blvd. N E
Albuquerque, NM 87112**

**Final Report for:
High School Apprentice Program
Phillips Laboratory**

**Sponsored by:
Air Force Office of Scientific Research
Bolling Air Force Base, DC**

and

Phillips Laboratory

August 1997

Chaotic Dynamics in a Nd:YAG laser

Erica S. Gerken
Manzano High School

Abstract

A diode pumped Nd:YAG laser was constructed. The pump beam was modulated in order to stimulate nonlinear dynamics. Bifurcation processes were investigated. Data was acquired using a 16 bit vertical resolution digitizer card and signal processor.

Chaotic Dynamics in a Nd:YAG laser

Erica S. Gerken

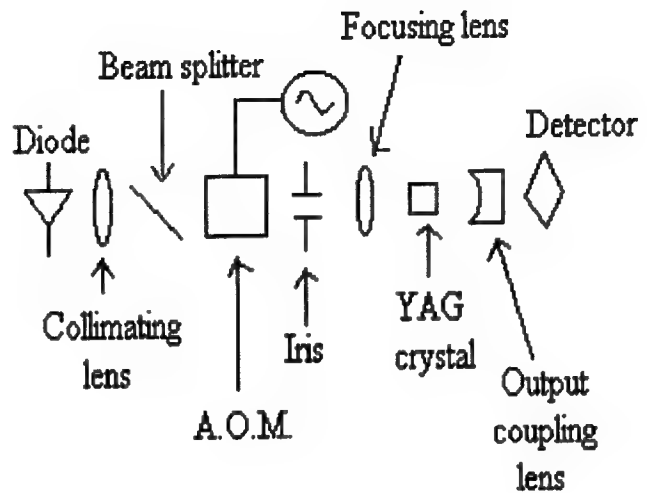
Introduction

Chaos was studied in an optical system using a custom built Nd:YAG laser. This laser can be modeled using two ordinary differential equations and hence is a class B laser. The pump beam was modulated to stimulate chaotic dynamics. A period doubling route into chaos has been predicted to exist for a Nd:YAG laser but has never been observed in a published experiment.

Construction

Figure 1 shows the experimental apparatus. A laser diode emitting at 810nm with up to 100mW power pumps the Nd:YAG crystal. The highly divergent light is collimated using an antireflection coated Newport FL-10 collimating lens. We may observe the pump using a beam splitter. The pump light can be modulated using one of two methods. The easiest way is to modulate the current of the laser diode. However, we found this introduces a substantial amount of noise in the pump beam. Also, the modulation is limited to 50kHz due to the limitations of the current driver. An alternative manner of modulation is to modulate the intensity of the pump beam using an acousto-optic modulator. An iris is used to control the intensity. The pump beam is focused on the crystal with a medium focal length bi-convex lens. The dimensions of the Nd:YAG crystal are 5mm by 2mm. One face of the crystal is coated for high transmission of 810nm and high reflection at the YAG wavelength of 1064nm. An output coupling mirror with 98% reflectivity is placed a short distance from the crystal. Thus, the cavity length is approximately 7mm. This makes the free spectral range of the cavity approximately 4GHz ($FSR = c/2nl$). With this large FSR, the laser operates in a single longitudinal mode for low powers of pumping. Furthermore, the laser can be made to operate in the Gaussian 00 mode. Finally, by careful alignment and proper pumping levels, the laser operates in 1 polarization eigenstate.

Fig. 1



Data Acquisition

One of the major impediments between theory and experiment is the resolution of the experimentally acquired data. While theorists routinely work with double precision machine data, experimentalists are limited to the vertical resolution of the digitizer. This is typically 8 to 10 bits. We have employed a state of the art data acquisition system that samples data at up to a 3 MHz rate with vertical resolution of 16 bits. The digitizer card is installed on a PC and the incoming data is processed by a Bittware Gamma Digital Signal Processor. It is necessary to program both the digitizer card and the DSP in order to synchronize the two.

Problems

Due to their high gain and nonlinear characteristics, laser diodes are extremely sensitive to optical feedback. The consequences are that the laser will mode hop and its intensity will oscillate in an erratic manner. The resulting oscillations will trigger relaxation oscillations in the Nd:YAG laser. Undesired feedback into the laser diode existed due to many sources. We found that reflections from poor collimating lenses are sufficient to induce

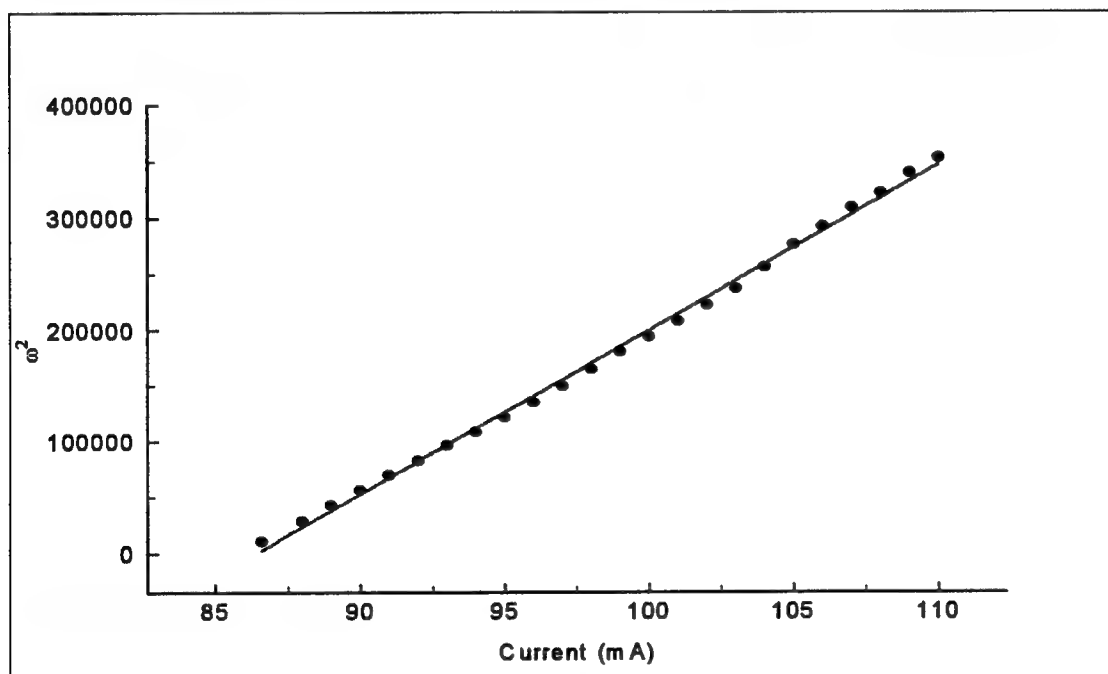
erratic behavior. We also found that reflections from the YAG crystal will stimulate this behavior. This, in fact, is our most daunting problem. The solution is to place optical isolators in the beam's path. Even this did not solve the problem completely.

Characterization of the Nd:YAG laser

Figure 2 is a plot of the square of the relaxation oscillation frequency versus the pump intensity. This relationship obeys the following equation

$$\omega^2 = \left(\frac{P}{P_0} - 1 \right) \frac{1}{\tau \tau_p}$$

where ω is the relaxation oscillation, P is the pump, P_0 is the pump at threshold, τ is the fluorescence lifetime, $240\mu\text{s}$, and τ_p is the photon lifetime.

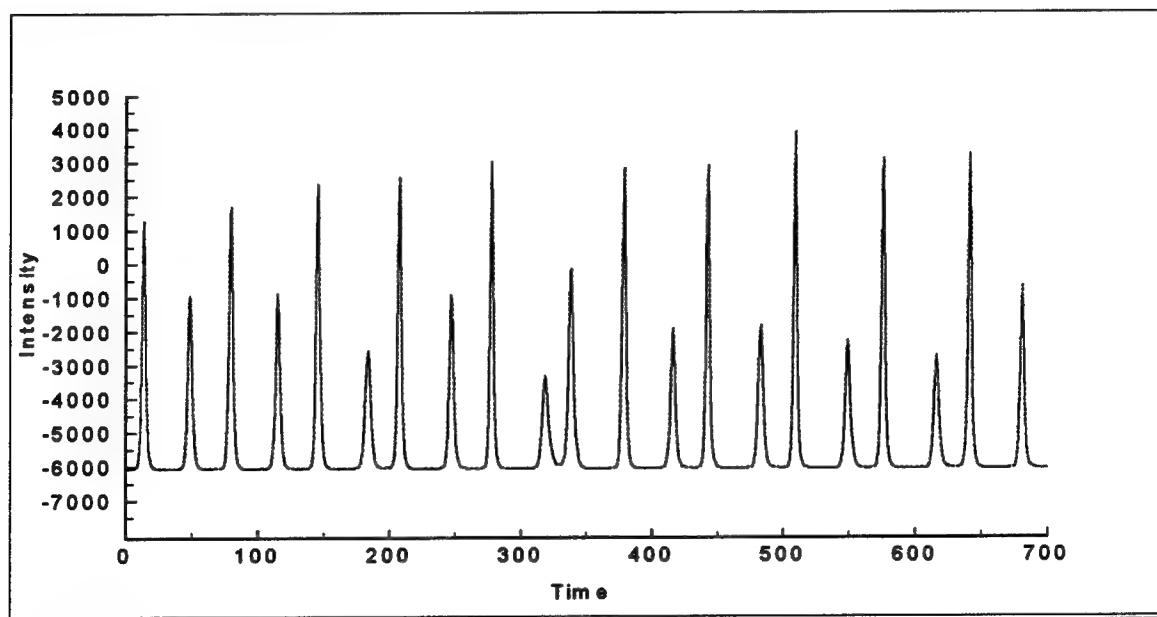


From this graph we find that τ_p is 3.28 ns.

Below, we looked at the relaxation oscillation as a function of the crystal temperature. However, we did not observe a clear trend in the data.

Temperature (°C)	Relaxation Oscillation (kHz)
10	22.89
11	17.40
12	10.08
13	10.14
14	10.14
15	10.14
16	17.46
17	27.23
18	25.40
19	18.07

Figure 3 is a time series of the pump modulated YAG. The modulated pump destabilizes the normally constant output. The result is a wavetrain of spiky pulses. Here the laser is operating in a chaotic state.



Conclusions

Our initial search was to observe a period doubling route into chaos. While we observed a limit cycle and a period two bifurcation, we saw no higher period doubling bifurcations. Instead, chaos was reached by an explosive type of bifurcation in which the period two orbit is suddenly replaced by the chaotic waveform seen in figure 3. We also observed

evidence of coexisting attractors. Here, the output jumped from low intensity oscillations to very large amplitude oscillations.

Acknowledgements

To Timothy C. Newell for his guidance throughout the experiment and for the help he gave me while I wrote this paper.

Associate did not participate in the program.

A STUDY ON OPTICAL PATTERNATION

Paul G. Loftsgard

Quartz Hill High School
6040 W. Ave. L
Quartz Hill, Ca 93593

Final Report for:
High School Apprenice Program
Phillips Laboratory

Sponsored by:
Air Force Office of Scientific Research
Bolling Air Force Base, DC

and

Phillips Laboratory

August 1997

Abstract

Optical patterning was studied in an attempt to create a three dimensional image of a liquid cone, created by a nozzle, of a specific angle, and composed of fluorescent water. The image is created through the use of Planar Liquid Laser-Induced Fluorescence(PLLIF). PLLIF is done by taking pictures, using CCD camera, of a laser sent through a spray containing a fluorescent dye. With the use of a fluorescent filter the camera is able to take accurate pictures of the spray and it's intensity. This type of picture is taken at successive heights and combined to form a three dimensional model of the spray.

Introduction

The use of high density sprays in many industrial fields has generated the need to have the sprays accurately diagrammed. The older method of attaining these diagrams, using a system of pipes and test tubes, was tedious and inaccurate. A spray would be activated over a field of holes connected to pipes, the liquid from the spray traveled down the pipes and into the test tubes. The amount in each test tube was then measured manually, consuming excessive amounts of time, for every picture taken anywhere from 576 to 221184 test tubes would need to be measured.. Through the use of PLLIF in the same sprays a much more accurate and time saving method was developed.

Approach

In order to establish the basic method of creating the three dimensional models a test spray was used. The nozzle formed a 45 degree symmetrical spray. The spray was water with fluorescent dye dissolved into it. The dye had a small concentration of approximately 0.00001 to 0.0001 molar. In order to induce florescence an Argon laser was, through the use of cylindrical lenses, turned into a sheet and sent through the spray.(Pic 1)

Experimentation

After taking several pictures of the spray at various heights, exposure times, directions(of the laser), gains, and accumulations, two main problems arose: the spray seemed to deplete from one side to the other, and particles out side of the laser sheet were being illuminated by scattered light.

The first problem was found to be caused by the depletion of the laser sheet when put through the spray, it was solved by sending a second laser sheet from the opposite side of the spray(Pic 2).

The second problem required a new method of taking pictures to minimize the scattered light. By sending just a single laser beam through the spray the amount of scattered light was greatly reduced. An aperture creating a focused laser approximately 1/16 of an inch wide was used. Pictures taken with just a beam though do not illuminate the entire spray(Pic 3). Only two main points are shown, the spots where the beam passes through the cone of the spray. A new method of taking pictures had to be used. It was determined to create a full sheet, pictures one pixel wide had to be taken and combined(Pic 4, Pic 5). This new method reduced the amount of light scattering and made the pictures more accurate. It also, however, made it much more time consuming to take the pictures of a full spray. For every one picture taken previously thirty to fifty now have to be taken, this method is still much less time consuming than the test tubes though, and was used.

Combining the pictures was done through a program created using FORTRAN. The rows of pictures are placed one on top of the other. Because of one pixel equaling just under one millimeter(the distance between pictures) the pictures of combined pixels are not to exact scale.

The first problem encountered after starting one pixel wide pictures was a reversal of peaks in the spray. When the laser was coming from the left the peak intensity would be on the right. When coming from the right, the right side would be extremely intense. The factor causing this was narrowed down to either the camera, the filter, or the spray nozzle.

The fluorescent filter was the first to be tested. The intensities remained on the wrong sides. After taking out the filter. Several other filters were also tried with the same results. The fluorescent filter was not the cause of the distorted pictures.

The nozzle to the spray was then taken off and cleaned. The pictures continued to be distorted. It was then taken off and looked at under a low powered microscope. Several large scratches and marks were found on the nozzle. The pictures returned to their expected

intensities after replacing it.

Just a few days later the same problem occurred once again. The nozzle was the first object looked at. Once again the nozzle developed scratches from an unknown source. Two filters were used(2 microns, 400 microns) to cleanse the water before it was put through the nozzle. Another assumed source of the problem was also taken out, this was how the nozzle was cleansed. To clean the nozzle, approximately once each day, it was put in a glass beaker and run through a sonic cleaner. It is believed that the glass beaker may have scratched the nozzle, it is now only put in plastic containers to be washed. Since the incident the spray has remained relatively symmetric.

As a result of the filters the pressure decreased to the nozzle disrupting the spray yet again. The 2 micron filter was taken out and the pressure was returned to normal. Throughout the day as the filter clogged the pressure slowly decreased, lowering the intensities on all pictures taken. The 2 micron filter was taken out leaving only the 400 micron filter to clean the water, this has not had any noticeable effect on the spray.

The next problem was the result of the laser. Its intensity ,for an unknown reason, decreased throughout the day. The intensity started at approximately .270 watts and decreased to approximately .250. The effect on pictures was minimal at best. It did not create any noticeable change in the pictures or the intensities within the pictures.

The laser was also the cause of another problem. After noticing that, on the pictures, the beam seemed to be heading not right through the middle but at an angle. This caused the pictures to appear lopsided. This was overcome by straightening the beam with the mirrors directing it. The laser from the left and the right, however, are not going through the exact same spot. This was taken care of by taking pictures at separate center pixels. The right was taken at the pixel 190 versus the left which was taken at 193. The completed sheets look correct.

After eliminating all noticeable problems with the method of taking the pictures, full

scans were taken. This involved taking 30 scans, from the left and right containing 30 to 50 pictures each, varying distances from the nozzle. The number of pictures in each scan differed depending on the width of the spray at the particular height of the scan. Each scan of pictures was then combined, resulting in thirty pictures of full sheets.

References

Talley, D.G., Verdieck, J.F., Lee, S.W., McDonell, V.G., and Samuelsen, G.S.

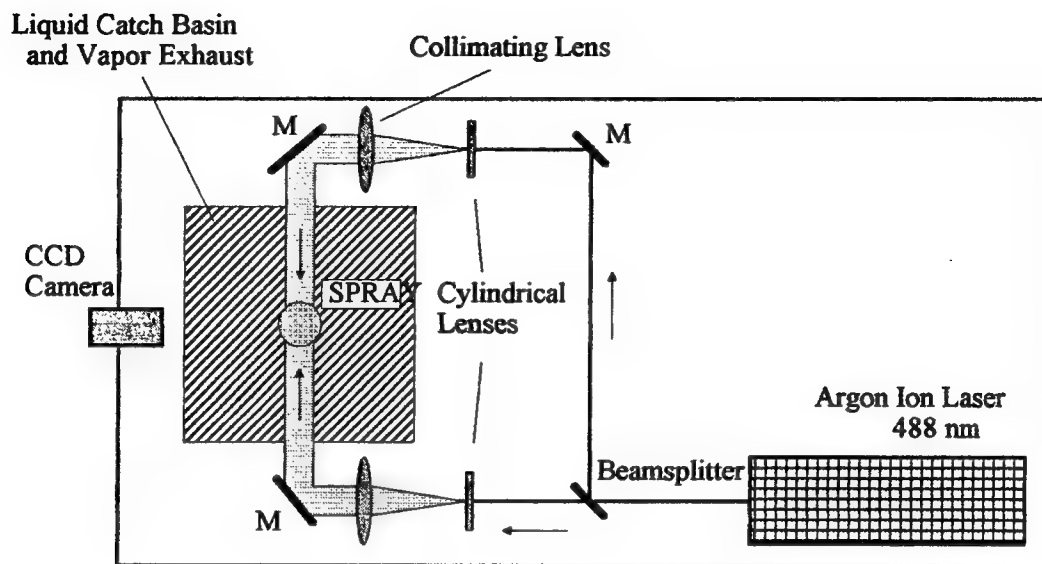
"Accounting for Laser Sheet Extinction in Applying PLLIF to Sprays"

Verdieck, J.F. "Experimental Investigation of Atomization and Droplet Processes at High

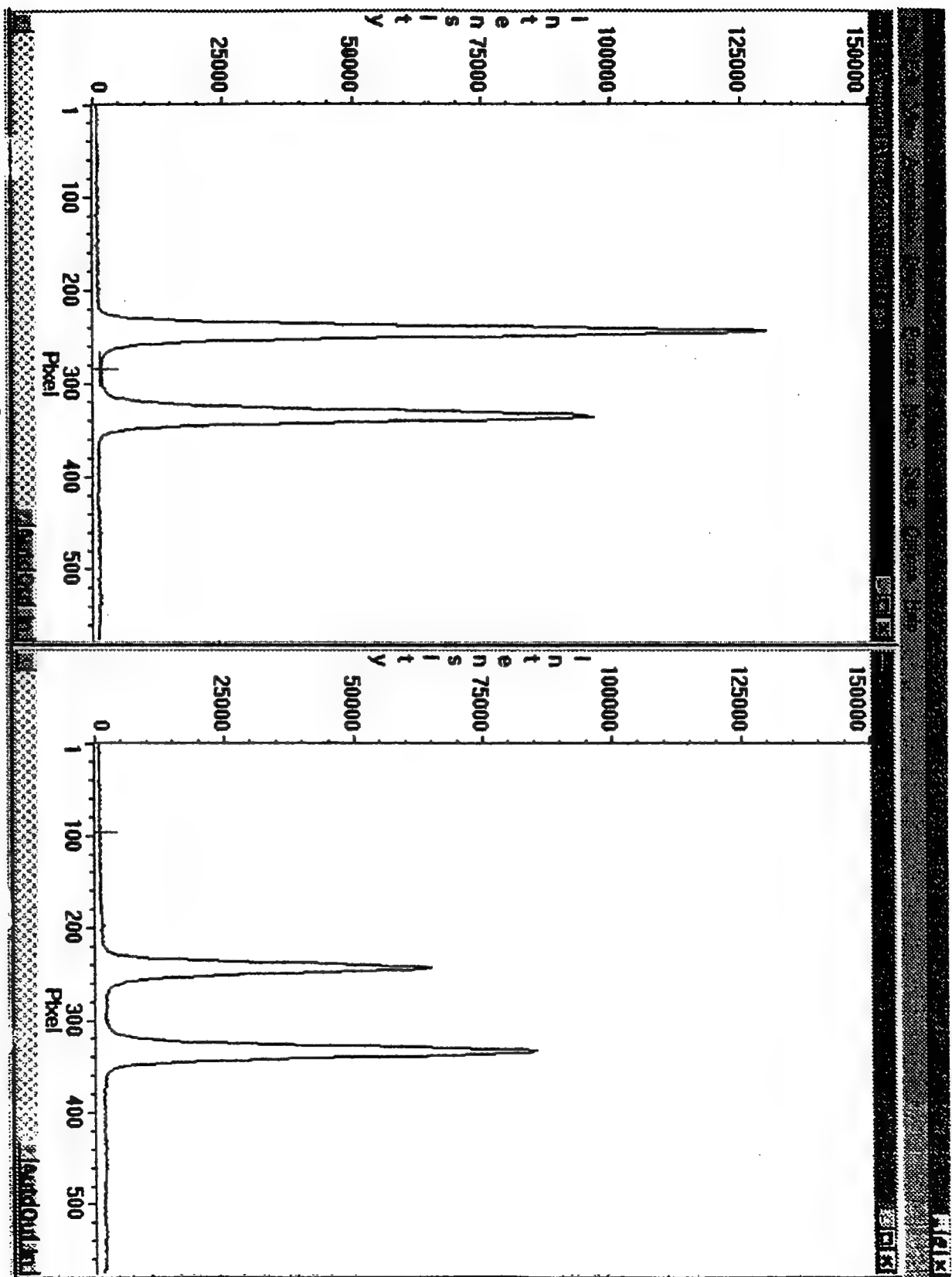
Pressures"

PICTURE #1

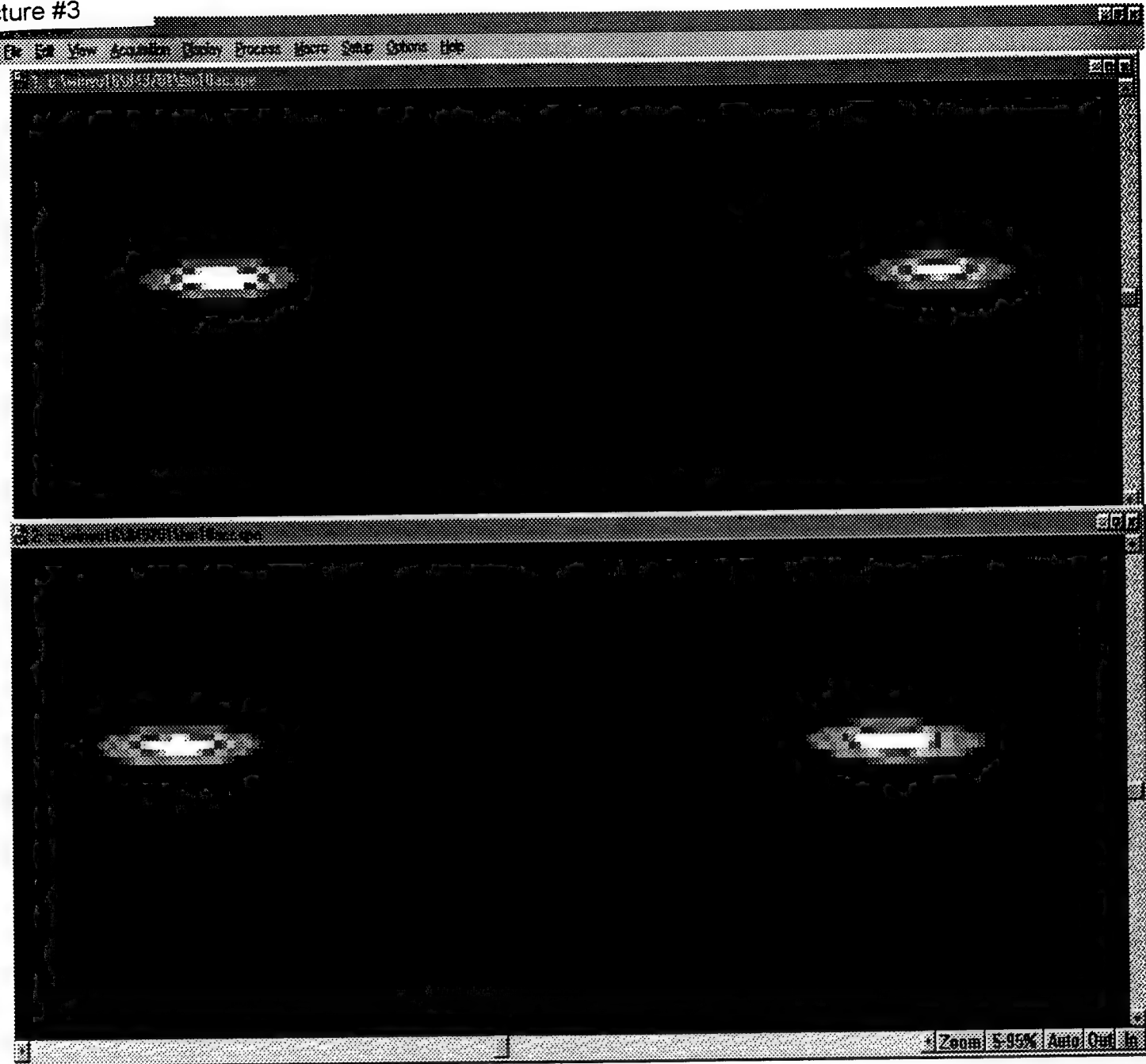
TWO LASER SHEET DIAGNOSTIC for CORRECTION
of EXTINCTION in DENSE SPRAYS : TOP VIEW



Picture #2

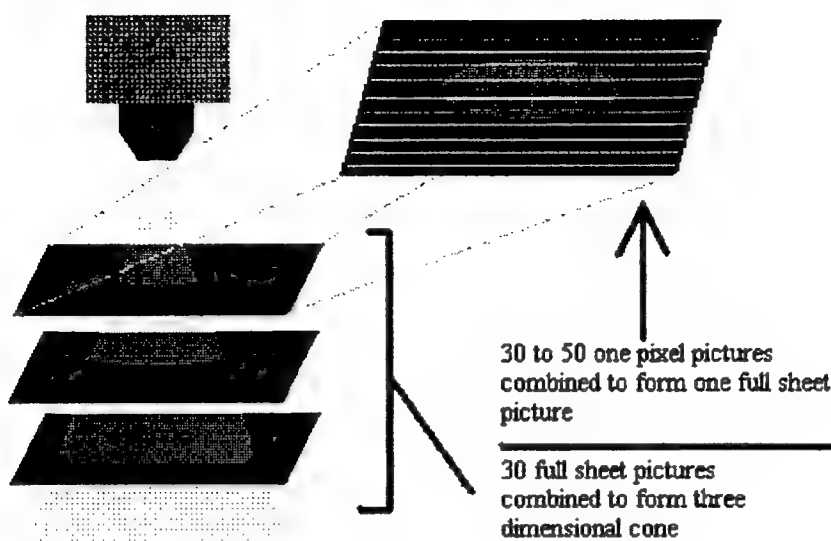


Picture #3



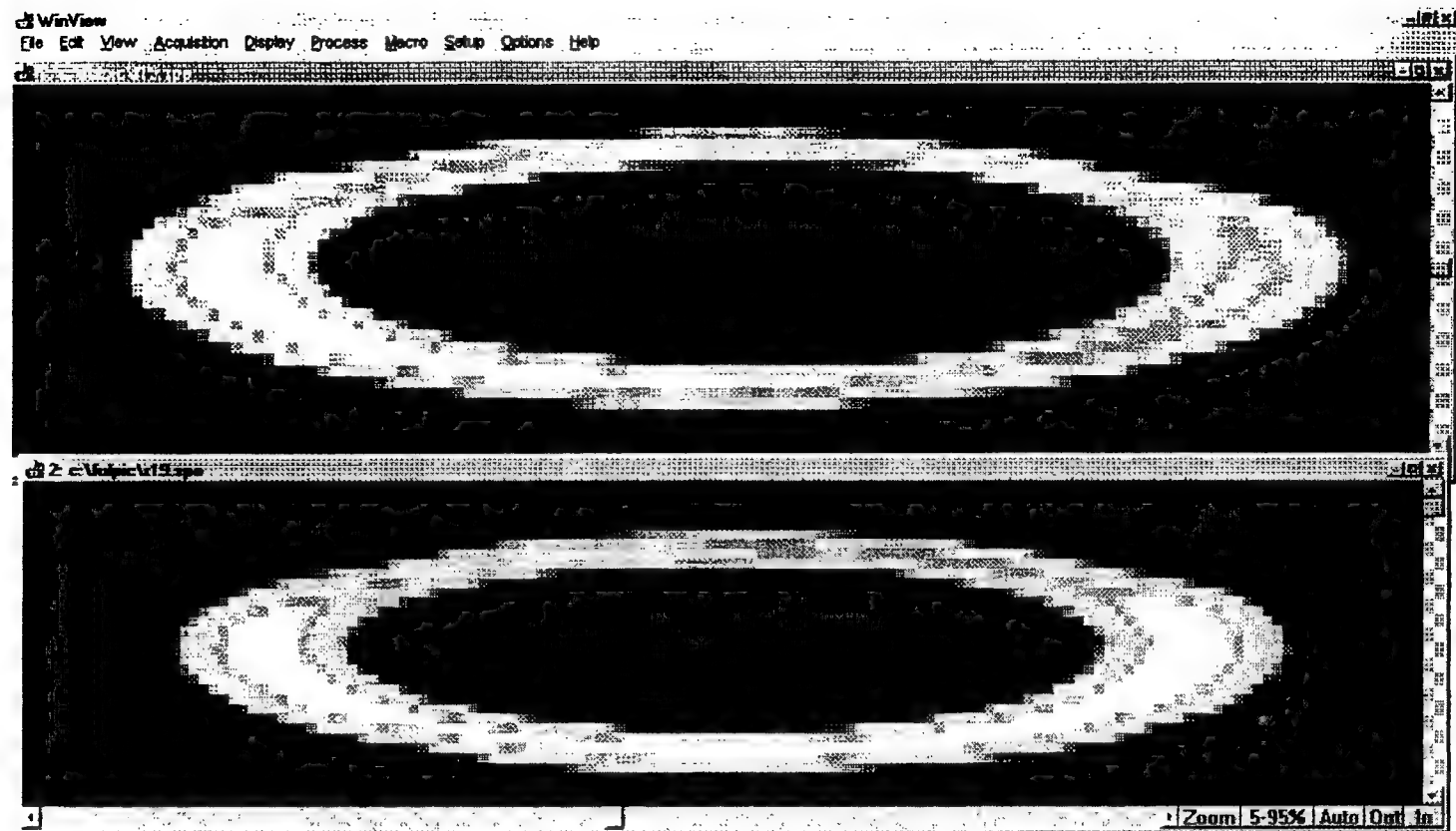
PICTURE #4

METHOD OFF CREATING FULL SHEET PICTURES



PICTURE #5

PICTURES CREATED BY COMBINING PICTURES 1MM WIDE FROM LEFT(TOP) AND RIGHT(BOTTOM)



A STUDY OF
SPACE STRUCTURE'S
ISOLATION

Fawn R. Miller

Manzano High School
12200 Lomas Blvd. NE
Albuquerque, NM 87112

Final Report for :
High School Apprentice Program
Phillips Laboratory

Sponsored by:
Air Force Office of Scientific Research
Kirtland Air Force Base, NM

and

Phillips Laboratory

July 1997

A STUDY OF
SPACE STRUCTURE'S
ISOLATION

Fawn R. Miller

Manzano High School

Abstract

Tests on the Taurus-2 mass-payload for the GFO Mission were completed. The tests utilized a 45,000 lb. shaker to provide controlled base motion. The first test was run without any isolation techniques, and then isolators designed by CSA Engineering were installed, and the test was run again. The isolators damp the satellite vibration during launch. These tests were performed to demonstrate the system performance under launch-like conditions.

A STUDY OF
SPACE STRUCTURE'S
ISOLATION

Fawn R. Miller

Introduction

As long as space craft have been in existence, their structures had to be tested to determine whether the materials were strong enough to withstand take-off conditions. When a rocket carrying a space vehicle takes off for space, high loads can damage such lightweight and delicate structures. Space vehicles and rockets have to be strong enough to withstand all these forces. These space craft cost thousands, even millions of dollars; thus, the companies that built them, don't want them to fall apart before they leave the earth. Long before a space craft even arrives at the launch pad, many tests are run on it to see if it can survive in this highly-strenuous launch situation. This summer's research was dedicated to the testing of one of these space structures; the Taurus-2 / GFO Mission satellite.

Methodology

This unique testing process required many preparatory steps for the protection of the satellite. The equipment required the use of a class 100,000 Clean-Room, so the satellite had to be handled carefully; more specifically, with protective gloves and clothing. The structure was moved with slow movements on a large crane. Since this equipment is very valuable, any drop could have resulted in thousands or more dollars in repairs or even a termination of the project.

A mass simulator was fabricated for this system-level isolation system test series, due to the highly abrasive program schedule. When the test article arrived in our High-bay,

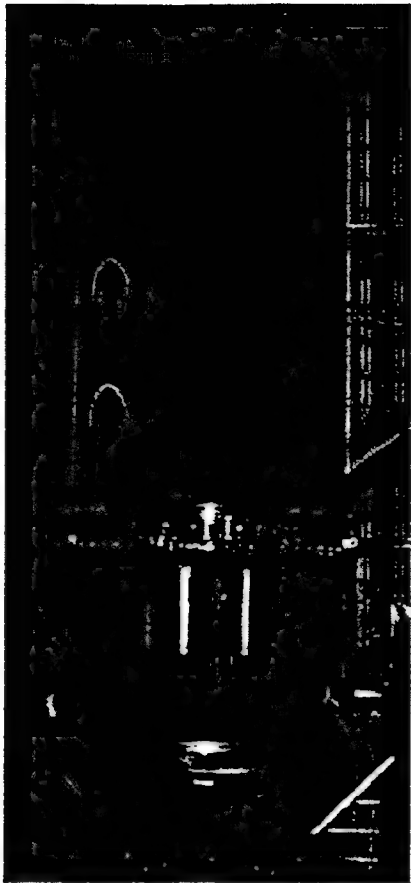


(Fig. 1) The Taurus-2 / GFO Mission test setup.

the 900 lb. structure was removed from the large shipping crate, and placed on padded blocks, so the setup process could begin. Twenty-two accelerometers were placed around the structure to test its movement at specific spots. These accelerometers measured the structure's acceleration along the X, Y, and Z directions. Each of the accelerometers had one corresponding cable that lead to a signal analyzer and shaker controller, which then measured the linear movement of each area.

The structure was placed on an adapter plate, which was in turn attached to the shaker table. When all this was performed, the accelerometer cables had to be attached and taped down so the moving cables did not create noise during the tests.

The structure consisted of an 800 lb. mass simulator of the actual payload, a separation ring, used to disconnect the satellite from the launch vehicle, and an avionics structure that was created from composite material. This complete structure was shaken in a thrust axis (vertical direction) and in a lateral direction, both unisolated. Then after the isolators were attached, the same thrust axis and the lateral directions were tested on the shaker table.

Results

When the structure was completely assembled for the unisolated tests, a low level sine test was run on the structure at 10 to 80 Hz, at 0.1g, for 0.2 Hz/second sweep. Then a random test using low level random input at 5 to 300 Hz, at 0.5g was run. These same tests were run for the lateral configuration, and then again for the thrust axial and lateral isolated tests at a higher level.

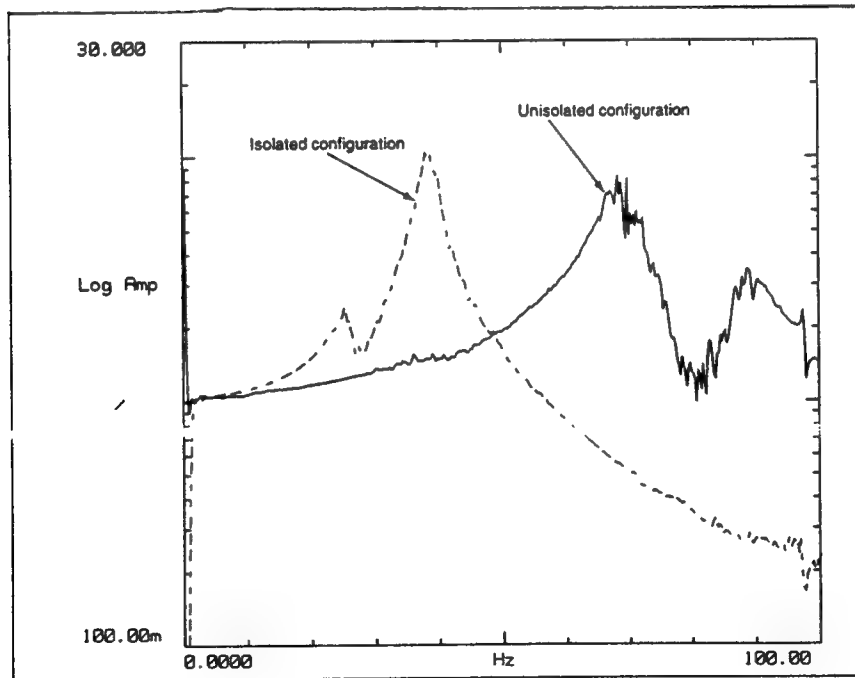


(Fig. 2) This shows how effective the isolators were when compared to the unisolated configuration at 0 to 100 Hz.

The isolators used for these tests worked well. The isolators showed a 5% in the axial (plunge) direction. The isolators created a reduction in the vibration from the whole structure, thus creating a safer environment for the satellite and its payload. When the isolators were attached, the structure was shaken harder, and the payload's movement was significantly less than when it was not isolated. Figure 3 shows measured acceleration transmissibility functions from thrust-axis tests, in both unisolated and isolated configurations. The isolators create a plunge mode at 38 Hz., producing isolation above 50 Hz. The unisolated resonance near 70 Hz. would cause damage to the satellite, as indicated by the composite models. The response in this frequency range is reduced by a factor of 26 dB.

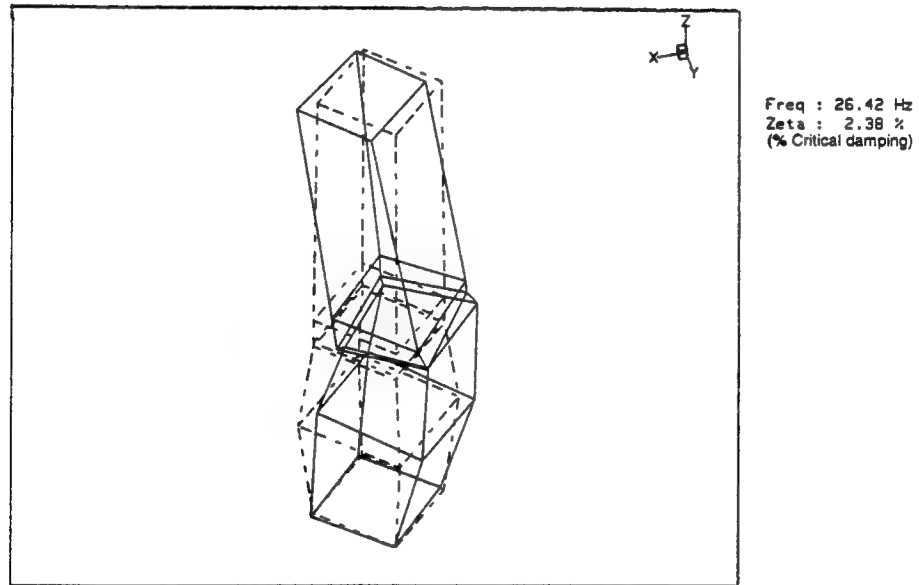


(Fig. 3) The mode bending in the X direction at 26 Hz.

The dotted line is the undeformed geometry; the solid line depicts the test article characteristic shape when mounted on the shaker expander head. A mode shape is the characteristic response of a structure at a particular resonant frequency. This bonding mode is of interest to the launch vehicle contractor, as it determines the amount of so-called rattle

space required around the satellite to accommodate its motion.

Conclusion

There are many satellites that are launched and are destroyed because they do not have any isolation system. These tests of the Taurus-2 / GFO satellite have shown that the isolation system will damp the payload a significant amount, thereby protecting the satellite from high launch loads.

Through the AFOSR Research Program, I gained hands on experience and learned valuable information on a product that may excel in protection of future spacecraft during their launches. Also to those who helped me out during this tour, a special thanks to these PL/VTV Employees and Contractors. Mainly: Jim Gooodding, Rory Ninneman, and Dino Sciulli.

References

Ewins, D. J.; Modal Testing: Theory and Practice. Research Studies Press LTD., Letchworth, Hertfordshire, England; 1984.

Netscape Technology Pages: Vibration Isolation, Accelerometers, Signal Analyzers, and CSA Engineering

A STUDY OF THE EFFECT OF FUEL SULFUR CONTENT
ON THE PRODUCTION OF AEROSOLS IN AIRCRAFT EXHAUST PLUMES

Amy W. Mok

Newton North High School
360 Lowell Avenue
Newtonville, MA 02160

Final Report for:
High School Apprentice Program
Phillips Laboratory

Sponsored by:
Air Force Office of Scientific Research
Hanscom Air Force Base, Massachusetts

and

Phillips Laboratory

August 1997

A STUDY OF THE EFFECT OF FUEL SULFUR CONTENT
ON THE PRODUCTION OF AIRCRAFT EXHAUST PLUMES

Amy W. Mok
Newton North High School

Abstract

In an attempt to discover the effect of fuel sulfur content on the production of contrail, several flights were conducted in which F-16 aircraft burned different types of sulfur fuels. A T39 collected and studied samples of the contrail and separated the sample with use of a mass spectrometer. This instrument revealed what was contained in the sample and how much of each was present. The results indicated that amounts of each of the masses did change due to the variation of the fuel sulfur content. More in-depth studies were necessary to prove and explain the differences.

A STUDY OF THE EFFECT OF FUEL SULFUR CONTENT ON THE PRODUCTION OF AIRCRAFT EXHAUST PLUMES

Amy W. Mok

Introduction

Two groups have recently been interested in the type of fuel being burned by their aircraft. Each of the groups had its own intention. One of the groups, the Air Force, was interested in learning how the contrail produced by its aircraft could be predicted. In doing so, at times of war, the nation's aircraft would be less visible to enemy fire and be in less danger. The second group, National Aeronautics and Space Administration, NASA, was interested in the atmospheric chemistry portion of this research. NASA believed that contrail affected cloud formation and therefore caused alterations in weather. It wanted to know if fuels of varying sulfur content would have different effects on the troposphere and stratosphere. In both cases, the purpose was to find the type of fuel that would benefit both security and environmental impact of the aircraft.

Methodology

In a span of three days, several scientists from the Hanscom Air Force Base in Massachusetts along with several others conducted a total of six flights. The scientists flew inside of a T39 while chasing F-16 aircraft. On each of the three days the F-16 being chased would burn a different type of sulfur fuel. Each type of fuel was tested twice; once at an altitude of 30,000 feet and once at 35,000 feet. The T39 collected samples of the contrail left behind by the F-16 through a flow tube that was connected to a mass spectrometer set up inside of the T39. The mass spectrometer, operated by the occupants of the T39, separated the sample and showed what the contents of the sample were by indicating each of the contents' mass and quantity on a graph. All data collected were stored in a program on the computer which was also linked to the mass spectrometer. The purpose of this experiment was to see if fuel sulfur content had an effect on contrail production. To answer this question, it was necessary to analyze all the collected data on the computer with the assistance of a program created by the scientists and a graphing program called AXUM. The computer program was designed by the scientists particularly for data analysis of this experiment. AXUM is a "technical graphics and data analysis package" produced by Trimetrix for Windows.

Collecting Samples and Data

Three special sulfur fuels were tested in addition to a control, or regular, fuel. On the first day, a flight with high sulfur fuel was conducted at an altitude of 30,000 feet. A flight with high sulfur fuel at 35,000 feet was also done that same day. On the second day, two more flights were done at the same two altitudes except this time with medium sulfur fuel. The third day was committed to low sulfur fuel.

Regular fuel was tested during all six flights for comparison to the special fuel results.

During each flight an F-16 aircraft would burn a special fuel and produce an exhaust plume. Scientists in a T39 along with a mass spectrometer, computer, and a flow tube would follow chasing after the F16 to collect samples of the exhaust plume for studying. Several samples were collected for each special fuel. After collecting an adequate number of samples the T39 would chase another F-16 which burned the regular fuel. More samples were collected from this aircraft. The mass spectrometer separated each sample into its different ions. The ions were represented by only their mass and a count of each was calculated. All data including the exact hour and minute of the day during which flight occurred was transferred to and stored inside the computer while the T39 was still in flight. The program in the computer performed many useful tasks. Mainly, it graphed the amount of each mass present throughout the flight against the actual time of the flight. The program also averaged counts during specified blocks of time, "block average", showed amounts of SO₂ and CO₂, displayed with markers periods where a calibration occurred , and many other helpful skills. All these features assisted with the study of the data.

The Analysis

While the T39 was chasing F-16s and the computer was busy storing data, the scientists were busy recording time and events by hand. Their logs included times when calibrations occurred, plume crossings, altitude of aircraft, power settings of the machines, flow rates, and other significant details of the flight. The first step of my analysis of the data was to compare the information on the computer with that of the written logs. Did the times match? After all, the written logs were based on times from a wrist watch. Did the graphs which the computer program produced agree with what was happening during the flight at the same times? In order to make the graphs more comprehensible, I printed them out and wrote the details of the events were written directly on the graphs. Comparison was repeated for all six flights. This process was to ensure the validity and accuracy of both sets of data.

During one of the flights, an extensive calibration experiment was done. This experiment was to test how much of each of five masses (60, 78, 96, 112, 114) were present in the emission when the SO₂ flow dial setting was varied. These five masses were chosen because they were presumed to be products of the

burning of the sulfur fuel used. There was a total of twelve settings: 50, 100, 150, 200, 300, 400, 500, 600, 700, 800, 900 & 1000. Viewing the graph of this calibration on the computer program indicated a fluctuation in the amounts of the five masses present with the varying settings. To find out exactly how they were changing, block averages were done on the five masses for each of the dial settings. The counts obtained for each mass and flow were recorded for later entry into AXUM. Counts for each mass were entered on to an AXUM data sheet along with their respective flow settings. AXUM then produced a graph of count versus SO₂ flow for all five masses. The only one of the five curves that appeared to be a straight line was that for mass 112. Another graph devoted just to mass 112 was made and indeed proved to be a straight line. This result meant that mass 112 increased consistently with the increase of SO₂. This conclusion was believed to be correct for mass 112 represented SO₅⁻ which is produced from the reaction of SO₂. The other four masses did not have consistent trends in their counts which may mean that with different SO₂ flows different reactions involving the masses are occurring. These reactions may be the cause of the varying amounts of the other four masses. Depending on which reactions took place at which settings, the amount of a certain mass present could increase or decrease.

An exact simulation of this comprehensive calibration experiment was performed in the laboratory on base. The same twelve SO₂ flow dial settings were used and block averages were done again on the computer program. Once again, a graph of count versus SO₂ flow indicated an expected straight line with mass 112. The data from flight and from the laboratory were agreed with each other which assured that the data obtained on flight was legitimate for use to make conclusions.

In addition to the extended calibration, short ones were also dispersed throughout the flights. At many times the valves of SO₂ and HNO₃ were turned on and then shut off after a minute or two ending the calibration. The valve for the SO₂ was turned on to a certain flow setting each time and the setting was recorded on the logs. Block averages were performed again for each calibration of the six flights. After average counts for the five masses were obtained, they were entered on to an AXUM data sheet. A graph of mass count versus SO₂ flow was produced to check whether the mass counts were consistent for each flow during all flights. In other words, all the counts for mass 112 should be the same for a dial setting of 600. More or less, the data was reasonably close to one another.

The following step in the study involved the use of newly obtained data. The new data consisted of the time of flight given in seconds and the concentration of CO₂ in parts per million (ppm). This new data will be described as "SN data" while the former data already in the computer program will be called "Jems data." Unlike the SN data, Jems data had the time given in hours and minutes and the CO₂ in counts.

For the SN data to be of any use the Jems data was converted to the same units as the SN data.

Converting hours & minutes to seconds was a fairly simple process, but, as for the CO₂, the conversion required a longer process. First, the SN data was imported to an AXUM data sheet and a graph was made of CO₂ ppm versus time in seconds. This graph was then used to compare with the Jems data for conversion. The AXUM graph was matched with the similar shape of the Jems graph from the scientists' computer program by locating the peaks of the curve. In the computer program values of the count at the peaks were found. These values were then compared with the values in ppm in the SN data that were recorded at the same time. At this point, CO₂ counts were matched with CO₂ concentration. By using AXUM again, a graph of CO₂ (ppm) to CO₂ (counts) was produced and an equation was obtained to convert one to the other. The equations for the six flights were, more or less, identical which was what was looked for. These equations were recorded for later use.

The next step in the analysis was very important. This was when SO₂ concentration was compared with CO₂ concentration. The scientists were especially interested in knowing the ratio of the concentration of these two products in determining the effect of different fuel sulfur contents. To start, calibrations (SO₂ valve is turned on so count is up) where plume crossings (CO₂ is up) were nearby in time were chosen for analysis. Details of each of these calibrations had to be found including start and end time of calibration, and mass 112 count during and just before/after the calibration. This information was then entered into the program to change the graph's units for SO₂ from counts to concentration. The graph then displayed the counts of CO₂ and the concentration of SO₂ versus time. By matching the two graphs for the same times pairs of SO₂ (ppb) and CO₂ (counts) were found. This newly recorded data was entered into AXUM and along with the equation that converted counts of CO₂ to concentration found earlier produced matching sets of SO₂ (ppb) and CO₂ (ppm). Graphs of SO₂ versus CO₂ concentration were then made; all of which produced lines. The ratio of SO₂ to CO₂ was found by calculating the slope of these lines through regression. The slopes represented the ratio of SO₂ to CO₂ present in the emission for the type of fuel used. It was found that with the higher sulfur content the slopes were greater. The slopes for the regular fuel lay between the values for medium sulfur fuel and low sulfur fuel. What this trend meant was that with more sulfur in the fuel the amount of SO₂ produced compared with the amount of CO₂ produced becomes greater. In other words, with more sulfur in the fuel, either SO₂ production increased or CO₂ production decreased or both. The slopes were also compared with the different altitudes and power. However, there wasn't enough information on these two factors to make any legitimate conclusions. All that could be deduced was a general trend of higher slopes with increasing altitude and power.

The research continued with a detailed analysis of every calibration in all six flights. Counts for the masses were found once again during and before/after the calibration. SO₂ flow dial settings were once again noted and entered with the counts for the computer program to produce a list of new information. The list included values for the absolute pressure, differential pressure, flow tube temperature, flow tube velocity, tube flow, SO₂ flow (sccm), SO₂ concentration, and the SO₂ calibration factor. Earlier in the analysis, the mass 112 was noticed to not have been constant throughout a calibration. With the new list of information, a search for trends was started by comparing graphs of each of the new factors versus time. After a long examination of the numerous graphs, several conjectures were made on why mass 112 counts were changing as they were. It seemed that mass 112 counts either increased or stayed steady throughout the calibration. The only decreases were very slight. After studying the graphs for the calibrations whose mass 112 counts increased with time, it appeared that some factors may be pressure, SO₂ concentration and tube flow. The calibrations with increases seem to have displayed high pressure with high velocity, low SO₂ concentration and high tube flow. As for the ones with somewhat steady mass 112 counts, low velocity with either high or low pressure, high concentration of SO₂ and low tube flow seemed to be the deciding factors. These results are assumed to only be conjectures because they weren't what was expected and the graphs were also not always accurate.

Further analysis was done concerning this experiment. Unfortunately, at the time of my departure from the program, there was more data which needed to be investigated in the computer. The scientists at Hanscom Air Force Base continued with the research and will hopefully discover new useful information in the near future which will benefit the Air Force, NASA and many other people in the world.

**THE SEPARATIONS AND REACTIONS OF
CYCLOHEXYL POSS COMPOUNDS**

Martin Morales

**Palmdale High School
2137 E. Ave. R
Palmdale, CA 93550**

**Final Report for:
High School Apprentice Program
Phillips Laboratory**

**Sponsored by:
Air Force Office of Scientific Research
Bolling Air Force Base, DC**

and

Edwards Air Force Base, CA

August 1997

THE SEPARATIONS AND REACTIONS OF CYCLOHEXYL POSS COMPOUNDS

Martin Morales
Palmdale High School

Abstract

Cyclohexyl POSS compounds are very useful in polymer chemistry. The collection and separation are vital steps taken in order to apply these compounds to rocket propulsion systems. The collection of cyclohexyl Poss compounds is long and tedious. The separation requires large amounts of solvent. Therefore, new methods for decreasing the amount of starting material were studied. Once isolated, functionality was added to them through corner capping reactions.

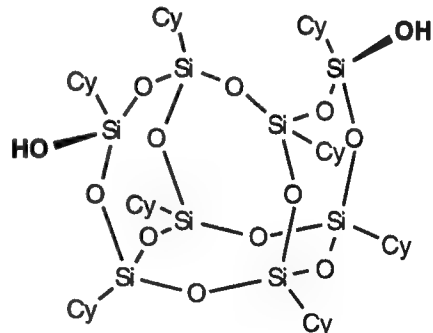
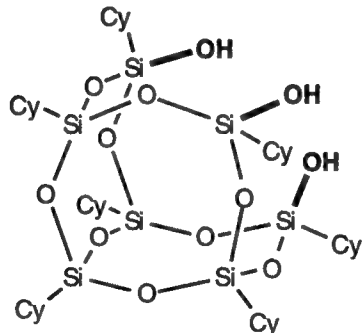
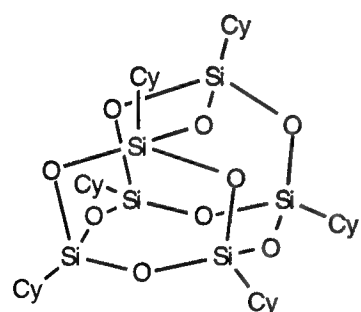
SEPARATIONS AND REACTIONS OF CYCLOHEXYL POSS COMPOUNDS

Martin Morales

Polyhedral oligomeric silsesquioxane (POSS) compounds are unique in composition. They are polyhedral caged compounds made up of oligomers of silsesquioxanes ($\text{RSiO}_{1.5}$). The composition of a POSS unit is intermediate between the mineral silica (SiO_2) and silicones (R_2SiO). Thus, they bridge the property space between sand and silicones. These POSS structures are building blocks to present and future applications as polymeric units for aircraft and rocket propulsion systems.

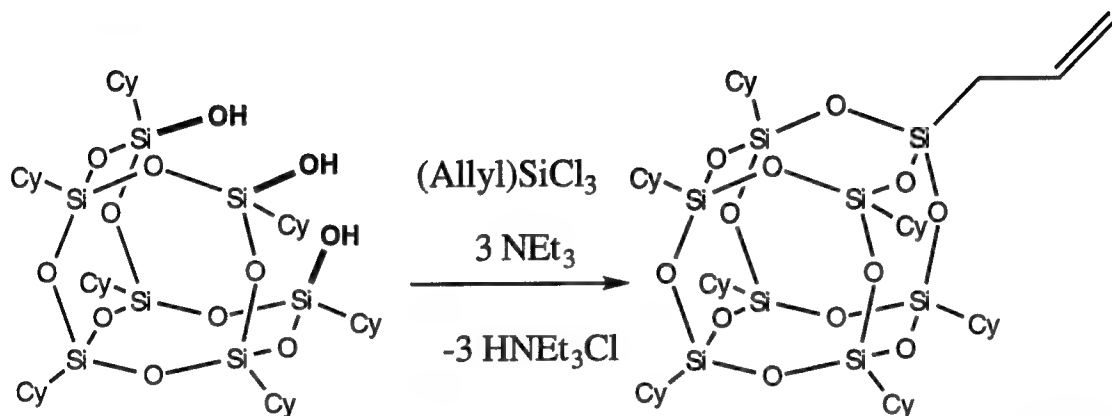
POSS building blocks can be used for numerous purposes. They can be chemically or physically incorporated into polymers, or used alone in applications ranging from catalyst support to medical agents. Their unique 3-D structures and tailororable chemical composition provide novel chemical starting materials for many useful polymeric compounds.

One promising class of POSS compounds is made from the hydrolysis of cyclohexyltrichlorosilane. Their synthesis yields a mixture of products with the following structures:



These compounds must be isolated and separated for further use.

A fundamental application of the T₇ compound is that of corner capping this triol with silane coupling agents to create a fully condensed POSS system. In one case, T₇, or triol, is reacted with allyl trichlorosilane in anhydrous THF, to yield a fully caged POSS allyl.



POSS structures are produced through a hydrolysis reaction consisting of 12L of Acetone, 3.2L DDI H₂O, and 650g CySiCl₃. The solution is placed in a five gallon carboy, stoppered, and set aside for an extended amount of time. Periodically, these carboys are harvested by filtration to collect the precipitated products and washing with acetone to remove resinous by-products. It is at this stage where the separation is done. For results from the third harvest see Appendix A.

The synthesis and separation of the POSS structures was first performed in 1960 by John Brown and Lester Vogt, Jr¹. Cyclohexyl T₆ was separated by either fractional crystallization from acetone or by extraction of the triol with cold pyridine. The T₇ was separated from the T₆ by fractional crystallization or extraction with pyridine and recrystallized from benzene-acetone. At that time, Cyclohexyl T₈ was undetected.

A similar method of separation was used by Feher². Feher isolated T₆ by stirring

the crude mixture in 5 times its weight with pyridine, and filtering the insoluble material from chloroform. The pyridine solution of T₇ and T₈ was crashed into aqueous HCl and washed thoroughly with water. T₇ and T₈ were then separated by a series of ether and chloroform fractional crystallization.

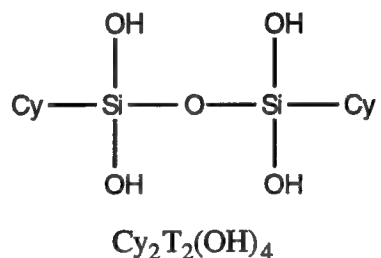
At Phillips Lab, the separation of T₆, T₇, and T₈ was once exclusively performed via the prep-HPLC method. However, this method consumes large amounts of solvent. Therefore, recrystallization of crude cyclohexyl POSS in hexane is done, removing forty percent of the starting material. This method crystallizes the T₇, while the T₆ and T₈ are left in solution. The solution, or mother liquor, is rotovapped and the material is collected. The prep-HPLC system then separates the remaining T₆, T₇, and T₈. In order to further decrease the amount of starting material, triethylamine washings are performed. This method is similar to the pyridine washings of Feher although the removal of T₆ is not quantitative.

The total collection from the third harvest of the hydrolysis reaction was 332g. This total is quite low in comparison to previous harvests. This crude material along with other crude was recrystallized in the hexane solution. In five separate crystallizations, 348g of material was produced. Of that, 291g was usable T₇ material. The remaining 57g contained all three structures. The mother liquor also contained all three structures. Further recrystallizations of this remaining material proved to be ineffective as pure T₇ was never collected.

Additional work is yet to be done for optimizing the separation of these compounds. It appears as though the recrystallization and triethylamine washings are a useful first step to the ultimate separation using preparative HPLC.

Another reaction performed involved the T₂ compound. This reaction was setup

similar to the hydrolysis of the previous three POSS compounds, only the ratio of water to acetone was different. A reactor was placed in an ice water bath. 1.2l of water was stirred in the reactor. 100ml of acetone and 32ml of cyclohexyltrichlorosilane was slowly added to the stirring water. The length of the reaction is about four days. At that time, the work-up requires filtration and acetone washing. Theoretically, 15.3g is expected, however, given the impurities, yields were well below average. The following is a picture of the T₂ compound:



In terms of the future, one consideration may be to research the triethylamine washes and its advantages. Alone, it separates a large amount of T₆, while leaving behind only small amounts of T₇ and T₈. In combination with another solvent, it could be possible to completely isolate the T₆. It also may be possible to do this by optimizing the amount of triethylamine in the washing procedure.

REFERENCES

1. J. Brown, Jr., L. Vogt, Jr., *Polycondensation of Cyclohexylsilanetriol*, 1965
2. F. J. Feher, D. A. Newman, J. F. Walzer, *Journal of American Society*, 1989, 1747

APPENDIX A
CYCLOHEXYLTRICHLOROSILANE HYDROLYSIS DATA

	Carboys	2nd Harvest			3rd Harvest			Amt	
		T6	T7	T8	T6	T7	T8	2nd	3rd
1	normal setup 650g CysiCl3 12l tech acetone 3.2l DDI water	3%	93%	3%	14%	35%	20%		46g
2	normal setup	1%	93%	6%	12%	39%	26%		23g
3	normal setup	2%	90%	8% 18%	35%	24%		23g	
4	normal setup	1%	91%	8%	16%	8%	47%		19g
5	normal setup	<1%	87%	8%	17%	4%	52%		13g
6	normal setup	<1%	86%	13%	15%	5%	39%		23g
7	normal setup	<1%	99%	1%	15%	8%	34%		11g
8	normal setup	<1%	97%	3%	13%	8%	45%		11g

9	normal setup	2%	92%	7%	20%	12%	44%		7g
10	650g CySiCl3 12l tech acetone 3.2l DDI water added in reverse fashion	21%	77%	2%	8%	46%	16%	210g	20g
11	650g CySiCl3 12l acetone 3.2l DDI water CySiCl3 was added last	20%	76%	4%	12%	57%	12%	140g	38g
12	same setup as #11	13%	80%	7%	12%	54%	21%	158g	49g
13	650g CySiCl3 118g Na Cl 12l acetone 3.2l DI water	17%	75%	8%	10%	42%	26%	250g	8g
14	650g CySiCl3 210g NaBr 12l acetone 3.2l DI water	22%	74%	4%	22%	48%	17%	210g	3g
15	650g CySiCl3 12l acetone 3.2l Tap water	23%	71%	6%	14%	62%	15%	230g	18g
16	650g CySiCl3 (clear) 12l acetone 3.2l DI water	16%	81%	3%	14%	41%	26%		1g
17	normal setup	16%	82%	2%	17%	53%	17%		5g
18	same setup as #16	13%	77%	10%	23%	53%	19%		2g

19	16%	79%	5%	13%	54%	19%	250g	10g
	650g CySiCl3 and trace acetone							
	12l acetone							
	3.2l DI water							
20	17%	79%	4%	13%	33%	35%		2g
	same setup as #16							
21				22%	39%	21%		2g
	650g CySiCl3							
	15l black liquid from carboys #4 and #10							
	5.5ml DDI water							

**INTRANET WEB PAGE,
DESIGN AND DEVELOPMENT**

David D. Parker

**Boron High School
26831 Prospect St.
Boron, CA 93516**

**Final Report for:
High School Apprentice Program
Phillips Laboratory**

**Sponsored by:
Air Force Office of Scientific Research
Bolling Air Force Base, DC**

and

Phillips Laboratory

July 1997

INTRANET WEB PAGE, DESIGN AND DEVELOPMENT

**David D. Parker
Boron High School**

Abstract

We attempted to create an attractive Intranet Web Page for Phillips lab through the process of trial and error as we attempted to use different forms of web page creating techniques. In the past few years there has been a drastic increase in the use of the Internet. This increase of usage has resulted in many new uses that often times include household and business uses that normally would not be considered in everyday discussions. On the business aspect, there are ways to create an intricate web page system for a business that is only available to that business. Other businesses can also receive permission to access the system by the operating center. The use of this type of business owned Internet system is often times referred to as Intranets. With this new capability of using Intranets, a business is able to communicate and broadcast all forms of information to their employees via a network system. This ability makes it possible for the businesses to save money on costs that would normally originate from memos and other forms of communication that is now much less economically sound..

INTRANET WEB PAGE, DESIGN AND DEVELOPMENT

David D. Parker

Introduction

The methods of creating web pages have expanded to a much larger scale today, then what it was years ago. The original techniques of web page creators consisted strictly of HTML and the use of a typing program permitting the creators to design and save their web pages to their computer. In the recent years there has been many advances in the field of web page creation that has permitted the pages to be more and more interesting and fun to view. These advances consist mainly of Java, Javascript, and Web Page Editors. Although Web Authorizing Tools make use of HTML, the creator never has to look at the programming language if they do not want. Web Page Authorizing Tools permit the creator to cut and past objects into and out of the page making it much easier and quicker to create a web page. The main drawback of web page authorizing tools, is that they do not allow you to have as much control as what you do while using strictly HTML. Java and Javascript, although two completely different languages, are an enhancement to HTML. Through the use of these languages the creator is now able to insert many things into their pages that had only been a dream a few years back. With these languages the creator can insert movies, songs, film strips, colored buttons, and many more items that are too numerous to list. Now that all of these advancements have become available to the general public there has been a huge increase in private parties that have created and operate their own web page.

Methodology

When creating anything the first step is planning and Naturally it is the same when creating web pages. We had to first develop a basic design, format, and outline for the system that you are going to create. After we finished that crucial step we began the ever lasting process of information collecting. When we had finished collecting information you we began to edit through it and pick out the most important sections that we would insert into the pages. After we had finished this step we had the task of learning HTML and inserting the information into the document that we had already decided what the basic format would look like. When we had inserted all the information we began to make the document more pleasing to the viewer. This consisted of anything from graphics to different text styles and colors or back ground colors. At the time when we had created all of the necessary pages we got to the step in which we put them onto a remote server and inserted and tested the links. This process can often times be very time consuming or flat out confusing, depending on whether or not the pages are incorporated into the same file. After we had gone through and checked to make sure all links were working, we gave it one last look over to check and see if everything was working and looked good. Finally we uploaded the web pages to a server making it possible for the intended audiences to view the finished product (In our case we used a Macintosh OS 7.5, with the server program MacHTTP.).

Conclusions

Through the research and study that I completed during the term of my internship I was able to develop opinions about web pages and the methods used to create them. For example, when using a program for creating a web page, that does not make you use the HTML tags, the creator has very little control. This forces placement of items to often times look nothing like what they had originally hoped for the finished product to look like. A Tag is a short description enclosed by less than and greater than signs. The opening tag for example, (creating bold text), then after you finish typing what you would like bold you end the phrase with a closing tag, . On the other hand though, with the use of strictly HTML and Notepad (a program on all windows based PC's), the creator is able to create a more precise and extravagant web page. For instance, you cannot insert sound clips into a web page with a web page creating program. With the use of the HTML Embed Tag you can insert a sound clip (MIDI File), that has a graphic with an active stop, play, pause, and volume control. The only advantage that I could find for web page creating programs is that they have a built in program to upload the page to the Internet. They also allow you to change color without having to know the six digit codes for the color. Other than those two small items, using HTML is a much better and more time efficient way of creating dynamic web pages.

THAT WAS CREATED



Operational Support Division (RKD)

[BACK TO PLE MAIN PAGE](#)

Double Click Here to Hear Test Music

****RKD SUBDIVISIONS******RKDI**

Information Technology Branch (RKDI)

RKDL

Logistics Support Branch (RKDL)

RKDSSafety and Environmental Operations
Branch (RKDS)**RKDT**

Technical Services Branch (RKDT)

E-MAIL

Please e-mail us here!

Mission:

The mission of RKD is to provide support that enhances the completion of the Propulsion Directorate Mission in the areas of Safety, Health and Environmental quality, Logistics, Human services, Security and Information Technology.

[Click Here to View RKD Org.](#)

Chart



Page Maintained By RKDI
This Page Was Last Modified On July 25, 1997

WHAT THE WEB PAGE LOOKS LIKE BEHIND THE BROWSER WINDOW

```
<HTML>
<BODY BGCOLOR="#FFFFFF">
<HEAD>
  <META HTTP-EQUIV="Content-Type" CONTENT="text/html; charset=iso-8859-1">
  <META NAME="GENERATOR" CONTENT="Mozilla/4.01 [en] (Win95; I) [Netscape]"><!-- RKD DIVISION WEB PAGE-->
</HEAD>
<BODY>
<CENTER><IMG SRC="PL_LOGO.GIF" ALT="PLE logo" HSPACE="5" HEIGHT="40" WIDTH="40" ALIGN="CENTER">Operational Support Division (RKD)<IMG SRC="AFRL.GIF" ALT="AFRL logo" HSPACE="5" HEIGHT="40" WIDTH="40" ALIGN="CENTER"></CENTER>
<CENTER><TABLE BORDER WIDTH="100%" HEIGHT="5%" BGCOLOR="#80FF80">
<TR ALIGN="CENTER" VALIGN="TOP">
<TD ALIGN="CENTER" VALIGN="TOP" WIDTH="25%"><B><FONT SIZE="-2"><A HREF="http://ple.af.mil">BACK TO PLE MAIN PAGE</A></FONT></B></TD>
</TR>
</TABLE></CENTER>
<EMBED SRC="SMPUMP.MID" AUTOSTART=FALSE LOOP=FALSE WIDTH=145 HEIGHT=55 ALIGN="CENTER">Double Click Here to Hear Test Music</EMBED>
<CENTER><TABLE CELLPACING="0" CELLSPACING="0" WIDTH="100%">
<TR>
<TD>
<CENTER><!--LEFT COLUMN--></CENTER>
</TD>
<TD ALIGN="CENTER" VALIGN="TOP" WIDTH="24%" BGCOLOR="#FFFFFF">
<TABLE CELLSPADDING="0">
<TR><CENTER><B><FONT COLOR=#000000>**RKD SUBDIVISIONS**</FONT></B></CENTER></TR>
<TR><TD>
<CENTER><BR><FORM METHOD="LINK" ACTION="/RKDI/RKDI.HTM"><INPUT TYPE="SUBMIT" VALUE="RKDI"></CENTER>
</FORM><CENTER><FONT COLOR=#000000><FONT SIZE="-2">Information Technology Branch (RKDI)</FONT></CENTER></FONT>
</TD></TR><TR><TD>
<CENTER><FORM METHOD="LINK" ACTION="/RKD/RKDL.HTM"><INPUT TYPE="SUBMIT" VALUE="RKDL"></CENTER>
</FORM><CENTER><FONT COLOR=#000000><FONT SIZE="-2">Logistics Support Branch (RKDL)</FONT></CENTER></FONT>
</TD></TR><TR><TD>
<CENTER><FORM METHOD="LINK" ACTION="/RKDS/RKDS.HTM"><INPUT TYPE="SUBMIT" VALUE="RKDS"></CENTER>
</FORM><CENTER><FONT COLOR=#000000><FONT SIZE="-2">Safety and Environmental Operations Branch (RKDS)</FONT></CENTER></FONT>
</TD></TR><TR><TD>
<CENTER><FORM METHOD="LINK" ACTION="/RKD/RKDT.HTM"><INPUT TYPE="SUBMIT" VALUE="RKDT"></CENTER>
</FORM><CENTER><FONT COLOR=#000000><FONT SIZE="-2">Technical Services Branch (RKDT)</FONT></CENTER></FONT>
```

```
</TD></TR><TR><TD>
<CENTER><FORM METHOD="LINK" ACTION="/RKD/mailform.htm"><INPUT TYPE="SUB
MIT" VALUE="E-MAIL"></CENTER>
</FORM><CENTER><FONT COLOR="#000000"><FONT SIZE="-2">Please e-mail us her
e!</FONT></CENTER></FONT>
</TD></TR></TABLE></TD>
<TD><!--CENTER COLUMN--></TD>
<TD ALIGN="LEFT" VALIGN="TOP" WIDTH="50%" CELLPADDING="0" CELLSPACING=
0" BGCOLOR="#FFFFFF">
<TABLE CELLSPACING="0" CELLPADDING="0">
<TR>
<TD><B><FONT COLOR="#000000">Mission:</FONT><B></TD></TR>
<TR>
<TD> <FONT COLOR="#000000">The mission of RKD is to provide support tha
t enhances the completion of the Propulsion Directorate Mission in the
areas of Safety, Health and Environmental quality, Logistics, Human ser
vices, Security and Information Technology.</FONT></TD>
</TR>
<TR><TD><HR></TD></TR>
<TR>
<TD><A HREF="RKDORG.GIF"><IMG HEIGHT=50 WIDTH=50 SRC="RKDORG.GIF" BORDE
R="0"></A><FONT COLOR="#000000"> Click Here to View RKD Org. Chart</FCN
T></TD>
</TR><TR>
<TD><HR></TD>
</TR><TR>
<TD><BR><CENTER><IMG SRC="rocket1.gif"></CENTER></TD>
</TR></TABLE></TD></FONT>
<TD><!--RIGHT COLUMN--></TD>
<TD VALIGN="CENTER" WIDTH="33%" CELLPADDING="0" CELLSPACING="0">
<TABLE CELLSPACING="0" CELLPADDING="0">
<TR><TD><IMG SRC="TSTIMG.jpg" usemap="#TSTIMG"></TD></TR>
</TABLE></TD></TR></TABLE></CENTER>
<HR>
Page Maintained By <A HREF="RKDI.HTM">RKDI</A><br>
This Page Was Last Modified On July 25, 1997
</BODY>
</HTML>
```

References

I. Internet References

<u>FUNCTION</u>	<u>TOOLS USED/ LANGUAGE</u>	<u>LOCATION</u>
Image Mapping	Mapedit	http://www.boutell.com/mapedit
Sound	Internet Libraries	http://www.aisp.net/mid.html-ssi
	HTML	http://www.midi-hits.com http://www.htmlgoodies.com
Frame	HTML	http://www.htmlgoodies.com
Graphics	GIF Libraries	http://he.net/~notasoul/animate.html http://geocities.com/SoHo/1085
Forms	HTML	http://http://www.htmlgoodies.com
Graphic Conversion	Paint Shop Pro 4	http://www.visitorinfo.com/software/paint.htm

II. Book References

A. HTML 3.2 & CGI Professional Reference Edition UNLEASHED

By: John December and Mark Ginsburg

B. JAVA 1.1 No Experience Required, Will Train

By: Steven Holzner

III. Software Used

A. Netscape Navigator 3.0

B. Netscape Navigator Gold

C. Netscape Communicator 4.01

D. Notepad for Windows 95

**SCIENTIFIC VISUALIZATION METHODS
AT THE
CENTER FOR PLASMA THEORY AND COMPUTATION**

Kimberly Robinson

**Sandia Preparatory School
532 Osuna Rd. NE
Albuquerque, NM 87113**

**Final Report for:
High School Apprentice Program
Phillips Laboratory**

**Sponsored by:
Air Force Office of Scientific Research
Bolling Air Force Base, DC**

And

Phillips Laboratory

August 1997

**SCIENTIFIC VISUALIZATION METHODS
AT THE
CENTER FOR PLASMA THEORY AND COMPUTATION**

Kimberly Robinson
Sandia Preparatory School

Abstract

Work in the field of scientific visualization allows computationalists to provide much depended upon support to experimentalists. Within this field, the World Wide Web and various graphics programs can be valuable tools for sharing information. The web enables computationalists to simulate a situation and put graphical representations of the results on a page that can be restricted by IP address or server domain, so that the experimentalist can see it the next day, without fear for security. This increases efficiency and gives experimentalists a tool by which to judge their results. As a demonstration, the results (charged particle positions and electromagnetic field values) of a Particle-In-Cell code simulation of a High Power Microwave device have been presented in the form of QuickTime animation. This animation was then placed within an outline set of web pages for the Center for Plasma Theory and Computation at the Air Force Research Lab. The individual frames of the animation were prepared with the Visualization Edition of Applications Visualization System/Express (AVS/Express).

**SCIENTIFIC VISUALIZATION METHODS
AT THE
CENTER FOR PLASMA THEORY AND COMPUTATION**

Kimberly Robinson

Introduction

The field of data visualization has recently become important to scientists, both experimental and computational. Experimentalists often perform measurements that require the accumulation and interpretation of large volumes of data. Graphical representations of the data may be used to allow a very fast comprehension of potentially complex data sets. Computer simulations are also used both to understand physical phenomena and to aid in understanding experiments. These too generate large amounts of data which are often most easily understood through some form of graphical representation.

The Center for Plasma Theory and Computation has three computer codes that are used to simulate High Power Microwave devices, among other things. In such devices, microwaves are produced by the interaction of three parts: a source of pulsed power, a beam/cavity interaction region, and an antenna. The pulsed power device is used to create a high voltage pulse (200-500 kV) with a duration of about 1 microsecond. This pulse is used to create a beam of electrons that are accelerated through the cavity. The beam is caused to bunch through some feature of the cavity (which is unique to each device), and this acceleration of the electron beam creates microwaves. The antenna is used to focus the microwaves in a desired direction.

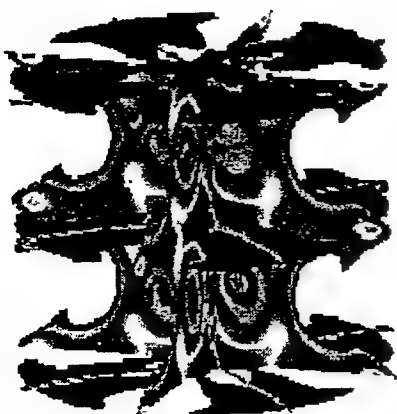


Figure 1: Mach3 was used to perform the first 3D simulated implosion of a cold-core gas puff. Shown in the picture are cut planes and isosurfaces of mass density (in kg/m^3) of radially-compressing plasma at 50 nsec.

Many pulsed power devices may be simulated using magnetohydrodynamic (MHD) calculations. High-density problems where the behavior is fluid-like lend themselves to the MHD technique. The MACH2 and MACH3 computer codes are examples of MHD codes that are used at the Air Force research Lab (AFRL). The beam/cavity interaction region contains a lower density beam and is more appropriately simulated with a particle-in-cell (PIC) code. The 3D parallel PIC code, ICEPIC, is used to simulate the cavity. There should be no particles in the antenna so this region may be simulated with a computational electromagnetics (CEM) code. The frequency domain code, PARANA, is used at AFRL to perform antenna simulations. Figure 2 is a PARANA simulation of a Vlasov antenna.

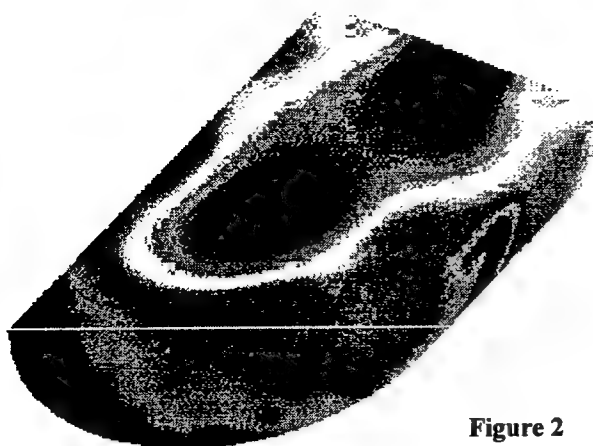


Figure 2

Methods

Visualizing data can serve many different purposes, depending on what the researcher, experimentalist or computationalist, wants to know. Making plots of everything from electric fields to densities at thousands of different points can be a very useful tool. There are many different plots that can be useful. As examples, ICEPIC computes electromagnetic field propagation; MACH computes density and magnetic fields; and PARANA computes modes (frequencies) in cavities and waveguides.

In order to start work in this field one needs to have a specialized tool. Applications Visualization System software (AVS) is one such tool. It is a powerful, object oriented program that allows the user to create specific sets of modules that can be used to visualize data in many different ways, depending on what is needed. In learning AVS, as with many other programs, it is best to begin by creating a simple example that may be extended later to more complex applications. For this example, it is useful to create a

data set that is simple enough to allow quick and easy debugging but that has features similar to the more complex data sets of interest. One such simulation that can be easily programmed, and then experimented with on AVS is the Earth orbiting the Sun. Its results are similar to the electron positions in ICEPIC in that the data is mostly position information that may be looped through time in order to create a movie. This problem is well known and the only difficulty lies in creating the module interface to make the visualization correct.

First, a program had to be written in order to create the data. The language that was chosen was C. That involved learning enough C to write the program. Once that was finished, the data had to be read into AVS, which, due to the complexity of the software and some bugs can be a difficult task. The easiest way is to create a “File_Import_Module”, which can be specially designed to suit the specific file that is to be read in. Once this is done, the three coordinates for each point that is to be plotted are interleaved into triplets. These can be run through a module to create a “field” (the basic AVS data structure that can include node positions, cell connectivity, node data, and cell data), and then outputted to the viewer. If all of the Earth-Sun data is read in at once, this creates a circle of dots around a single dot for the Sun. Eventually, a kind of “back door” method was discovered that would show only one dot for the Earth and one for the Sun at a time, and then cycle through them, giving the appearance that the Earth was orbiting the Sun. This works because of a Loop module within AVS. The arrays of data can be indexed so that only the values indexed at the current loop count will be shown, and as the loop cycles the points change. One must also create some kind of reference boundary to prevent the window from rescaling at each step. The easiest way of doing this is to build a big box that encloses all the data and has a set relationship to the maximum data value at each time step.

Working primarily with ICEPIC data, creating a template for making a QuickTime movie was an interesting process. There were more problems involving data, and how to render it, than in the simpler program. In order to make a movie, it was necessary to create a loop that would read through sets of numbered files, taking pictures of each one once the information had been processed. The size of each data set was over 10 MB and there were about 500 data sets, so this could often take several hours, sometimes days. In order to make a movie out of the newly outputted files it was necessary to have other software that

could render a QuickTime movie. This work was performed on a Silicon Graphics High Impact workstation which comes with simple tools to turn a series of numbered GIF files into an animation.

In creating the individual frames to be made into the movie, there were three parts, each requiring a different visualization technique: the device geometry, the particles, and the fields. For each time step, there was new particle information as well as new fields while the geometry stayed the same throughout. The geometry was built from a set of quadrilaterals strung together to create a 3D boundary of the device.



Figure 3

Figure 3 shows the geometry without the particles overlaid. More and more particles are created as the electric field continues to propagate through MILO. As time passes, they move around within the device so that all of them need to be replotted at each time step. The electric field values are specified on a mesh lying in the $x=0$ plane. This plane divides the device in half and is a plane of symmetry. Because the mesh is not complete (there are places in the device where the electric fields cannot penetrate) the electric field values are not read in as a

structural mesh, but as a point mesh which was later converted into a standard field format. Each of the points in the mesh was then colored according to the magnitude of the electric field. A second set of electric field values in the plane $y=150$ at the downstream end of the device (past the antenna) was also used to give an indication of the fields in 3D. These field plots were placed at the top of the screen by adding 100 to all of the "y" values for that plot before interleaving the three coordinate arrays. The two pictures (particles and fields) used the same loop so that the information on both always corresponded. Figures 4 and 5 show different frames from the MILO movie. Figure 4 is from the very beginning at time = 0.5 nsec. Figure 5 is at time = 150 nsec. The particles are the dots that group around the core of the device.

An object, or set of objects, can be mapped to a specific color to allow better visualization. Nodes, cells, or regions of the screen may also be mapped to a color based on data (such as the electric field here)

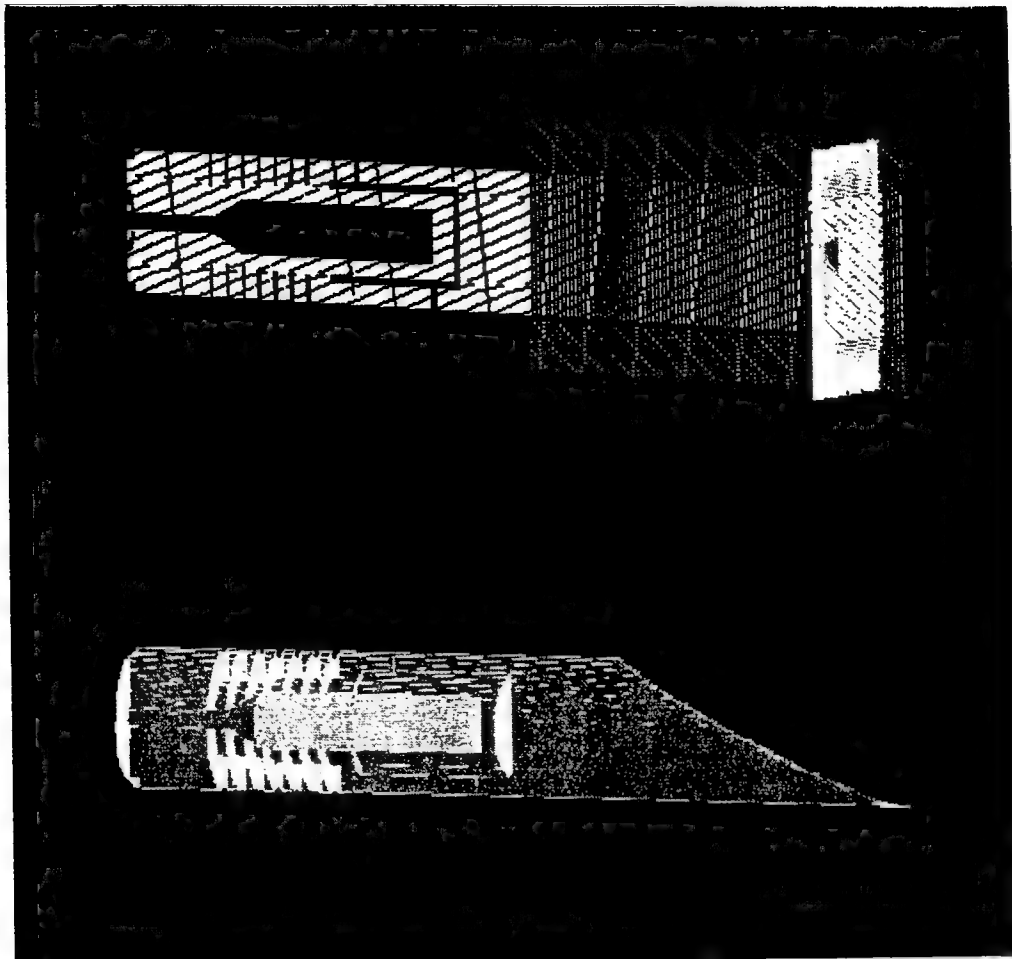


Figure 4
Time: 0.5 nsec

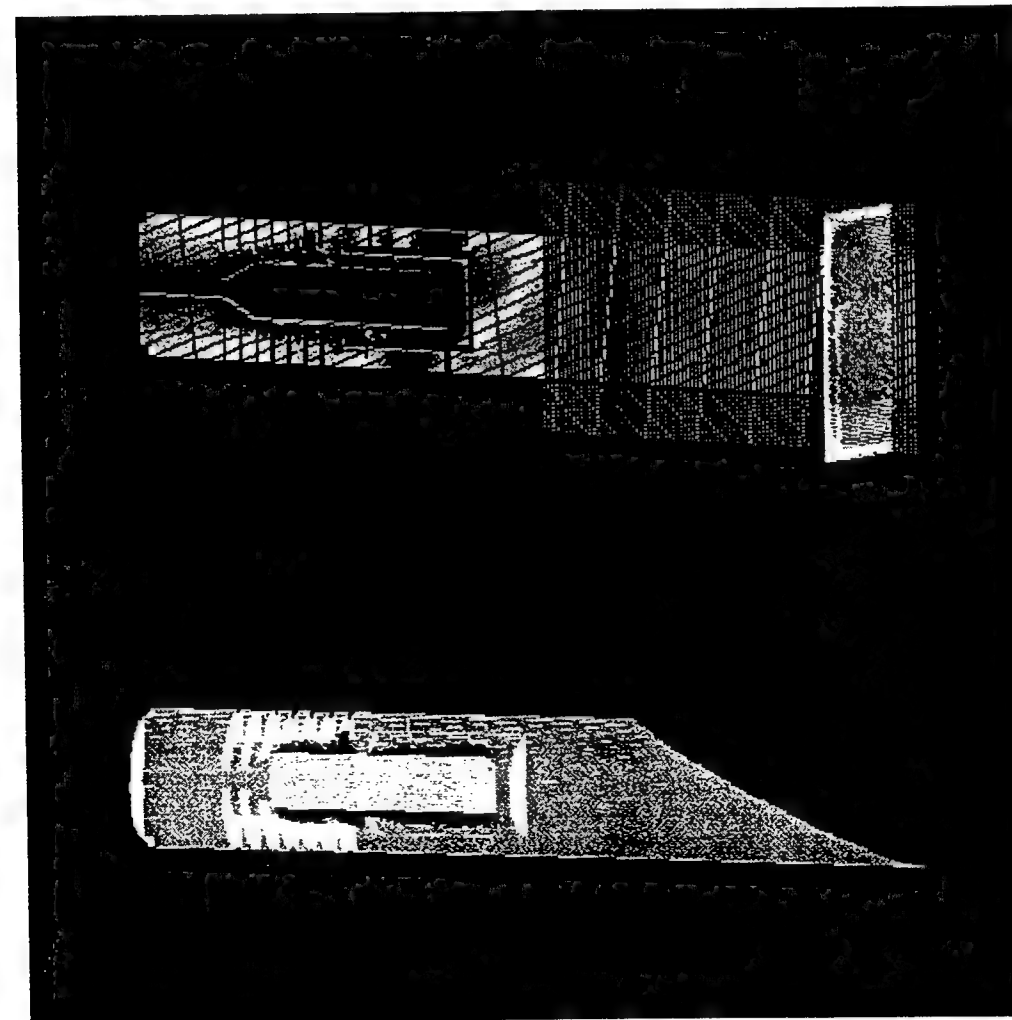


Figure 5
Time: 150 nsec

that is located at each of the nodes. Node data can be assigned by using the “File_Import_Module” and routing the results through a module that will change arrays of numbers into node data. One problem that arose within the electric fields was that the magnitude at some points was considerably higher than the magnitude at other points, so that important data was being obscured when using the default datemap. The datemap module in AVS is not particularly user friendly, but there is a way of creating multiple ranges within the map, so that for a specific range of values, an essentially separate datemap is defined. The drawback to the approach of creating new colormaps that repeat colors in other colormaps is that some colors will be the same, even though the field magnitude that they represent might be very different. There should be a way around that problem, too, with an option called sub-ranges. However, we were not able to make these work correctly.

Related to the field of data visualization is the necessity of a way of sharing the information that can be found in pictures of experiments. One way that this can be done is through the World Wide Web. This vast network of computers can be very useful for telling other people what goes on inside the labs. It can also be a way of sharing information with co-workers no matter where they are.

A set of general web pages was designed to share information about the Center for Plasma Theory and Computation codes and projects. They are filled with pictures from all three of the codes, as well as information and explanations of the projects. Examples of the information available are detailed descriptions of the codes and algorithms, user’s manuals, publication lists, sample input files, and instructions for obtaining the codes. The pages are an easily accessible place for people to find those descriptions.

Graphics are well known to be a “first sight” way of judging a web page, and the graphics produced by AVS can be a way of interesting people in the web page, as well as a method of explaining the experiments. The MILO movie is a good example of this. By putting it on a web page, it is easier to understand what happens within the experiment than by having it explained.

Another vision of the Center is to be able to maintain their own web site that will have pages that are open to the public as well as pages that can be locked. These closed pages can be limited by password, server domain, or IP address so that specific people who are allowed in can see new results or images that

have not yet been cleared by Public Affairs. This would enable the personnel on base to share information more quickly.

The idea of putting un-cleared information on the web is a security concern, but it can be now implemented safely with the help of new server technology. The Microsoft NT Server allows certain directories' visibility to be limited to or from certain computers. This is the slightly more difficult way of doing things, but it does work. A more desirable way to do it, which is being investigated currently, is to limit entry to the pages based on server domain. Ideally, these pages would be accessible only to people on computers based within the plk.af.mil domain (at the Phillips Lab).

Results

Through this project several things have been accomplished. There is now a template for creating movies with AVS. Other members of the group should be able to apply this template to their own data and with a small investment of time produce high quality movies. It should only be a matter of replacing the "File_Import_Module" to suit the new data, and possibly some new plot modules, if a different kind of plot is needed.

In addition to that, there is a set of web page outlines that can simply be added to until they are ready to be published. They were written in HTML in the frame format, but with new browser/editors, they can be edited one frame at a time so that it is not necessary to learn HTML or Java to add to the pages.

The MILO movie should be on the web soon. Once the site has been completed and has cleared Public Affairs, it can be seen at <http://oblivion.plk.af.mil/wsqt/wsqt.htm>.

Conclusion

The web pages will provide the Center with higher visibility as well as simplifying the distribution of software. They can also make the sharing of results of simulations more efficient between the computationalists and the experimentalists, allowing the computationalists to serve their basic function. If the server idea is instituted, it will also be a safe medium, without fear of releasing sensitive information.

Visualization of scientific data is a very powerful and important tool. Animations such as the MILO movie are an example of this. With the combination of the electric field propagation and the movement of the particles, the relationships become more obvious to the viewer.

With the creation of the AVS movie template, the technique that was used is an example for further visualization of other problems. This saves other people's time and energy because the way to make the movies is already there. It simply needs to be customized for the data.

Scientific Visualization is beneficial in many ways. The experimentalists may be given a better idea of what to look for in their measurements; the computationalists' results are often impossible to understand without pictures; and people who do not know what exactly they are looking at can understand because the pictures help to explain things, which is the main function of the Center for Plasma Theory and Computation.

**A STUDY OF THE EFFECT OF HEAT FLOW ON THE PERFORMANCE
OF AN ALKALI METAL THERMAL-to-ELECTRIC CONVERTER**

Michael P. Schoenfeld

**New Mexico Military Institute
101 West College Boulevard
Roswell, NM 88201-5173**

**Final Report for:
High School Apprentice Program
Phillips Laboratory**

**Sponsored by:
Air Force Office of Scientific Research
Kirtland Air Force Base, NM**

and

Phillips Laboratory

August 1997

A STUDY OF THE EFFECT OF HEAT FLOW ON THE PERFORMANCE
OF AN ALKALI METAL THERMAL-to-ELECTRIC CONVERTER

Michael P. Schoenfeld
New Mexico Military Institute

Abstract

The concentration of heat flow into an Alkali Metal Thermal-to-Electric Converter (AMTEC) was studied to determine if the efficiency of the Thermally Regenerative Electrochemical System (TRES) would increase when heat flow is concentrated into the Beta-Alumina Solid Electrolyte (BASE) tubes and evaporator by insulation techniques. Two experimental insulation techniques were used to see which one could direct and use the heat in the most efficient manner. Min-K was used as a standard insulator. Two experimental insulations, alumina powder and multi-layer foil, were used in two different set ups in conjunction with the Min-K. Based on results, it was hypothesized that alumina powder tended to sinter, thus increasing its thermal-conductivity which allows a larger fraction of the heat to move through the powder instead of into the cell top. The multi-layer foil was found to direct a larger fraction of the heat into the top, reducing the amount of heat lost by conduction through the alumina powder.

A STUDY OF THE EFFECT OF HEAT FLOW ON THE PERFORMANCE OF AN ALKALI METAL THERMAL-to-ELECTRIC CONVERTER

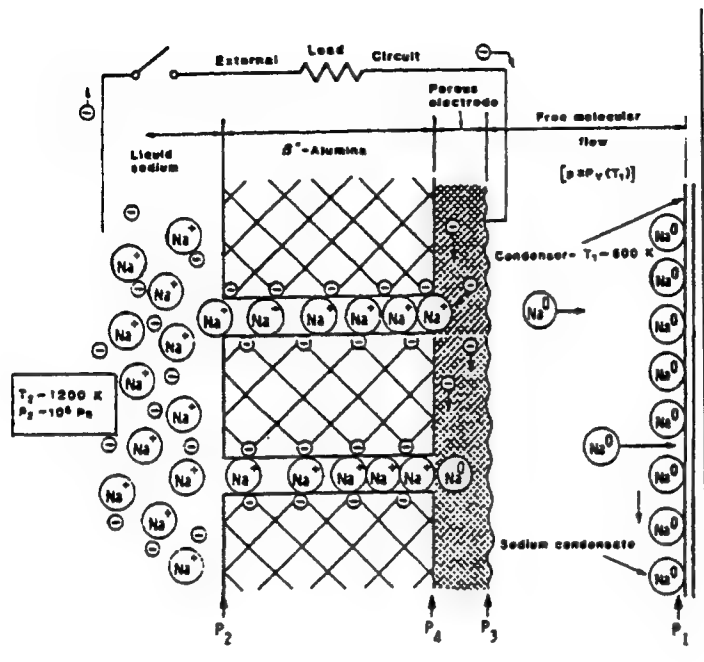
Michael P. Schoenfeld

Introduction

The AMTEC cell directly converts heat to electrical energy using Beta-Alumina Solid Electrolyte (BASE) tubes and sodium ions. These BASE tubes are composed of $\text{Na}_{5/3}\text{Li}_{1/3}\text{Al}_{32/3}\text{O}_{17}$ and have crystal structure such that spacing of the O^{2-} ions above and below the Na^+ planes have a low activation energy barrier that allows for rapid diffusional motion of sodium ions. The reaction $\text{Na}^\circ \longrightarrow \text{Na}^+ + \text{e}^-$ occurs at the high pressure side of the BASE. At open circuit, Na^+ ions move through BASE because of a pressure differential across the BASE. The differential is caused by a temperature differential. An electric field builds up in the BASE until it is strong enough to stop the flow of Na^+ ions. The open circuit voltage is given from the Nernst equation $V_{oc}=RT_2F^{-1}\ln(P_2/P_4)$ where R is the gas constant, F is the Faraday, P_2 is the vapor pressure of sodium at T_2 , and P_4 is the sodium at the BASE-porous electrode interface. When the circuit is complete, electrons flow through the external load and return to the low pressure side of the BASE where they recombine with the sodium ions. This causes the reaction, $\text{Na}^+ + \text{e}^- \longrightarrow \text{Na}^\circ$, to complete. Sodium atoms in their vapor state, leave the porous electrode, and release their heat of condensation on the condenser. The heat input creates a pressure differential that creates a voltage across the BASE tubes. This voltage drives electrons along current collectors producing electrical work. The sodium is then "wicked" along the condenser, through the artery, and to the evaporator by capillary forces. When it reaches the evaporator it becomes vapor, travels to the BASE tubes and cycles through the process again (See figure 1).

Figure 1

AMTEC



Governing Equations

$$V_{oc} = \frac{RT_2}{F} \ln \frac{P_2}{P_4}$$

$$V(i) = V_{oc} - iR_{internal}$$

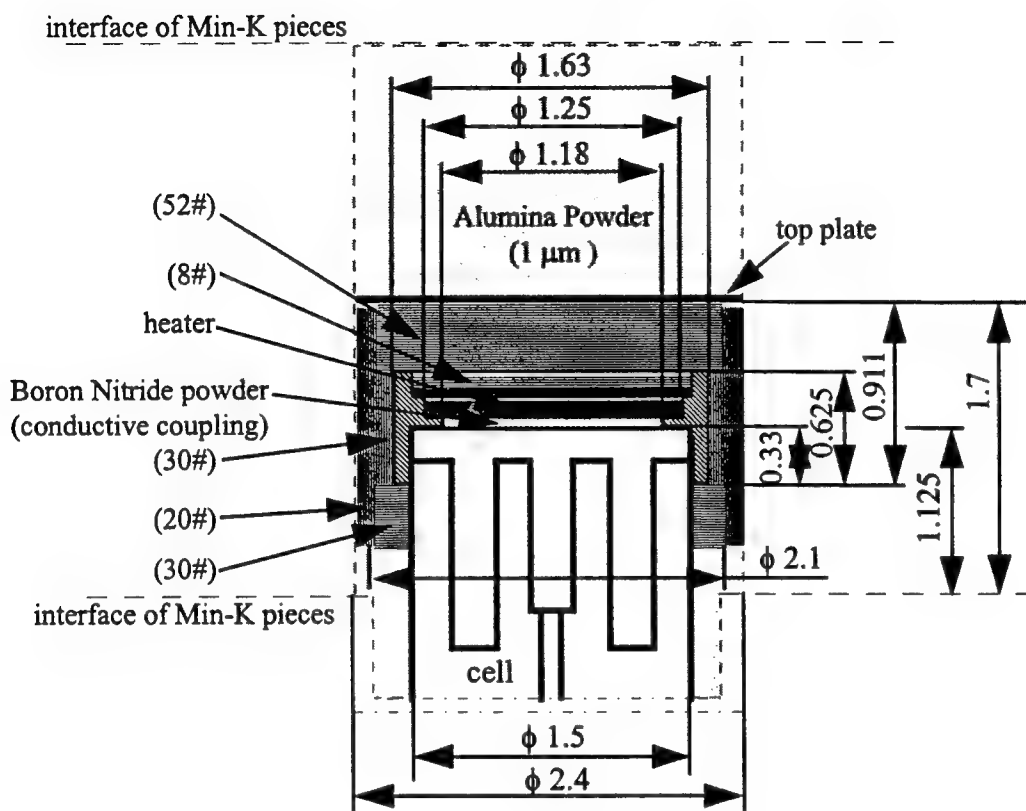
$$P = iV_{oc} - i^2 R_{internal}$$

$$\eta = \frac{P_{out}}{Q_{in}}$$

$$\eta = \frac{Vi}{i \left\{ V + \frac{[L + Cp(T_2 - T_1)]}{F} \right\} + Q}$$

Figure 2

Multi-Foils Shielding for Electric Heater (for Cell PX-4B)



All dimensions are in inches.

Molybdenum foils: $\delta = 7.62 \mu\text{m}$

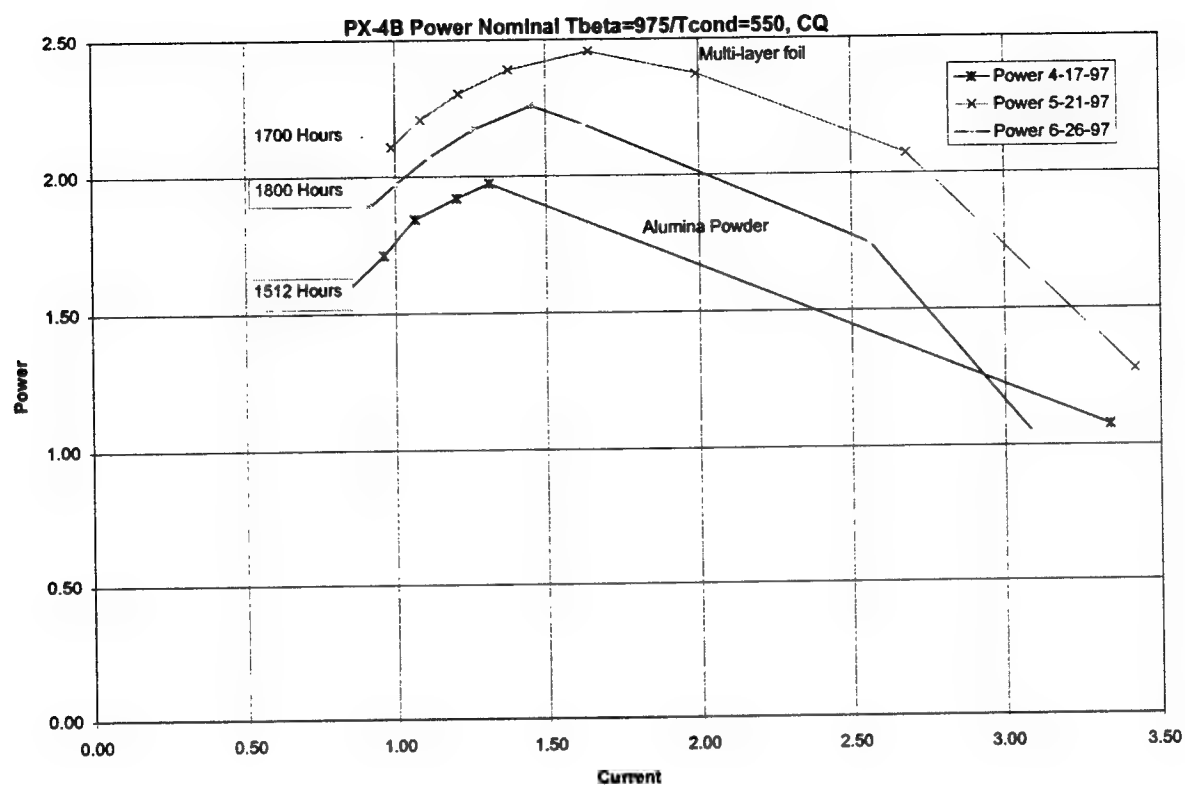
spacer: Zirconia powder, $D_p = 0.23 \mu\text{m}$

the thickness of multi-foils: 0.0055"/layer

Methodology

The process of converting heat to electricity using an AMTEC cell is achieved by supplying heat to an evaporator and BASE tubes. Heat can be supplied by concentrated solar energy, radioisotope decay or other nuclear sources, fossil fuels, or I^2R heating. Since efficiency of the system is a function of parasitic heat loss and internal resistance, it is important to keep the heat flow concentrated into the BASE tubes and evaporator (cell top). Experiments were conducted with two different insulation configurations to determine which design would keep the heat as concentrated as possible. One experiment was designed with alumina powder and the other with multi-layer foil (both in conjunction with Min-K). In one experiment the cell was placed in a circular cut out in the middle of the Min-K. Then the gap between the Min-k and the cell was filled with alumina powder. The other experiment was set up similarly, but the top of the cell and heater were shielded with multi-layer foil. The space below the foil was filled with the alumina powder. The multi-layer foil was placed with spacing in between each other to keep the emissivity very low (as in the equation $Q=\epsilon\sigma A\cdot(T_b^4-T_c^4)$ for radiation heat transfer). Small beads of zirconium oxide were placed on the foil to prevent direct contact between layers of foil. Not only would this lower the amount of heat lost by radiation, but would also increase the reflectivity. Therefore, most of the heat is concentrated to the BASE tubes and evaporator. Results showed that over time (1512 hours) the alumina powder sintered which increased the amount of heat lost from the BASE tubes and evaporator by conduction. Then at 1700 hours the multi-layer foil was set up and the power output increased because more heat was concentrated into the cell. Then, at 1800 hours, new unsintered alumina powder was used to replace the multi-foil insulation. Results indicate that the initial power curve (1512 hours) had suffered degradation caused by the Al_2O_3 partially sintering. Recovery of this power was shown in the 1800 hour case where fresh Al_2O_3 powder was used with no multi-layer foil. The 1700 hour power curve shows that multi-layer foil significantly increase the ratio of heat input which goes directly into the top of the cell (versus the heat lost by conduction down the side walls) (See figure 3).

Figure 3



A STUDY OF THE CHARACTERIZATION OF REDUCED TOXICITY MONOPROPELLANTS

Thomas Jonathan Shea

Tehachapi High School
711 Anita Drive
Tehachapi, CA 93561

Final Report for:
High School Apprentice Program
Phillips Laboratory

Sponsored by:
Air Force Office of Scientific Research
Bolling Air Force Base, DC

and

Phillips Laboratory

August 1997

A STUDY OF THE CHARACTERIZATION OF REDUCED TOXICITY MONOPROPELLANTS

Abstract

Selected characteristics of RK-124A, RK-124B and HAN-based monopropellants were investigated. Literature data on safety precautions and effects of hydrazine along with the different monopropellants were collected before the laboratory work was begun. Each liquid monopropellant was characterized including their kinematic viscosity in relation to temperature, performance (Isp, Density, Combustion Temperature), density at four different temperatures, Department of Transportation (DOT) Thermal Stability, and heat capacity. All observations were recorded in the duration of an eight week period. A desktop computer was used to calculate the theoretical performance and the Isp, Density, and Combustion Temperature were recorded. A viscosity and density measurement was made for each sample at 0°C, 20°C, 25°C, and 40°C, and the resulting calculations were recorded and graphed. However, RK-124A was not evaluated at 0° because of its melting limitations but it was used in the thermal stability test. In the DSC Heat Capacity test all monopropellants produced accurate results. Unstabilized NASA HAN was made to help in comparison with the newly developed stabilized HAN, and was included in all safety and performance tests. The goal of the experiment was to evaluate the physical properties of the four monopropellants and to test their capabilities as a possible substitute to hydrazine in the future.

A STUDY OF THE CHARACTERIZATION OF REDUCED TOXICITY MONOPROPELLANTS

Introduction

In the vast world of monopropellant propulsion, there are three basic types of liquid monopropellants. (1) Single substances (molecular compounds) that contain an oxidizing agent and combustible matter in the same molecule, such as nitromethane. (2) Intimate mixtures of compounds that are stable under normal conditions, such as HAN, and (3) Thermodynamically unstable chemicals, such as hydrazine. Upon ignition, the first two types of monopropellants will undergo combustion much like a bipropellant combination. The first is an oxidizer and a fuel in one molecule, which allows it to burn very easily. The components in the second type must be compatible at normal temperatures, but react when ignited or heated under pressure to give hot combustion gases. It is an "intimate mixture" because it combines the efforts of two or more molecules for oxidizing and fueling purposes. The third type decomposes to produce hot gases by means of a catalyst or a thermal source. In hydrazine, there is no real combustion. The compound is unstable in the presence of a catalyst, and when it decomposes it makes ammonia, hydrogen, and nitrogen. The monopropellants under these three main categories, specifically monopropellants with hydrazine, have been the most acceptable and useful in a wide variety of systems to date.

Hydrazine's ease of catalytic decomposition has led to its becoming the principal fuel for low-thrust satellite propulsion. It has replaced hydrogen peroxide in almost all monopropellant applications because of its better storability and higher performance. Various alternative propellant compositions have been evaluated as a mean of improving monopropellant performance compared to hydrazine. The four samples (RK-124-A, RK-124B, Unstabilized NASA HAN, and Stabilized NASA HAN) have been made with the desired outcome to improve the overall performance and reduce the toxicity of the current monopropellants that are in use. Some key monopropellant characteristics were tested in the following experiments to see if they have potential as a suitable replacement to hydrazine. An equal or better

performance than that of hydrazine itself will indicate the substance's feasibility as a replacement and ability to increase the energy capacity of the existing and future satellites in orbit.

Methodology

Safety Standards on Dangerous Materials

Hydrazine- Anhydrous or aqueous solutions of hydrazine are toxic by ingestion. Inhalation of vapors or contact with the skin causes systematic effects of physical breakdown. It can affect the nervous system resulting in hernia, convulsions, and death. Some of the diseases hydrazine can cause include pulmonary edema, irritation upon the eyes and respiratory tract, fatty necrosis if there is liver damage, and interstitial nephritis if there is damage to the kidneys.

Hydroxyammonium Nitrate, Glycine (HAN)- HAN can cause abnormalities of the lungs and liver. Animal data indicates it would be a sensitizer. Some of the diseases it could cause include dermatitis and allergic dermatitis. Lethargy, ataxia, coma, alopecia, hyperactivity, brown staining of the nose and mouth, soiling and wetness in the anogenital area, and alopecia were all observed in lab experimentation of various animals. The exposure limit in humans is about 300 mg/cuM for 15 minutes. In small animals like rats, the fatal limit is 250 mg.

Acid protective gloves, laboratory coat, skin and eye protection, and foot protection are essential when handling these hazardous materials. TLV (Threshold Limit Value), PEL(Permissible Exposure Limit), and LDL (Legal Dose Limit) are three of the many safety standards looked at when various substances are tested.

Theoretical Calculations

Theoretical Isp, density, and combustion temperature all are essential in the initial formulating stages of a monopropellant because they usually give accurate predictions of how the substance will perform. The achieved number in each of these categories must meet a certain standard in monopropellant performance, density, combustion temperature, and hopefully, a product that has reduced toxicity. A thermodynamic equilibrium calculation program using an imputed ingredient library is used to obtain theoretical monopropellant formulation numbers. The optimized performance

calculations of unstabilized NASA HAN, stabilized NASA HAN, RK-124A, and RK-124B will be shown in the results portion of this presentation.

Viscosity and Density

To determine the viscosity of each of the four monopropellants, many elements need to be fulfilled before the actual testing of the material take place. The first step is to calibrate the glass kinematic viscometer that is going to be used in the experiment.

A Cannon-Fenske Viscometer was used at sizes 50 and 100 (See Figure 1). The theoretical approximate constant for serial tube A-37 (50) was found to be 0.004 and the approximate constant for serial tube B-45 (100) was found to be 0.015. A liquid standard having a flow time of at least 200 seconds and no more than 1000 seconds is the ASTM standard used in the experimentation process. To calculate the viscosity constant (V_c), a standard must be used along with the following equation:

$$V_c = C_s / t \quad \{1\}$$

In the equation, C_s stands for the number at centistokes in a given temperature, and t stands for the time it takes to go through the viscometer test. Once the viscosity constant for the viscometer is obtained, experimentation on the monopropellants can begin. Once the constant is found, it can be multiplied by the time to obtain the number of centistokes of the various monopropellants.

$$C_s = V_c * t \quad \{2\}$$

To obtain the centipoise (C_p), the density of the product was determined using a pycnometer. A standard must be used to find the volume of the pycnometer, which can be calculated from the following equation.

$$V = g / D \quad \{3\}$$

Once the volume is obtained from the standard being used, it becomes the constant for the monopropellants that are to be tested in the pycnometer. Once the weight of each propellant is obtained, it can be divided by the volume of the standard to achieve the density.

$$D = w / V \quad \{4\}$$

Once the density is determined from each product, the centipoise (C_p) of each monopropellant

can be calculated. The equation to get the centipoise is as follows:

$$C_p = Cs / D \{5\}$$

The numbers achieved are explained in the results portion under density. The complete viscosity spreadsheet can be seen on tables 2 and 3 and the viscosity vs. the temperature along with the density vs. the temperature can be observed on figures 3 and 4 respectively.

Heat Capacity and DOT Thermal Stability Test

Heat capacity is the amount of heat required to raise the temperature of one gram of material one degree centigrade. Specific heat capacity is the heat capacity of a sample divided by the heat capacity of water. The heat capacity of a material changes with its temperature. Historically, it has been measured at 25° C and assumed not to change with temperature. The DSC Heat Capacity software however, calculates the actual heat capacity at any temperature in the DSC scan. The heat capacity calculations require three DSC scans: baseline, reference, and sample. The baseline scan is used for baseline subtraction from the reference and sample data. The subtraction removes all systematic instrument effects from the heat capacity results. The reference scan, usually done with sapphire, is used to calibrate the calorimetric response of the DSC versus temperature. The sample scan can be used to calculate the heat capacity of the sample at any temperature. The heat capacity of a material undergoing a constant heating or cooling ramp is proportional to the heat flow at any temperature:

$$C_p = E_t * Q_t / H_r * M \{6\}$$

In this equation C_p is the specific heat capacity, E_t is the cell constant, Q_t is the heat flow due to the actual sample at a temperature, H_r is the heating or cooling rate, and M is the mass of the sample. The DSC Heat Capacity program should correct the measured heat flow for all files by subtracting the contribution due to the sample pans, correct the measured beat flow in the reference and sample files for the corrected baseline signal, and calculate the actual heating / cooling rate at each point from the sample temperature data. It should also calculate the heat capacity of the sample at each point, integrate the total heat transferred to or from the sample across the analysis region, and allow the user to exclude contributions due to reactions or transitions within the analysis range. Finally, the DSC machine should

analyze sample heat capacities from increasing or decreasing temperature scans.

In the DOT thermal stability test, a sample is tested to see if ignition, explosion, color change, and weight loss occur. A sample up to 50 grams is placed into a beaker, covered with a watch glass, and weighed. The beaker is then placed into an oven at 75 °C for 48 hours. If an explosion occurs during this time period, the sample has failed. After the two day period, the sample is taken out of the oven, re-weighed, and determined if any of the sample has been lost based on the weight of the sample before and after the test excluding moisture and volatiles. A 0 % error is desirable, but a sample re-weighing anywhere between 0% to 3% error is considered passing in the experiment.

Results

Safety Standards on Dangerous Materials

The rules provided in the GenCorp Aerojet safe handling of HAN materials, the A3L Safety Update, and AF form 55 (EF-V1) helped develop precautionary measures with the hydrazine salts that were used. The potential splashes of hazardous liquids, working near hot equipment, working in an area where explosives are stored, chemical exposure, and the handling of the monopropellants were all taken into account in the lab area. The experimentation resulted in no injuries or broken equipment because of the careful consideration of the potential hazards.

Theoretical Calculations

In each of the four monopropellants, the theoretical Isp, combustion temperature, and density was taken and compared with the numbers achieved in hydrazine. In unstabilized NASA HAN, the theoretical Isp was at 208.703 seconds, the combustion temperature was 1300.78 °K, and the density was recorded at 1.330 g / cc. In stabilized NASA HAN, the Isp was taken at 209.618, the combustion temperature was at 1306.00 °K, and the density is 1.332 g / cc. There is no real significant change from the two compounds other than the use of stabilizers. The data from both monopropellants coincide with each other. PL candidate RK-124A had an Isp of 264.267 seconds, a throat temperature of 1991.48 °K, and a density of 1.398 g / cc. With RK-124B, the Isp was recorded at 252.126 seconds, the throat temperature at 1808.00 °K, and the density at 1.370 g / cc. much lower than that of RK-124A. The densities of ingredients in the

RK-124 monopropellants were estimated. An overview of each of the monopropellants anticipated performance in density, combustion temperature and Isp / Density can be seen on Table 1 and Figure 2.

Viscosity and Density

Before the viscosity experiment began two viscometer tubes were calibrated. Using viscosity standard S6, Tube A-23 (50) was found to have a viscosity constant of 0.004376 {1}, very close to the 0.004 reading of the theoretical constant. However, due to the small capillary in the viscometer of the A-23 tube, all four monopropellants exceeded the 1000 second limit. The Cannon-Finske B-45 (100) viscometer did meet the needs of ASTM time requirements of the standard S6 and the monopropellants. It had an average viscosity constant at temperatures of 20⁰, 25⁰, and 40⁰ of 0.014329 {1}, compared to the theoretical constant of 0.015.

The monopropellants viscosity in centistokes was determined using equation {2} and the number ranged as high as 11.7835 for unstabilized HAN at 0⁰ C to as low as 3.1710 at 40⁰ C on RK-124B. The exact calculations may be observed on the viscosity tables.

In order to calculate the pyncrometer volume {3}, the standard that was used for the pyncrometer was distilled H₂O. The water was found to have a volume that equaled 9.2356 at 25⁰C. The units of the monopropellants in the pyncrometer at 0⁰ C, 20⁰ C, 25⁰ C, and 40⁰ C were divided by the calculated volume of the distilled H₂O {4} to get the density of the monopropellant at that specific temperature.

Once the density was obtained, the centipoise {5} could be calculated. The centipoise ranged as low as 2.2051 at 40⁰ with RK-124B to as high as 10.8481 at 20⁰ with RK-124A. The results can be seen with all of the monopropellants on Tables 2, 3, 4 and Figures 3 and 4.

Heat Capacity and DOT Thermal Stability Test

A reference file for the DSC Heat Capacity machine was used to help determine the achieved data taken from the monopropellants. 35.56 mg of sapphire was used in a pan weighing 23.36 mg as a standard in the experiment. Distilled H₂O was tested twice in a hermetically sealed pan, both weighing in at 7.90 mg. The heat capacity in the test was found to be lower than the actual heat capacity of water

(4.184 J / g $^{\circ}$ C and 1.000 cal / g $^{\circ}$ C). The actual number achieved was 4.019 J / g $^{\circ}$ C and 0.959 cal / g $^{\circ}$ C which gave about a 4.0% error in the monopropellant work.

Using equation {6} in the TA DSC Heat Capacity machine, the data recorded in all of the monopropellants produced consistent numbers. RK-124A had 7.9 mg of solution in the pan and had an average of 1.789 J / g $^{\circ}$ C (0.427 cal / g $^{\circ}$ C) and RK-124B had 6.4 mg of solution in the pan and had an average of 1.836 J / g $^{\circ}$ C (0.438 cal / g $^{\circ}$ C). The unstabilized NASA HAN had 6.4 mg of solution and averaged 2.191 J / g $^{\circ}$ C (0.523 cal / g $^{\circ}$ C) while the stabilized HAN had 7.9 mg of solution with a heat capacity of 2.495 J / g $^{\circ}$ C (0.595 cal / g $^{\circ}$ C). Each of the monopropellants showed fluctuations in the graphs, but relatively stayed constant during the experimentation. The heat capacity graphs of each of the monopropellants can be observed on Tables 5 and Figure 5.

In the DOT Thermal Stability Test, RK-124A was used in the experiment. The monopropellant was weighed in a beaker and had a total mass of 41.3811 g, close enough to the 50 g needed for experimentation. The monopropellant was placed in an oven over a two day period at 75 $^{\circ}$ C. When it was taken out, it was re-weighed and found to have a new mass of 41.3808. The 0.0003 g difference could be the result of either human error or vaporization of the H₂O in the water based material. The monopropellant had a 99.9992 % of the material left with a surprisingly small 0.0008 % error. The RK1+A monopropellant did well during the 48 hour period and passed the thermal stability test.

Conclusion

The results that were gathered for each of the monopropellants have shown consistency with literature data and of each other. In the theoretical calculations, the end result in the Isp, density, and combustion temperature and the information obtained on the monopropellants have produced distinct similarities and differences with each other and with hydrazine. Unfortunately, the monopropellants have a much higher throat temperature than hydrazine, but the density is high which helps increase its energy capacity and possibility of a stronger and longer life in satellite propulsion. The viscosity decreases with temperature, and the time for the solution to run through the viscometer tube increases with lower temperatures. In the viscosity vs. temperature graph (Figure 3), stabilized and unstabilized

NASA HAN have virtually the same points with stabilized HAN being slightly more viscous than the unstabilized.

Another interesting point is the fact that RK-124B is less viscous than the two HAN products, and RK-124A has the highest viscosity than all three. The theoretical densities of the products are accurate based on the comparison of the achieved densities on Figure 4. The heat capacity of the monopropellants show consistency in the data (Table 5) and relatively stable line graphs in the plots (Figure 5).

All monopropellants have distinct advantages over each other and can be very beneficial propulsion industry someday. They all have potential for use in satellites in the future. Stabilized HAN, in particular, has stabilizers included in the compound and is more thermally stable than unstabilized NASA HAN. The goal to develop a monopropellant that can run longer, cost relatively cheap, and have a lower toxicity will someday become a reality based on the positive data achieved on the four different monopropellants worked on in this lab work.

Acknowledgments

1. Brand, Adam. General Information, Report and Presentation Assistance, Theoretical Calculations, and Lab Assistance, 1997.
2. McKay, Milton (Mac). General Information, DOT Thermal Stability Test, 1997.
3. Jones, Paul. Density, Viscosity, and Heat Capacity lab and report assistance, 1997.
4. Wilson, Angelica. Viscosity Lab Assistance, 1997.
5. LaRue, JoAnne. Viscosity Lab Assistance, 1997.
4. Ismail, Ismail. Heat Capacity Plotting and Graphing, 1997.
5. Schwartz, Daniel. Theoretical Calculation, Viscosity, and Density plotting and graphing, 1997.
6. Bach, Duyen. Theoretical Calculations, 1997.
7. Hawkins, Tom. Literature Data, Report and Presentation Assistance, 1997.

References

1. P. Ander and A.J. Sonnessa, Principles of Chemistry: An Introduction to Theoretical Concepts. The Macmillan Company, 1965.
2. N.I. Sax, Dangerous Properties of Industrial Materials. Van Nostrand Reinhold Company, 1984.
3. P.A. Smith, Derivatives of Hydrazine and other Hydronitrogens Having N-N Bonds. The Benjamin / Cummings Publishing Company, 1983.
4. F.S. Forbes, Liquid Rocket Propellants. Academic Frontier, 1987
5. G. P Sutton and D.M. Ross, Rocket Propulsion Elements: An Introduction to the Engineering of Rockets. Wiley-Interscience, 1976.
6. A. Katzakian, Safe Handling of HAN Materials. GenCorp Aerojet, 1991.
7. J.W. Beckmann and W.M. Kalliomaa, Rocket Propulsion Experimental Facilities at the Phillips Laboratory, Edwards Air Force Base, California. SAE International, 1993.
8. G.M. Clark, A3L Safety Update. GenCorp Aerojet, 1992.
9. Du Pont Instruments, DSC Heat Capacity Data Analysis Program. TA Instruments, 1991
10. The Defense Logistics Agency, Department of Defense Explosives Hazard Classification Procedures. 11A-1-47 Air Force, 1989

Figure 1
Viscosity and Density Instruments

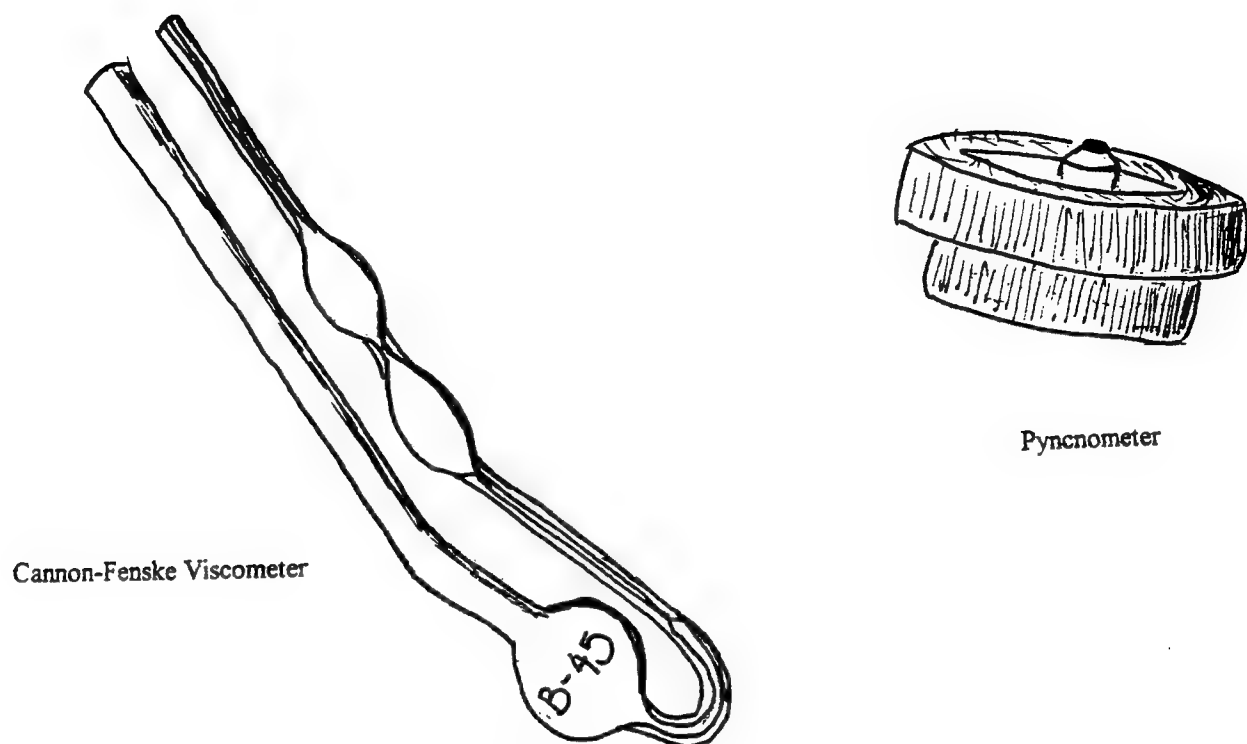


Table 1
Theoretical Calculations

	RK-124A	Stabilized NASA HAN	Unstabilized NASA HAN	RK-124B	Hydrazine
Isp	264.627	209.618	208.703	252.126	232.796
Density Isp	369.948546	279.211176	277.5749	345.41262	235.12396
CT	1991.48	1306	1300.78	1808	756.79

Figure 2

Monopropellant Performance Calculations

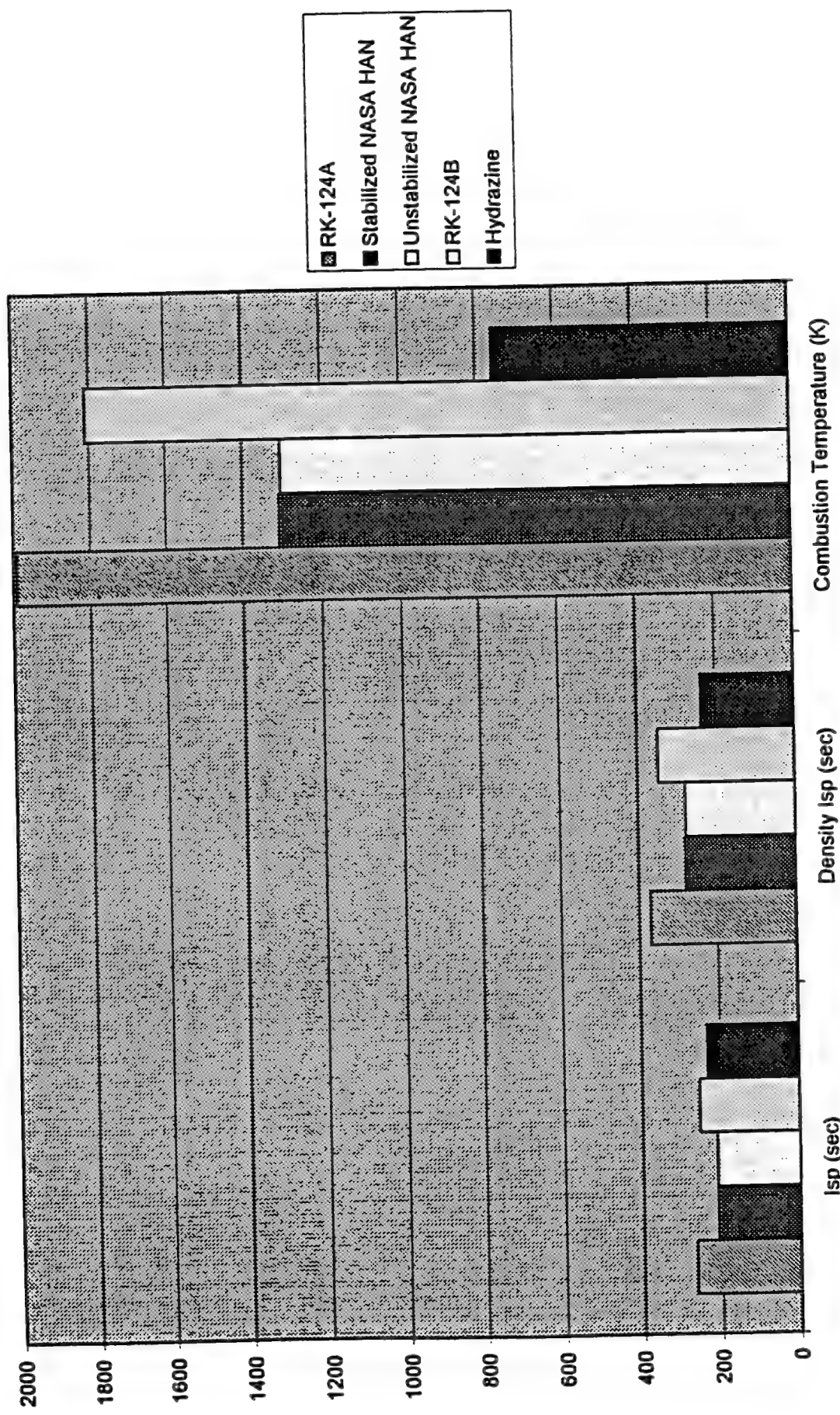


Table 2
RK-124A and RK-124B Viscosity Calculations

MONOPROPellant Viscosity Worksheet						
Sample Name	Temp	Time	Constituent	CENTIPOISE (cP)	Density	MEAN
JK-126A	20	15.00	0.01420	10.401	1.412	7.01040471
	20	15.00	0.01420	10.362	1.412	7.024603566
	20	15.00	0.01420	10.359	1.412	7.024472277
	20	15.00	0.01420	10.451	1.412	7.010864065
	20	15.00	0.01420	10.472	1.412	7.023432304
	20	15.00	0.01420	10.224	1.403	6.980436094
	20	15.00	0.01420	10.235	1.403	6.981569587
	20	15.00	0.01420	10.284	1.403	6.984399456
	20	15.00	0.01420	10.279	1.403	6.983558807
	20	15.00	0.01420	10.207	1.403	6.982737936
	20	15.00	0.01420	10.079	1.411	6.994482144
	20	15.00	0.01420	10.073	1.411	6.992238608
	20	15.00	0.01420	10.007	1.411	6.997919411
	20	15.00	0.01420	10.046	1.411	6.994868452
	20	15.00	0.01420	10.039	1.411	6.912586412
	20	15.00	0.01420	10.032	1.411	6.97632544

NONPROPELANT VISCOSITY WORKSHEET

SAMPLE NAME	TEMP	TIME	CONSTANT	CANTENITY(KA)		DENSITY	CENTIPOISE (CP)	MEAN
				0.010329	0.010329			
RK-1248	0	719.52	0.010329	0.010329	0.010329	1.001	7.15907945	7.15907945
	0	719.5	0.010329	0.010329	0.010329	1.001	7.15907441	7.15907441
	0	719.48	0.010329	0.010329	0.010329	1.001	7.15907166	7.15907166
	0	719.39	0.010329	0.010329	0.010329	1.001	7.144464609	7.144464609
	0	720.31	0.010329	0.010329	0.010329	1.001	7.367094932	7.367094932
	0	720.32	0.010329	0.010329	0.010329	1.001	7.358153418	7.358153418
	20	352.81	0.010329	0.010329	0.010329	1.001	2.610243457	2.610243457
	20	352.81	0.010329	0.010329	0.010329	1.001	3.616083326	3.616083326
	20	352.5	0.010329	0.010329	0.010329	1.001	3.613535556	3.613535556
	20	352.16	0.010329	0.010329	0.010329	1.001	3.610020047	3.610020047
	20	352.66	0.010329	0.010329	0.010329	1.001	3.6131251684	3.6131251684
	23	314.61	0.010329	0.010329	0.010329	1.001	3.241766144	3.241766144
	24	314.46	0.010329	0.010329	0.010329	1.001	3.124216103	3.124216103
	25	314.43	0.010329	0.010329	0.010329	1.001	3.1096	3.1096
	25	314.91	0.010329	0.010329	0.010329	1.001	3.219968359	3.219968359
	25	314.17	0.010329	0.010329	0.010329	1.001	3.244234335	3.244234335
	40	271.84	0.010329	0.010329	0.010329	1.001	3.237257265	3.237257265
	40	271.33	0.010329	0.010329	0.010329	1.001	2.39371684	2.39371684
	40	271.35	0.010329	0.010329	0.010329	1.001	3.295487617	3.295487617
	40	271.41	0.010329	0.010329	0.010329	1.001	2.393679461	2.393679461
	40	271.3	0.010329	0.010329	0.010329	1.001	2.29432044	2.29432044

MONOGRAPHIA VISCOELASTICITATIS

12-14

Table 3
Stabilized NASA HAN and Unstabilized NASA HAN
Viscosity Calculations

12-15

SAMPLE NAME	TEARF	TIME	CONSTANT	CENTISTOKE (cS)	DENSITY	CENTISTOKE (cP)	MEAN
Stabilized NASA HAN	0	021.35	0.014329	11.7035	1.3617	1.3617	1.65551254
	0	021.46	0.014329	11.7664	1.3617	1.3617	8.60963302
	0	022.36	0.014329	11.7925	1.3617	1.3617	8.660130719
	0	021.18	0.014329	11.7658	1.3617	1.3617	8.64135252
	0	021.33	0.014329	11.7688	1.3617	1.3617	8.641712604
	0	446.34	0.014329	6.3939	1.3617	1.3617	4.78045377
	20	446.1	0.014329	6.3923	1.3531	1.3531	4.72608003
	20	446.84	0.014329	6.4021	1.3531	1.3531	4.75847041
	20	446.73	0.014329	6.4013	1.3531	1.3531	4.74265311
	20	446.1	0.014329	6.3922	1.3531	1.3531	4.73760905
	25	301.79	0.014329	5.9307	1.3566	1.3566	4.02671681
	25	301.79	0.014329	5.9303	1.3566	1.3566	4.02671681
	25	302.41	0.014329	5.9196	1.3566	1.3566	4.0233265542
	25	303.42	0.014329	5.9497	1.3566	1.3566	4.033343147
	25	302.43	0.014329	5.9487	1.3566	1.3566	4.031703175
	40	267.16	0.014329	5.8281	1.3551	1.3551	2.814951568
	40	268.13	0.014329	5.8412	1.3551	1.3551	2.814951511
	40	267.81	0.014329	5.8174	1.3551	1.3551	2.81182053
	40	267.6	0.014329	5.8344	1.3551	1.3551	2.82900671
	40	261.56	0.014329	5.8319	1.3551	1.3551	2.80616185

SAMPLE NAME	TEARF	TIME	CONSTANT	CENTISTOKE (cS)	DENSITY	CENTISTOKE (cP)	MEAN
Unstabilized NASA HAN	0	000.34	0.014329	11.4691	1.3502	1.3502	8.89263031
	0	000.07	0.014329	11.4655	1.3502	1.3502	8.892223671
	0	000.85	0.014329	11.4754	1.3502	1.3502	8.892027119
	0	001.15	0.014329	11.4797	1.3502	1.3502	8.89222169
	0	000.98	0.014329	11.4774	1.3502	1.3502	8.89318462
	0	001.74	0.014329	6.1466	1.3468	1.3468	4.54292554
	20	426.73	0.014329	6.1166	1.3468	1.3468	4.54020594
	20	426.64	0.014329	6.1133	1.3468	1.3468	4.31912979
	20	426.41	0.014329	6.1109	1.3468	1.3468	4.34690227
	20	426.51	0.014329	6.1115	1.3468	1.3468	4.31791288
	25	375.54	0.014329	5.3783	1.3443	1.3443	4.000967046
	25	375.53	0.014329	5.3411	1.3443	1.3443	4.0232615
	25	375.98	0.014329	5.3374	1.3443	1.3443	4.017581572
	25	375.81	0.014329	5.3321	1.3443	1.3443	4.00364592
	25	375.6	0.014329	5.3302	1.3443	1.3443	4.001570632
	40	233.07	0.014329	5.6262	1.3405	1.3405	2.70049825
	40	231.69	0.014329	5.6257	1.3405	1.3405	2.704535291
	40	231.2	0.014329	5.6281	1.3405	1.3405	2.706215526
	40	233.38	0.014329	5.6207	1.3405	1.3405	2.708264926
	40	231.55	0.014329	5.6311	1.3405	1.3405	2.710251794

Monopropellant Viscosity vs. Temperature

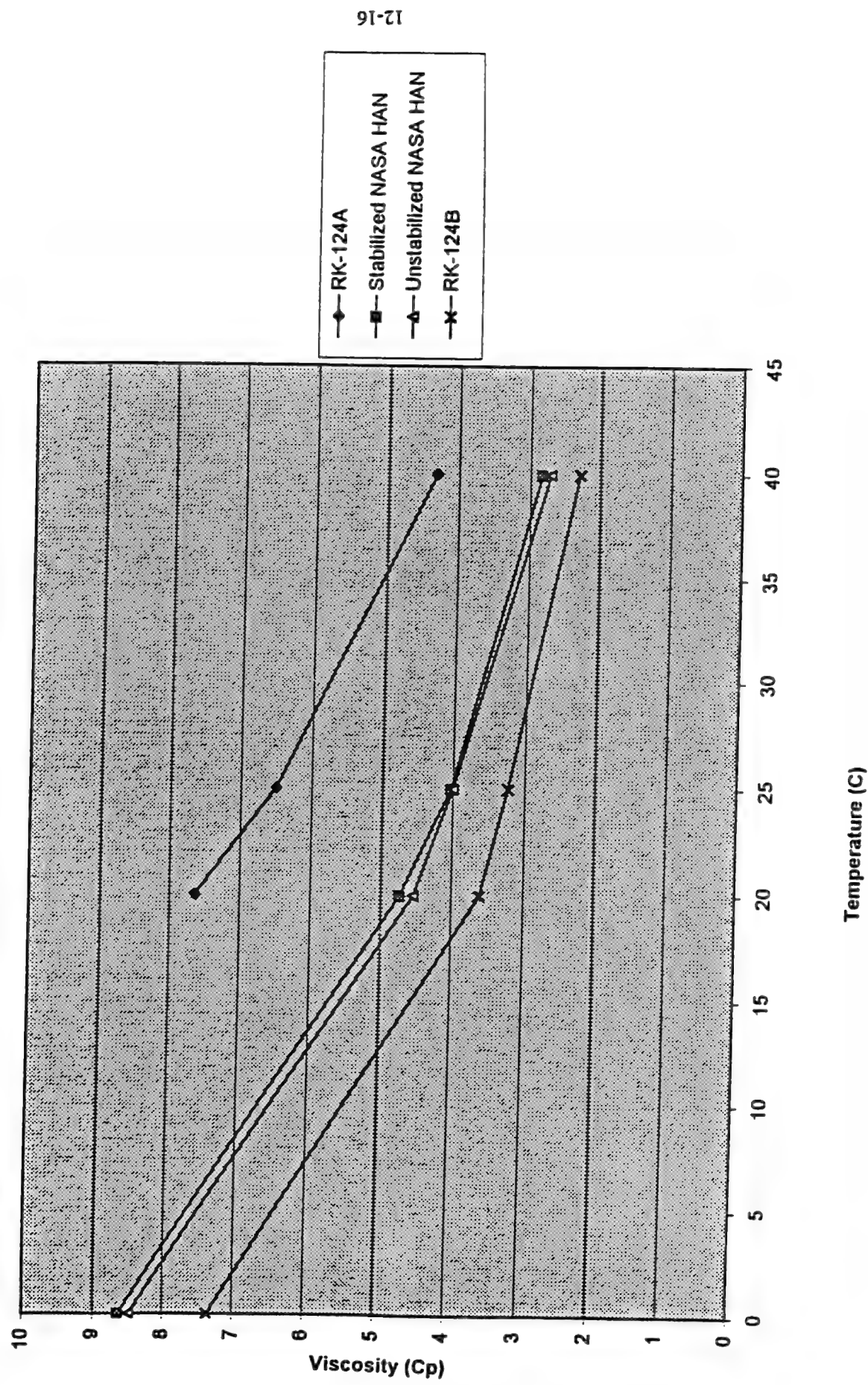
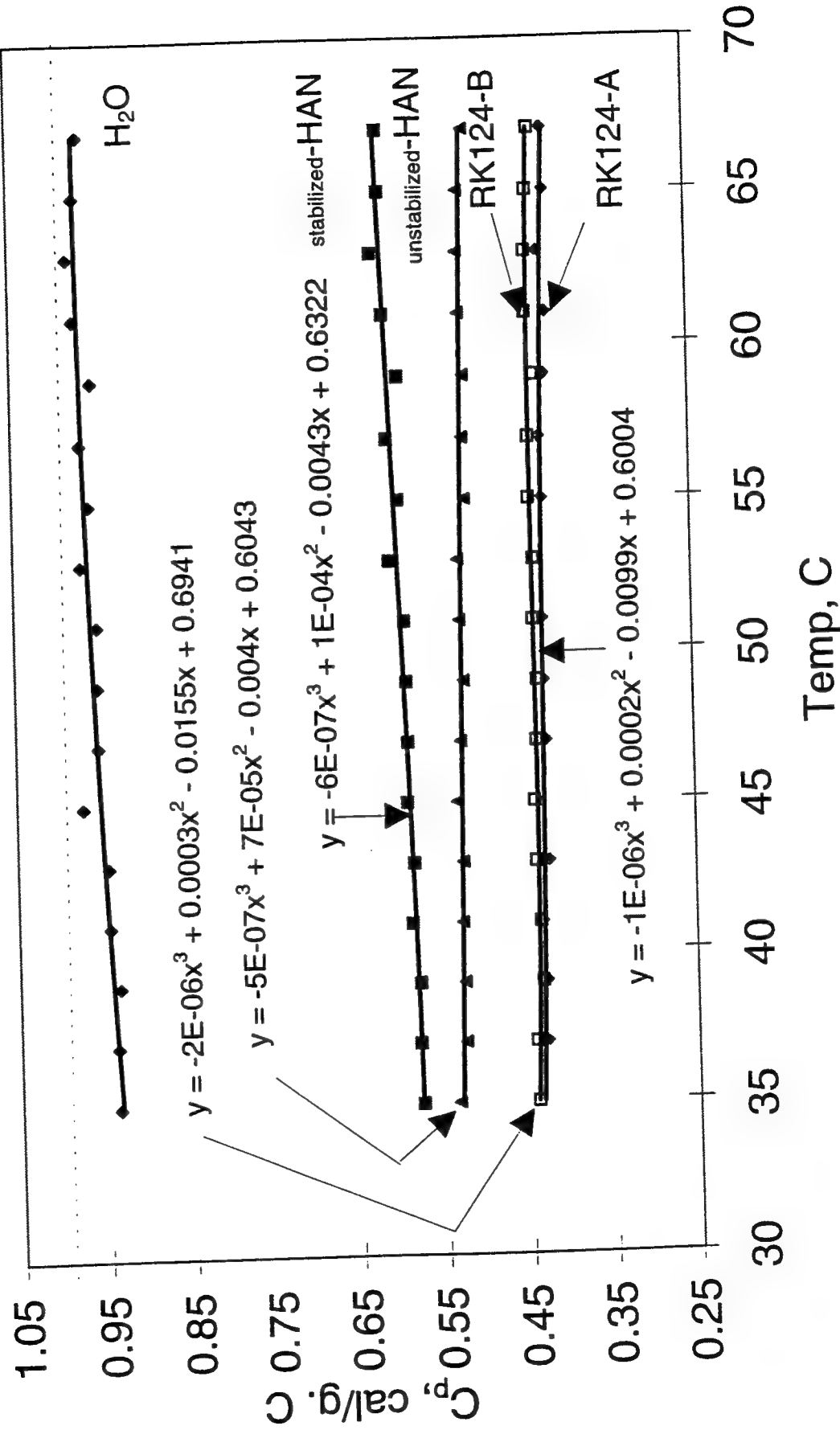


Table 5
Heat Capacity Calculations

Heat Capacity DATA										
Temp, C	H2O		US-HAN		RK124-A		RK124-B		S-HAN	
	J/g.C	J/g.C	J/g.C	J/g.C	J/g.C	J/g.C	Cal/g.C	Cal/g.C	Cal/g.C	Cal/g.C
31	2.9051	1.9603	1.5858	1.3693	1.4068	31	0.693341	0.467852	0.378473	0.326802
33	3.788	2.3346	2.1553	1.7765	1.8292	33	0.904057	0.557184	0.514391	0.423986
35	3.9287	2.4219	2.2427	1.8429	1.8529	35	0.937637	0.578019	0.535251	0.439833
37	3.9334	2.4307	2.2046	1.8013	1.8558	37	0.938759	0.580119	0.526158	0.429905
39	3.9178	2.4264	2.2046	1.7985	1.8195	39	0.935036	0.579093	0.526158	0.429236
41	3.9619	2.4591	2.2099	1.8134	1.825	41	0.945561	0.586897	0.527422	0.432792
43	3.9627	2.4451	2.2029	1.7766	1.8419	43	0.945752	0.583556	0.525752	0.42401
45	4.0804	2.4734	2.2226	1.833	1.8454	45	0.973842	0.59031	0.531265	0.43747
47	4.004	2.4656	2.2043	1.7824	1.832	47	0.955609	0.588449	0.526086	0.425394
49	4.0023	2.4678	2.185	1.7886	1.8235	49	0.955203	0.588974	0.52148	0.426874
51	3.9998	2.4716	2.1997	1.7892	1.8368	51	0.954606	0.589881	0.524988	0.427017
53	4.0722	2.5413	2.204	1.814	1.8289	53	0.971885	0.606516	0.526014	0.432936
55	4.0306	2.4928	2.1641	1.7825	1.8474	55	0.961957	0.59494	0.516492	0.425418
57	4.0674	2.5435	2.1703	1.7911	1.8451	57	0.97074	0.607041	0.517971	0.42747
59	4.0098	2.4852	2.161	1.761	1.8199	59	0.956993	0.593126	0.515752	0.420286
61	4.0917	2.5535	2.1784	1.7478	1.8481	61	0.976539	0.609427	0.519905	0.417136
63	4.1151	2.6065	2.1833	1.7841	1.8443	63	0.982124	0.622076	0.521074	0.4258
65	4.0806	2.5641	2.1739	1.7475	1.8329	65	0.97389	0.611957	0.518831	0.417064
67	4.0574	2.5677	2.1404	1.7522	1.8159	67	0.968353	0.612816	0.510835	0.418186
Average	4.019	2.495	2.191	1.789	1.836	Average	0.959	0.523	0.427	0.438

Heat Capacity of H₂O, HAN and Monopropellants

12-18



A STUDY OF THE INTERRELATION OF CLOUD THICKNESS
AND CLOUD LIQUID WATER CONTENT IN MARITIME STRATOCUMULUS

Carl W. Steinbach

Lincoln-Sudbury Regional High School
390 Lincoln Road
Sudbury, MA 01776-1012

Final Report for:
High School Apprentice Program
Phillips Laboratory

Sponsored by:
Air Force Office of Scientific Research
Bolling Air Force Base, DC

and

Phillips Laboratory

August 1997

A STUDY OF THE INTERRELATION OF CLOUD THICKNESS
AND CLOUD LIQUID WATER CONTENT IN MARITIME STRATOCUMULUS

Carl W. Steinbach
Lincoln-Sudbury Regional High School

Abstract

A statistics software package was used to evaluate data collected from a vertically pointing millimeter-wave cloud radar and from a vertically pointing two-channel microwave radiometer. Descriptive statistics were produced for pertinent variables as well as a regression analysis of cloud thickness in relation to cloud liquid water content. The results of these tests indicate that cloud thickness and cloud liquid water content are highly correlated, and that a straight line model describes this relationship.

A STUDY OF THE INTERRELATION OF CLOUD THICKNESS
AND CLOUD LIQUID WATER CONTENT IN MARITIME STRATOCUMULUS

Carl W. Steinbach

Introduction

Nascent attempts have been made, such as those of the Defense Meteorological Satellite Program (DMSP), to sense integrated cloud liquid water using the Special Sensor Microwave/Imager (SSM/I) instrument aboard the current generation of DMSP satellites. *Greenwald et al.* [1993] conducted an analysis of SSM/I-retrieved liquid water values, comparing them against ground based radiometer retrievals and found a theoretical average error between 25% and 40%, dependent on atmospheric/surface conditions and the amount of liquid water present in the cloud.

Techniques are also being devised to sense cloud layer thickness using orbiting radars. *Uttal* [1997] points out that despite the fact that most clouds are thin, less than 1.5 km, and the range resolution of 0.5 km of these proposed satellite radars would leave most clouds undersampled. Furthermore, studies have found that the cloudy atmosphere will have clouds present at more than one level roughly 50% of the time [*Uttal* 1997].

Existing ground based vertically pointing millimeter-wave radars, however, already provide detailed information about cloud layers and thicknesses and also exhibit a high sensitivity to hydrometeors and relative insensitivity to ground clutter. For example, the 8.7-mm wavelength NOAA/K Doppler radar is able to attain resolutions of 37.5m over 328 range gates. Used in conjunction with satellites and other atmospheric data collection devices, ground based millimeter-wave radars are playing a valuable role in weather prediction and research efforts.

Current experiments with such radars, besides testing the effectiveness of this technique, have also resulted in data which can be used to gauge correlations between cloud thickness, liquid water content and ice water content. These studies reaffirm the value of radars in an integrated data collection system by evidencing the frequency of multiple cloud layers.

The purpose of my project was to find a correlation between cloud thickness and cloud water content through a statistical analysis of data gathered in the Atlantic Stratocumulus Transition Experiment (ASTEX) [*Albrecht et al.* 1995]. A high correlation between these two variables would allow analysis systems to infer one from the other. It would also indicate that cloud water content values retrieved with SSM/I equipped satellites could be used to estimate cloud thicknesses. The accuracy of such estimates can be approximated by combining the standard error of the LWP/cloud thickness regression analysis with the standard error of the LWP retrieval. The accuracy that is achievable with this approach can then be compared with the accuracy of another method, under development at Phillips Laboratory, for retrieval of cloud thicknesses.

Methodology

As part of ASTEX, the NOAA/K field system was deployed to Portugal's Puerto Santos Island in 1992. Located in the subtropical Atlantic Ocean, Puerto Santos is positioned under a portion of the atmosphere where marine

stratocumulus cloud cover is predominant. This type of cloud covers large parts of the ocean's surface, and consequently plays a great role in the global climate. Data used in this paper results from a 27 day period of consecutive observations made in June using the NOAA/K millimeter-wave radar and a two-channel microwave radiometer.

Cloud layer and liquid water path data collected, respectively, by the NOAA/K radar and microwave radiometer, were archived at the National Oceanic and Atmospheric Administration's Environment Technology Laboratory (NOAA/ETL). Later, the cloud layer data were processed using CLDSTATS, a cloud boundary detection algorithm for vertically pointing radar data [Uttal *et al.* 1993]. CLDSTATS objectively determined cloud base and cloud top heights using user defined thresholds and distinguished between different cloud layers. Data from both sources were combined into data records. These records were provided at 3 s intervals with a separate record for each cloud layer.

Data records were filtered. Records with liquid water path values less than zero were deemed instances of insignificant cloud layer and were removed. Information entries contained in the output which were not pertinent to this investigation were also removed. An initial analysis of the processed data indicated that there were many records representing high altitude cirrus clouds. Figure 1 shows the original cloud top height frequency histogram which clearly indicates the presence of two distinct cloud layers representing different cloud types. As my study was only concerned with the lower altitude stratocumulus layers, the decision was made to remove all data points with cloud top heights above 3 km. This had the effect of eliminating the statistical outliers, i.e. the records representing cirrus cloud layers.

Analysis software constraints forced a further reduction in the size of the filtered dataset. 75% of the processed records were discarded using an algorithm that saved every fourth entry. This sampling method avoided making the data subset biased chronologically. Though only one data subset was used for detailed study, a total of four were created, each with different values. This allowed statistical comparisons to be made between the four subsets to assure that they were statistically identical. Each subset contained 13,046 records and had an observational interval of 12 s. Values such as the mean and median of the data subsets were computed for individual variables and then compared. These values differed by less than 0.01% between the different subsets.

The data subset was analyzed using the Microsoft Excel statistical software package. The analysis included the computation of descriptive statistics for variables including cloud base and top height, cloud thickness, and cloud liquid water content. The statistics software was also used to conduct a regression analysis of the dataset to find qualitative links between computed cloud thicknesses and corresponding recorded cloud liquid water path (LWP) values. To this end an analysis of variance (ANOVA) test was performed and regression statistics were calculated to assess the validity of the straight line model found through regression analysis. Values for the correlation constant r and square of the correlation constant r^2 were given by:

$$r^2 = \frac{SSY - SSE}{SSY}$$

where

$$SSE = \sum(Y_i - \hat{Y}_i)^2$$

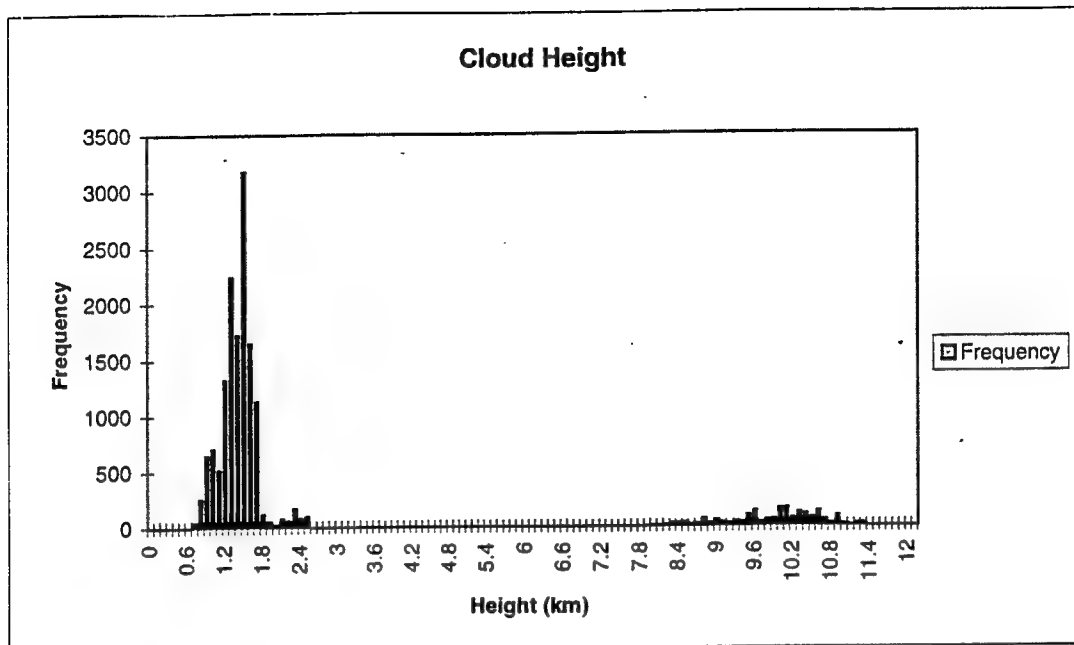


Fig. 1. Original cloud top height frequency histogram.

<i>Cloud Thickness</i>	<i>Cloud Base</i>
Mean	0.481144412
Standard Error	0.002417327
Median	0.41
Standard Deviation	0.276104842
Sample Variance	0.076233884
Range	2.34
Minimum	0.07
Maximum	2.41
Count	13046
Confidence Level(95.0%)	0.004738317
	Mean
	1.446543002
	Standard Error
	0.00313966
	Median
	1.41
	Standard Deviation
	0.358609094
	Sample Variance
	0.128600482
	Range
	2.44
	Minimum
	0.48
	Maximum
	2.92
	Count
	13046
	Confidence Level(95.0%)
	0.006154197

Fig. 2. Descriptive statistics summaries for cloud thickness, cloud base height, and cloud top height.

<i>Cloud Top</i>	
Mean	1.446543002
Standard Error	0.00313966
Median	1.41
Standard Deviation	0.358609094
Sample Variance	0.128600482
Range	2.44
Minimum	0.48
Maximum	2.92
Count	13046
Confidence Level(95.0%)	0.006154197

and

$$SSY = \sum(Y_i - \bar{Y})^2$$

where the summation is carried out over all data records i . Y_i is a cloud thickness value, and SSE and SSY are the Error Sum of Squares and Y Sum of Squares respectively. \bar{Y}_i is the sample mean for the Y_i 's and \hat{Y}_i denotes the estimated response at X_i (a LWP value) based on the fitted regression line.

Results

Descriptive statistics results for cloud thickness, cloud base height, and cloud top height are summarized in Figure 2. The mean cloud thickness value of 0.48 km agrees with other studies [*Uttal*].

Frequency distribution histograms of cloud thickness, cloud top height, and cloud base height (Figures 3, 4, and 5 respectively) illustrate the distributions of these variables. These histograms also illustrate the cumulative frequency of the variables. From Figure 3 it can be determined that 95% of the sampled clouds were less than 1.0 km thick. Similarly, it can also be determined that 95% of the sampled clouds had tops below 2.0 km and bases below 1.5 km.

Regression statistics and ANOVA test results are listed in Figure 6. The value of the correlation coefficient (r) for the regression analysis, 0.745, indicates that there is a high degree of linear association between the cloud thickness variable and liquid water content variable. The value of the square of the correlation coefficient (r^2), 0.55, indicates that 55% of the variation in the cloud thickness variable can be explained by variations in the cloud liquid water path variable. Collectively, the values of the correlation coefficient and its square indicate that it was valid to use a straight line model to approximate this relationship.

The equation for the line, of the form

$$y = \beta_0 + \beta_1 x$$

had a y intercept value, β_0 , of 0.305, and an x coefficient value, β_1 , of 0.00338. These results and other related values are summarized in Figs. 6 and 7.

Conclusion

My analysis of the cloud data made it clear that the millimeter-wave cloud radars are valuable research tools. Their ability to provide a highly detailed picture of the vertical structure of cloud masses is a great asset. This situation will not likely change. Proposed satellite radars with resolutions of 0.5 km would be ineffective at gauging vertical cloud structure as 95% of clouds sampled were found to have thicknesses of less than 1 km.

One concern that should be considered is that the datasets upon which this study is based are relatively small and restricted in terms of geography and season. More observations with vertically pointing millimeter-wave radars in different parts of the world at different times of the year need to be made before any greater significance can be drawn from these limited results.

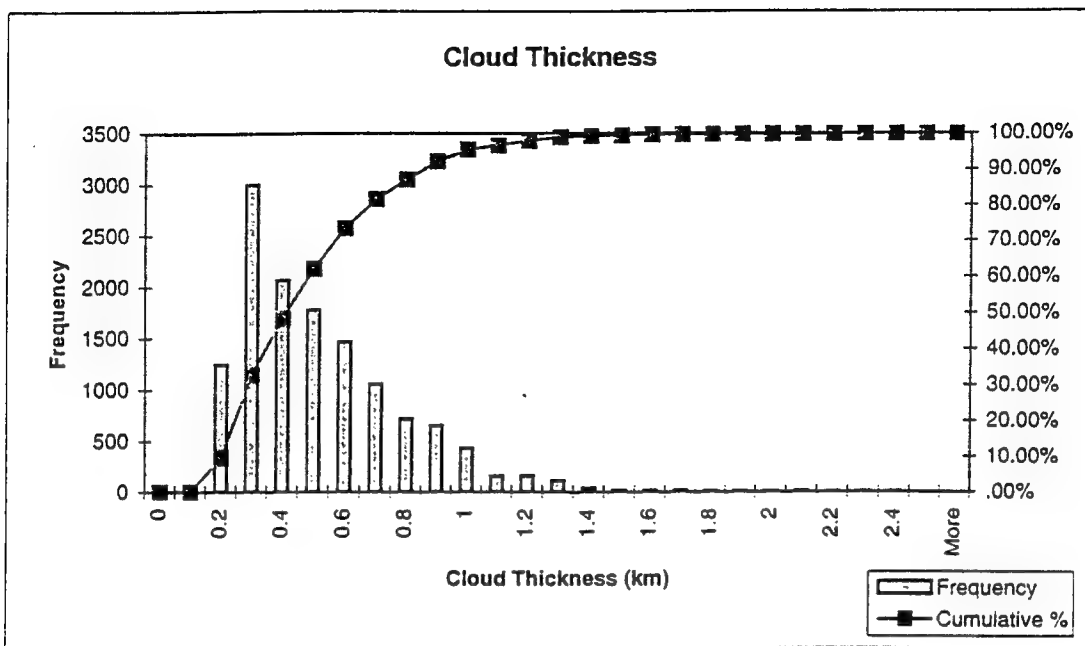


Fig. 3. Combination frequency distribution/cumulative frequency histogram of cloud thickness.

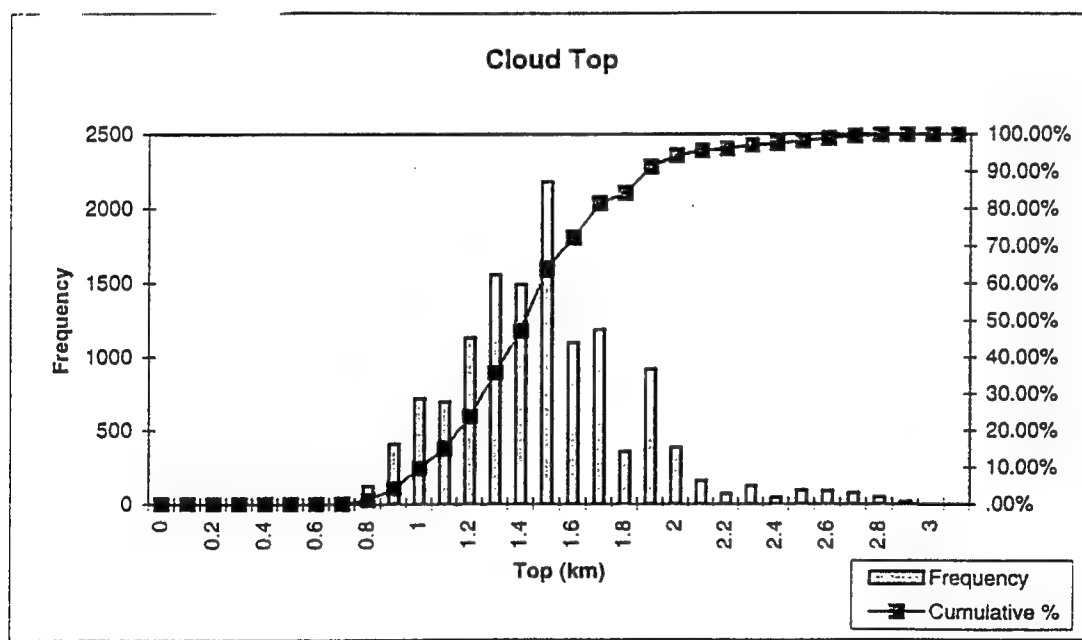


Fig. 4. Combination frequency distribution/cumulative frequency histogram of cloud top height.

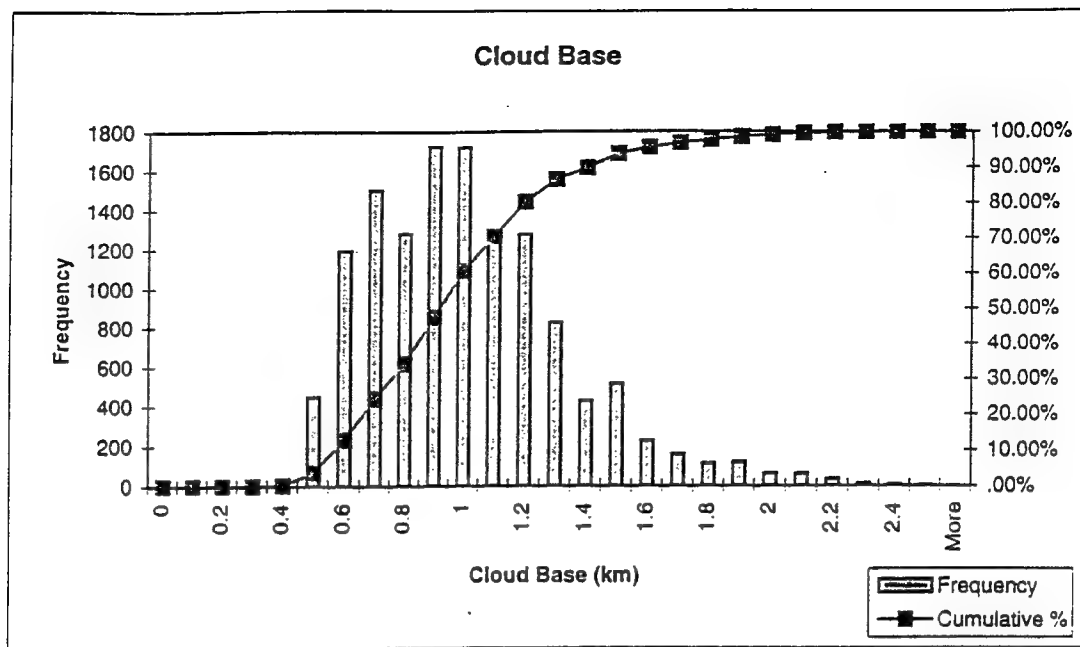


Fig. 5. Combination frequency distribution/cumulative frequency histogram of cloud base height.

ANOVA

	<i>df</i>	<i>SS</i>	<i>MS</i>	<i>F</i>	Significance <i>F</i>
Regression	1	551.2319481	551.2319	16222.1	0
Residual	13044	443.2390658	0.03398		
Total	13045	994.4710139			

	Coefficients	Standard Error	t Stat	P-value
Intercept	0.305282598	0.002123947	143.7336	0
X Variable 1	0.003376238	2.65082E-05	127.366	0

Regression Statistics	
Multiple R	0.744511012
R Square	0.554296647
Adjusted R Square	0.554262477
Standard Error	0.184337469
Observations	13046

Fig. 6. Regression statistics and ANOVA test results.

Cloud Thickness vs. Liquid Water Path

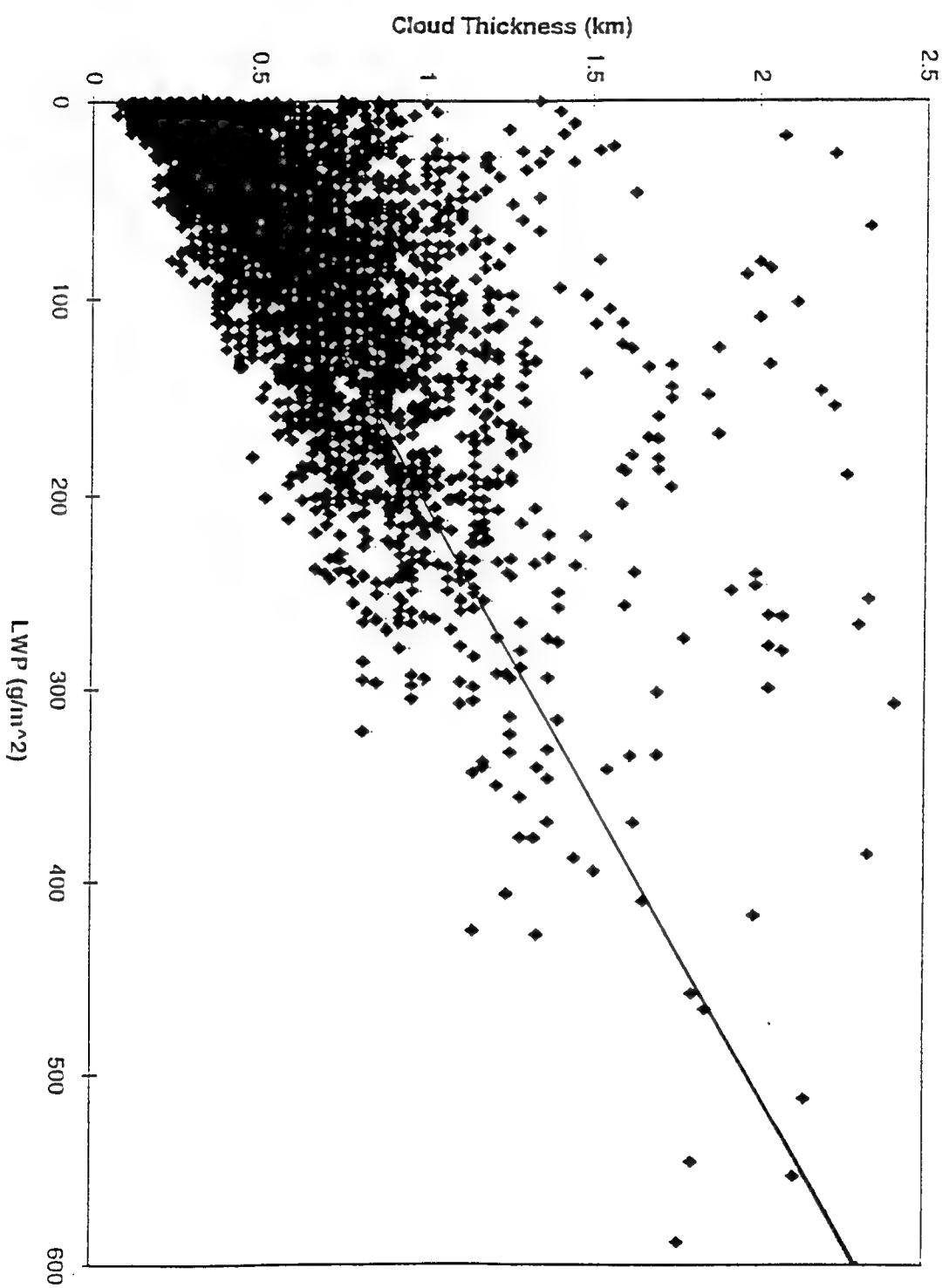


Fig. 7. Cloud thickness vs. LWP scatter plot with regression line.

Finally, it should be noted that in addition to all of the advantages of millimeter-wave vertically pointing radars, there are some disadvantages as well. Of these problems the most serious is the inability of millimeter-wave radars to function appropriately during rainstorms, hurricanes, etc. This factor significantly reduces the number of possible applications of this instrument.

Acknowledgments

This study is based upon data collected by the National Oceanographic and Atmospheric Agency's Environment Technology Laboratory and posted on the World Wide Web at <http://www6.etl.noaa.gov/data/#astex>.

References

Greenwald, T. J., G. L. Stephens, T. H. Vonder Haar, and D. L. Jackson, 1993:

A physical retrieval of cloud liquid water over the global oceans using Special Sensor Microwave/Imager (SSM/I) observations. *J. Geophys. Res.*, **98**, 18471-18488.

Albrecht, B. A., C. S. Bretherton, D. Johnson, W. H. Schubert, and A. S. Frisch, 1995:

The Atlantic stratocumulus transition experiment--ASTEX. *Bull. Am. Meteorol. Soc.*, **76**, 889-904.

Hogg, D. C., F. O. Guiraud, J. B. Snider, M. T. Decker, and E. R. Westwater, 1983:

A steerable dual-channel microwave radiometer for measurement of water vapor and liquid in the troposphere, *J. Climate Appl. Meteor.*, **22**, 789-806.

Uttal, T., 1997:

Detection of cloud boundaries with 8 millimeter-wave radar. [Http://www6.etl.noaa.gov/review/tav](http://www6.etl.noaa.gov/review/tav).

Uttal, T., L. I. Church, B. E. Martner, and J. S. Gibson, 1993:

A cloud boundary detection algorithm for vertically pointing radar data. *NOAA Tech. Memo. ERL WPL-233*, NOAA Environmental Research Laboratories, Boulder, CO, 28 pp. [Available from the National Technical Information Service, 5285 Port Road, Springfield, VA 22161]

**OPTICALLY ADDRESSED SPATIAL LIGHT MODULATORS
AS REAL-TIME HOLOGRAPHIC MEDIA**

Nhi T. Tran

**Manzano High School
12200 Lomas Blvd. NE
Albuquerque, NM 87112**

**Final Report for:
High School Apprentice Program
Phillips Laboratory**

**Sponsored by:
Air Force Office of Scientific Research
Bolling Air Force Base, DC**

and

Phillips Laboratory

August 1997

**OPTICALLY ADDRESSED SPATIAL LIGHT MODULATORS
AS REAL-TIME HOLOGRAPHIC MEDIA**

Nhi T. Tran
Manzano High School

Abstract

An optically addressed spatial light modulator (OASLM) and its effects on a compensated imaging process using real-time holography were studied. Use of a spatial light modulator to improve efficiency of real-time adaptive optical corrective techniques for telescope and atmospheric-induced path aberrations is significant because it makes the development of large, lightweight, low-optical-quality primary mirrors possible.

OPTICALLY ADDRESSED SPATIAL LIGHT MODULATORS AS REAL-TIME HOLOGRAPHIC MEDIA

Nhi T. Tran

Introduction

In recent years, the usage of an optically addressed spatial light modulator (OASLM) for works related to real-time adaptive optical correction for telescope and atmospheric induced path aberrations have come forth with new technology. Traditional telescope imaging can have defects due to atmospheric disturbance, misalignment of telescope optics and primary mirror distortion. In addition to the construction problems arise the problem of transporting heavy, high-optical primary mirrors into space. However, compensated imaging techniques have been studied as possible solutions to the problem by correcting the usage of low-optical-quality primary mirrors for imaging.

Background:

Spatial light modulators (SLM) are optical modulators constructed so as to spatially modulate, to a prescribed input, a readout optical beam where the input can be either optical or electrical{1}. The overall function of the SLM is to use optical techniques in processing the two-D information in which the input data is processed. SLMs are used in a variety of different fields such as fiber-optics communication systems, imaging, communicating data, and delivering optical power through an aberrated optical media.

Methodology: Experimental Setup{2}

Using the output from a helium neon laser operating at 543nm, an object point source at infinity is simulated by illuminating a 20mm pinhole and collimating the transmitted light with a six-inch diameter f/6 parabolic reflector. The collimated light is then directed towards the membrane mirror telescope. Next, the output from the 5mW green helium neon laser is used as the local beacon wavefront for the membrane mirror telescope. The output is then expanded and guided through a null corrector, with positive and negative lens, and onto the primary mirror surface. From the null corrector, a f/6 parabolic wavefront is produced and coincides with the normal center of curvature of the membrane primary mirror. After generating through the focus and illuminating the membrane

mirror, the beacon wavefront is retroreflected and recollimated by the null corrector. In the pupil plane produced by the null corrector, the beacon wavefront optical path difference relative to a planar wavefront is equal to twice the membrane mirror surface optical path difference from the ideal parabolic surface. The pupil plane is then directed to the "write" side of the OASLM where it interferes with a mutually coherent plane wave derived from the same laser to record the phase aberration information in the hologram. In this demonstration, near diffraction limited imaging was achieved using a membrane primary mirror with more than 200 waves of aberration.

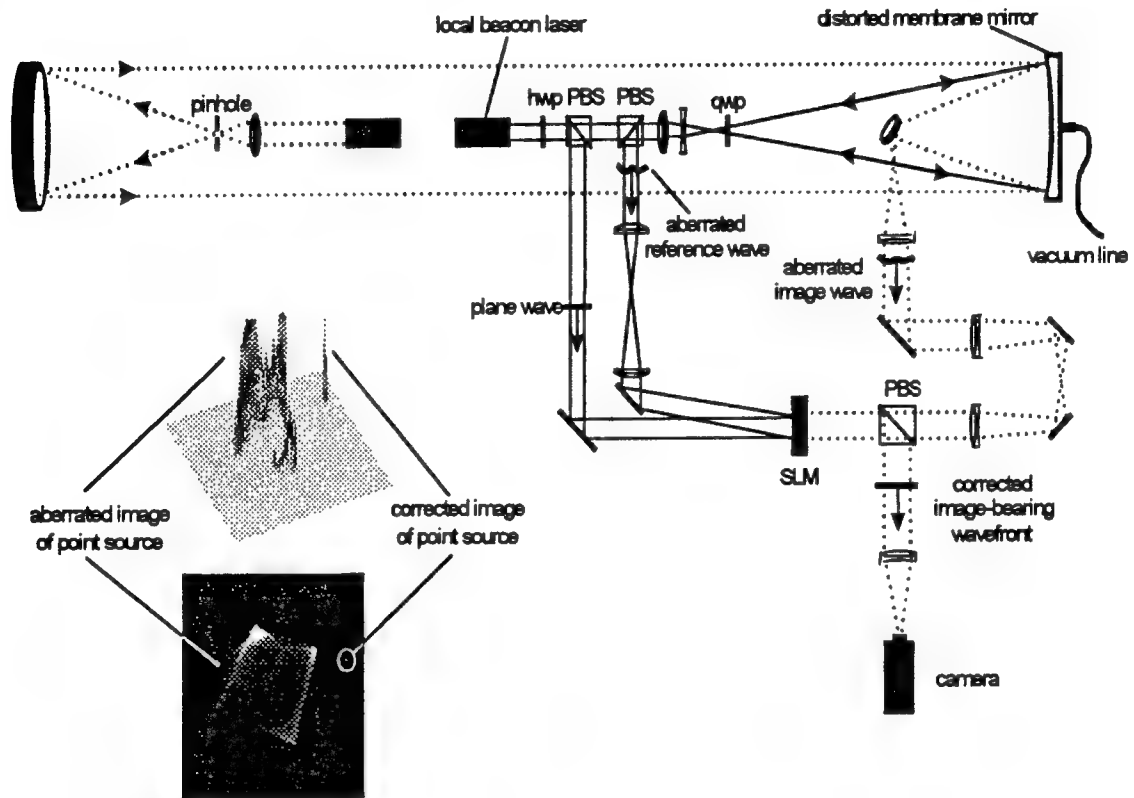


Figure 1. Experimental setup along with a two-dimensional photograph and three-dimensional intensity contours of aberrated and corrected images of a point source imaged by a low-optical-quality membrane optics using a real-time holographic phase subtraction technique. SLM, spatial light modulator; hwp, half-wave plate; qwp, quarter-wave plate; PBS, polarizing beam splitter.

Membrane mirror{2}:

The membrane mirror consists of a six-inch diameter, high-reflectivity-coated, four-micron-thick, nitrocellulose membrane attached to a vacuum flange and held under partial vacuum to approximate an f/6 primary mirror. The surface is characterized using an f/6 parabolic wavefront at one-micron wavelength in an interferometer setup to write the hologram in Figure 1.

SLM{2}:

A Displaytech ferroelectric OASLM operating at 300Hz acts as the real-time hologram. The aberrated image-bearing light is directed to the "read" side of the SLM that lies in the pupil plane for the image light. Due to the internal reflection, the OASLM generates diffracted light in the backward direction. The reflected light is propagated to a camera located in an image plane for the pinhole.

Problem

The purpose of the experiment was to transmit the image through distorting media using a SLM as a means of compensating for path distortions. However, to accomplish this mean, the diffraction efficiency of the SLM must be maximized. Commercially available parallel aligned nematic devices produce analog diffraction hologram with demonstrated efficiencies in excess of 30%{3}. For that purpose, the Hamamatsu parallel aligned nematic liquid-crystal spatial light modulator (PAL SLM), model number X5641, was tested to show the greatest amount of diffraction efficiency.

In Figure 2. the PAL nematic OASLM was tested using a green helium-neon laser at 543nm. The SLM is placed on a rotating stage where the resolution can be observed. The line spacing on the SLM is dependent on the angle of the two beams using the equation

$$p = \theta \text{ (in radians)}$$

$$\lambda$$

The SLM needs a certain angle to achieve a certain amount of line spacing. In order to achieve this, the SLM is lined up perpendicular to one beam. Using the rotating stage, a certain degree changes the surface on the SLM to

get the second beam to retroreflect where the angle between the two beams is equivalent to the angle on the rotating stage. From there, the diffraction efficiency is recorded.

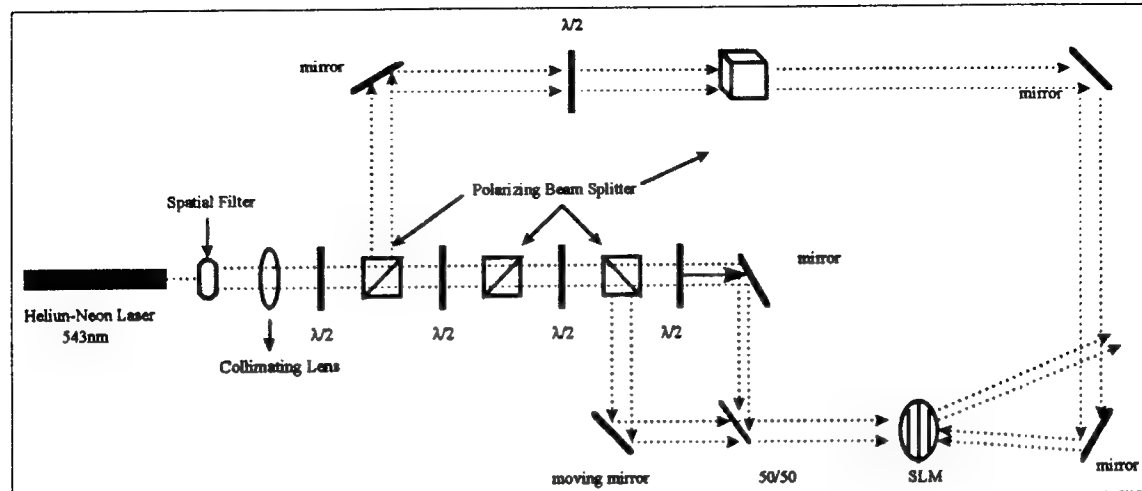


Figure 2. Experimental setup for the PAL nematic OASLM and the diffraction efficiency data recording. $\lambda/2$, half-wave plate; SLM, spatial light modulator.

Results

Working with various situations such as changing the resolution or the crossing-angle of the two beams, the diffraction efficiency never achieved the set amount of 30% according to the Hamamatsu handbook{3}. In Figure 3., the diffraction efficiency was at its highest level reaching about 23% with the spatial frequency at 10 lines/mm. Figure 4. shows different spatial frequency recorded and the diffraction efficiency that was generated.

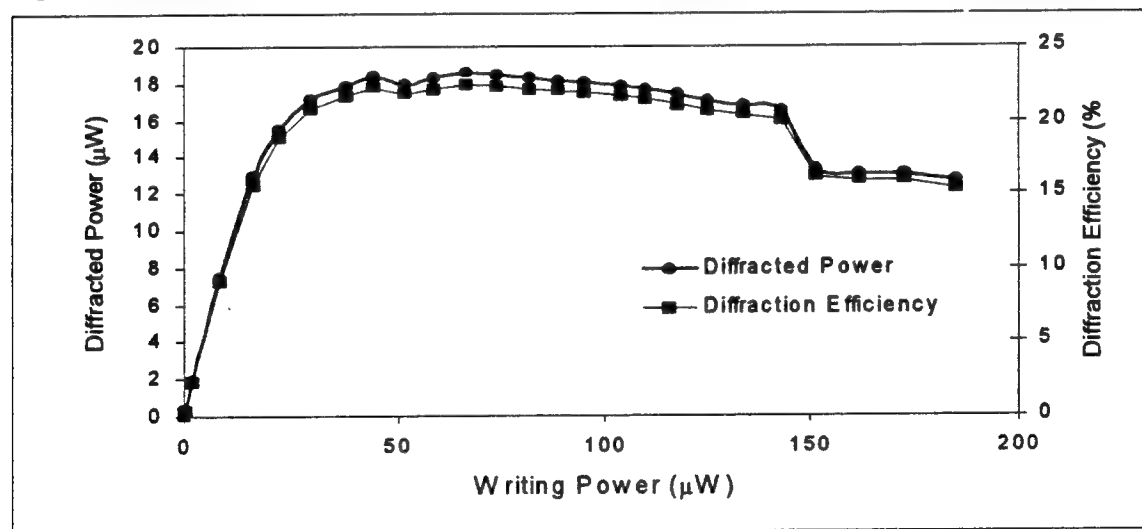


Figure 3. The highest level for diffraction efficiency of the Hamamatsu SLM. Crossing angle: 0.310 degrees; spatial frequency: 10 lines/mm; scaling information: 0.727953; readout power: 82.3 μm ; reference beam: 254 μm ; input beam (both): 184.9 μm ; input beam (first): 93.3 μm ; input beam (second): 91.9 μm .

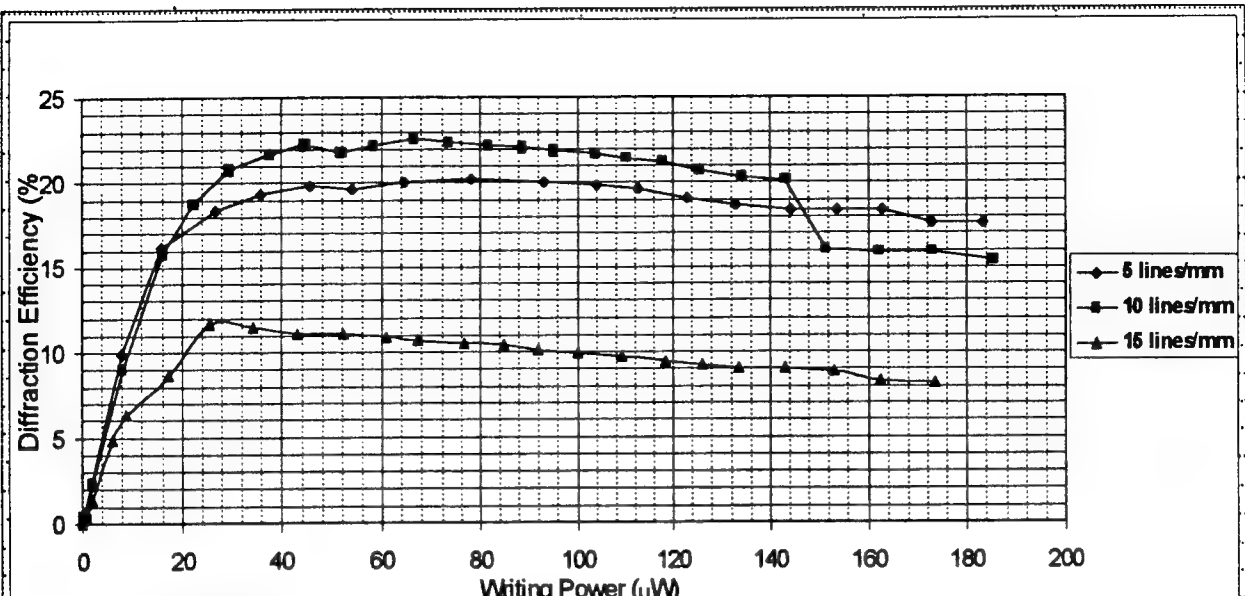


Figure 4. Diffraction efficiency comparison for different resolution.

Conclusion

The low net efficiency may be caused through variable problems associated with the use of the SLM. First, the interface of the SLM is amorphous-silicon resulting in the loss of diffraction of the image light upon reflection. Also, the SLM could also absorb light causing the efficiency to decrease.

Due to the low net diffraction efficiency of the SLM, the severity of the aberration that can be corrected in the application to the low-optical-quality primary mirror is limited. Improving the resolution to greater than 100 1/mm while maximizing the diffraction efficiency would make the SLM adequate for this application.

Acknowledgments

Special thanks to Mark Gruneisen, Chris Clayton, Roger Ramsey , and Mike Woods for their guidance in writing this paper.

References

1. Efron, Uzi "Spatial Light Modulator Technology: Material, Devices, and Applications". Marcel Dekker, Inc. New York,1995..
- 2.M.T. Gruneisen and J.M. Wilkes, "compensated Imaging By Real-Time Holography with Optically Addressed Spatial Light Modulators," Spring Topical Meeting on Spatial Light Modulators, Lake Tahoe, NV, March 17-19, 1997, Paper STuB5.
- 3.Hamamatsu technical data sheets for model X5641 PAL-SLM parallel aligned nematic liquid-crystals spatial light modulator.

Constructing a Computer Model of the Space Shuttle
and
The Effects of Lasers on Materials in Space

Jeremy L. White

Sandia Preparatory School
532 Osuna Rd NE
Albuquerque, NM 87113

Final Report for:
High School Apprentice Program
Phillips Laboratory

Sponsored by:
Air Force Office of Scientific Research
Bolling Air Force Base, DC

and

Phillips Laboratory

August 1997

Constructing a Computer Model of the Space Shuttle
and
The Effects of Lasers on Materials in Space

Jeremy White
Sandia Preparatory School

Abstract

The possibility of a space based war is ever increasing due to the advantages of carrying out certain tasks in space. It is important to have an accurate assessment of the situation in any war because it helps you to make important decisions during the battle, and these decisions can either help you win or loose the war. There is only one problem with using conventional methods of gathering intelligence information, and that is that they will not work. These methods will not work because they involve traveling to the target and observing the area, and that is not possible in space because it is so inaccessible. Satellites can be used to monitor the situation but visual information is still limited. That is why three dimensional modeling is being used, because there is always a visual representation that can be updated. Since the original is still available, the two images can be compared to more accurately assess the status of the target.

Another thing that has to be considered is the use of lasers. Since they are such a new weapon, the effects are still being researched, but that information is needed in the case of a war, because if you don't know what a laser can do to an orbiting spacecraft, then you can't accurately judge the status of a target that has been under laser attack. It also helps one to know what you can do to an enemy spacecraft.

Constructing a Computer Model of the Space Shuttle
and
The Effects of Lasers on Materials in Space

Jeremy L. White

Introduction

With the growing interest in the exploitation of space, there is also an increasing risk of war activities being conducted in space. One of the most important things that one can have in a war is accurate intelligence. A computer program called IDASS, which stands for Intelligence Data Analysis System for Spacecraft, is being developed in order to improve our intelligence capabilities in the possible case of a space based war. One technique that has been used in this program is the exploitation of computer generated three dimensional models of orbiting spacecraft. This allows for the use of visual intelligence information, which is sometimes the most helpful form of information. One other important thing that has come up is the possible use of lasers as weapons. Since lasers have never been used as weapons before, research is being done in order to find out how a laser can affect a target. This research will most likely play an important part in the gathering of intelligence data.

Discussion of the Problem

There really was no problem involved with the work I did on modeling the space shuttle. There were attempts to do it by other people working at the lab, but there just

was not enough time to construct a model quite as detailed as the one that I made. In other words, this project was just something that needed to be done. The problem with the advent of high powered laser technology, is that they will likely be the weapon of choice if a space based war ever breaks out. This causes difficulty in being able to anticipate possible damage from enemy weapons, because we still do not know exactly what a laser could do to a spacecraft. We do know that a laser could burn a hole into the craft, but there could be other things that might be a direct result of the burn damage. There is a possibility that the laser burn would not completely cripple a satellite, or spacecraft, but the things that we do not yet know about could finish the job. When damage is being inflicted upon anything, there will always be some debris resulting from that damage. We do know how to predict what the weapon will do in terms of debris, and also what that debris will do. A major difference between the environment in space, and the environment on earth is that there is no air in space. Space is a vacuum, so therefore any debris, especially small debris, will behave differently due to the lack of resistance. This fact makes it impossible to predict what will happen with that debris, because we have never seen little debris affect anything because the particles in our atmosphere put a stop to their movement before they can get anywhere. The other thing that prohibits the anticipation of debris damage to spacecraft is the fact that there is an absence of gravity in space. This will also change the way that all debris will behave, because the particles will not fall to the ground, but they will go in every direction, uninhibited, unless they hit something else floating around in space. One other thing, which has not been found to really affect the flow of debris, is the extreme low

temperatures which are found in space. The only thing that these low temperatures have been proven to affect, is the effectiveness of the laser. A laser does damage by heating, melting and weakening the material. The low temperature will prolong the heating process, because it has to start from a lower temperature than those encountered on earth. We can replicate the lack of air in space, by using vacuum chambers, and by also using liquid cooling processes, we can simulate the low temperatures of the space environment. The biggest problem with trying to simulate the space environment is that we do not yet have an effective way of simulating a zero gravity environment. So research done on earth will not be totally accurate.

Methodology

As part of my summer research program I was privileged to be able to construct a three dimensional model of the space shuttle for use with IDASS, using a program called SMT, or Satellite Modeling Tool. The first step in this process was to find a detailed representation to base my model on. The most important part about this representation was that it include measurements for the shuttle, because my model needed to be made to scale accurately. The next thing to do was to then test the different scales in the modeling program with the space shuttle measurements in order to find a scale that will allow the space shuttle to fit on the screen, and that scale turned out to be meters. Once that was done, I began to fabricate parts of the shuttle. I measured each component on the picture, and then converted those into the scale within the program. Within the modeling program there is a set of predetermined shape formats with which you must

construct your model with. They range from cones, to cubes, to cylinders. To make a shape with these formats, you must input the points, on a three dimensional coordinate plane, which the computer uses to build the shapes. This is how every piece of the model is formed. The name for the basic part of a model is called an element, which can have multiple shapes inside them. Creating the elements is one of the most difficult and time consuming parts of the process because there are so many of them involved. Once that was complete, then came the difficult task of assembling all of those pieces, correctly, into the form of the shuttle. In order to do this, the elements must be combined into assemblies. The angles and positions of the elements must be manipulated within the assemblies to form the correct shape. Then the assemblies must be joined together into larger assemblies, until the last assembly, which forms the entire model of the shuttle. This was a very difficult and time consuming part of the modeling process. The reason that this was so difficult was that in order to place the shapes into the correct positions, I had to manipulate each aspect of every shape within the three dimensional coordinate plane. I was forced to make changes on each axis of every shape, x, y, and z axes. This included manipulating the angles of each shape according to each axis, and also I had to specify the distance from the center of the axis that each shape was placed. As soon as the shuttle was completely assembled, I then proceeded in designating which parts of the model could be moveable. In order to do this I put the coordinates of the point on the grid where the axis of rotation would begin for each moving part. After that was complete I set the limitations of movement for the part on each three hundred and sixty degree axis. In order to check and make sure that the rotation parameters were set

correctly I brought up that shape into the dynamics tool to animate the movement. Then, if it wasn't moving the way that I had wished it to, I would modify the rotation parameters. I would then animate that shape again, and this cycle was repeated until the correct settings were found. This did get easier, however, as I became more familiar with the way that each input into the rotation settings affected the movement of the part. The next and final part of the modeling process was to assign the correct material properties for each part of the space shuttle. This was simple, as there was a list of properties to pick from, but because I had to go and set this for some individual elements, it took a long time to complete. Since there are special coatings and paint and other such things that can be put on the outside of the parts, the material of the bulk of the part, and the surface of the part, both had to be individually assigned, whether it be an assembly or an element. With the completion of that, the task of modeling the shuttle was complete. The next part of the modeling, was to mate the shuttle with another, previously constructed model of the Mir Space Station, which was of an equal scale. The only thing I had to do to accomplish this was to again find a detailed picture of the two while the shuttle was docked. I constructed a docking module for the two and attached the two pieces of it in their correct places. Then, using the picture, I aligned the shuttle up with the space station, and joined the two spacecraft, and that completed my task of modeling the space shuttle.

The next project that I was involved with was studying the effects of lasers on different materials in space. The process for setting up these tests were not terribly complicated. The first thing to do is to go around and turn on all of the machines. The

list of machines was incredibly long, but it consisted mostly of various calorimeters, and computers and cameras. Once the computers had booted up, the other lab personnel would bring up the proper programs to be used during the test. I never learned how do this, or to really learn how to use the programs, except for the slide scanning software. Then we would uncover all of the optics and ready the laser for a test shot. Before firing the laser we would line up the optics, so that the laser beam would be in the right position. With that completed, we would set a graphite block in front of the vacuum chamber so that the laser would not damage anything inside the chamber, and we always put on protective goggles, which block out the wavelength of light that the laser operates in, which is a wavelength of $1.315\mu\text{m}$. The other safety precaution that was taken was the use of lenses that have an AR, or anti-reflective coating for that same wavelength. This prevented any unwanted stray laser beams in the lab. On the test shot, or shots, depending on whether all of the equipment was functioning properly or not, we would use an infrared light detector card which would show where the laser beam hit, to see that the laser was lined up in the right place with all of the various instruments. Then we would mount the target on an aluminum plate which was bolted to a fixed stand within the vacuum chamber. For the next test shot after that, the graphite block was removed, and the alignment of the laser beam with the target was checked using that same infrared light detector card. During this test, there would be an attenuator lens in front of the laser, which would only transmit some of the lasers full power through to the target. The rest of the light was directed towards another, larger graphite block behind the laser. The reason that graphite blocks were used to stop the laser beam, is that they have almost zero

reflectance, which kept the beam from going else where, and because they can withstand high amounts of heat. We would then adjust the position of the target according to where the laser beam hit it, unless the beam was much higher than it should be, then we would adjust the last lens before the vacuum chamber to compensate. Once the target was aligned, the sensors inside the chamber would be checked to make sure they were in the right place, and making contact. A slide would also be mounted perpendicular, and right next to the target in order to collect the debris from the burn. We used several kinds of these: a glass slide, a polished copper slide, and a high index of refraction piece of glass. These varied as the people on the analyzation part of the test series ran into problems detecting the data, or debris, collected with their instruments. Once everything was found to be correctly positioned and setup, the vacuum chamber would be sealed up and pumped down. A roughing pump took care of most of the pressure, and then, a molecular pump would bring it the rest of the way down. We would let the molecular pump bring the pressure down to around 3×10^{-5} torr for every test, in order to simulate the conditions in space. This measurement was recorded, as it was important to know this in the case of any problems that might be run into, or other unexpected things that happened, which needed explaining. This would usually take about an hour or so to pump it down, and consequently, this limited the number of tests which could be done in a day. For some of the tests, we would also cool off the target using a cold finger, which we would use to take the target down to about -70 degrees centigrade, and this number would also be recorded. When the cold finger was used, the number of tests was limited even more, because if you broke vacuum before the target was back up to room

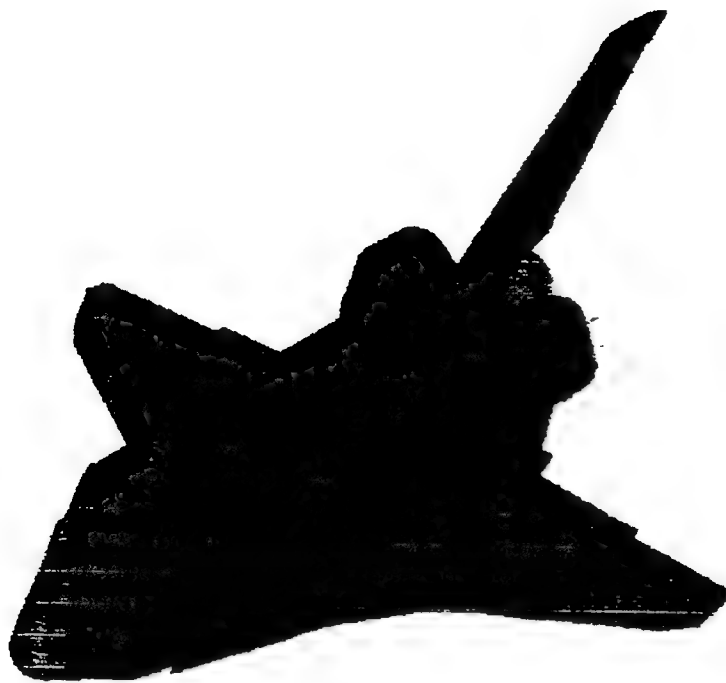
temperature, frost would form on the debris collection slide and ruin the collected data. The warming process would take all night, until the heat tape was installed to help it along. The heat tape, both inside, and outside of the vacuum chamber, was wrapped around the cold finger. This heat tape was able to bring it up to a temperature that would prevent the formation of frost on the data collection slide, in about one hour. Although the heating process was sped up considerably, the use of the cold finger stopped, because it appeared to have no effect upon the test results. While the vacuum chamber was pumping down, we would do a pre-test scan of the data collection slide(except not with high index of refraction glass due to different shape). This was done by computer control using a laser, and voltage detector mounted inside the chamber on a motor driven platform. Depending on which type of slide was used, the voltage reading from the photoelectric detector would be one of transmission (glass slide), or one of reflectivity (copper slide). This reading would be input onto a graph on one of the computers. As the motor moved the laser/detector assembly along the length of the slide, the voltage would change, which would show how much debris was on the slide. After this test, the computers would be reset, and everything would be readied for the final shot. Once the chamber was completely pumped down, we would all put on our protective goggles, and fire the laser. There would be no attenuator for this shot, and the test would last only a matter of seconds, anywhere from 3 - 25. Once all of the instruments had timed out, and stopped collecting data, we recorded the calorimeter data. This data included the runtime of the laser and most importantly, the average irradiance of the laser on the target. This was the measure of power put on a square centimeter. We proceeded in

doing a post-test scan of the slide with the same setup as the pre-test scan. This helps to see if the data is useable or not, but it still has to pass a scan using the other instrument with the group of analysts. Then the target is taken out after the warm up, and preparations for another test are made.

One more thing which I was able to do, was to use a laser profilometer. This piece of equipment is a laser triangulation gauge used to determine the surface structure of what ever object you choose to put underneath it. This laser profilometer consists of two servo motors, a motor power supply and control box, and a computer. A program on the computer, called 3d pro runs the laser triangulation gauge. It tells the motors what to do, according to the scale and grid dimensions that you input into the program. It then collects the data points and stores them in either an ASCII or binary file format for further processing. This program runs the gauge on a Cartesian coordinate plane, but there is also another program which does the same thing, called RT pro, only it runs on a polar coordinate plane. Then the file can be run in the surfer program, where a grid file is produced, which can be viewed as a three dimensional picture on the monitor which can be manipulated. This piece of equipment is used to determine how evenly the laser burned the target. The reason that this equipment is used, rather than visually checking it, is because the profilometer has a much higher resolution. It has a resolution of about 38 microns, but the size of the object is limited, because it can only handle a maximum of 14,400 points. This level of resolution makes for a much more accurate picture of the surface of the burned object.

Results

The only results which I can show you, are the pictures of the model of the space shuttle. I have no results from the laser tests, because the part of the experiment which I helped with, was not with analyzing the data and determining the results of the tests, but actually performing the tests, or the laser profilometer, because that was only busy work until I could start on the lab work.



I have chosen two pictures of the space shuttle model which I feel represent all the aspects of the model. I have also included a picture of the space shuttle while docked



with the Mir Space Station, because I helped with the finishing touches of that model,
and with the joining the two spacecraft.



Conclusion

This has been one of the best learning experiences that I have had in my life, and to make it better it was also very enjoyable. I was able to see and work on real experiments and projects, where the results would actually be used, not just some busy work that was given to me so that I would have something to do. One very important thing which happened to me during the time I spent working at Phillips Laboratory, is that it influenced my decision on what kind of a career I would like to pursue in the future. I learned how to use a computer to make a three dimensional model of a real

object, which is a skill that I think will come in very handy with the growing use of computers to aid in designing various objects. I also experienced what it was like to work in a laboratory environment, which is something that I think I would enjoy being a part of my job.

References

Hicks, Kerry, Major USAF. Chief, Systems Analysis and Integration's Branch.

Interview. June. 1997.

Joels, Kerry Mark, and David Larkin. The Space Shuttle Operators Manual.

New York: Ballantine Books, 1982.

Phillipson, Darrell, Lieutenant USAF. Satellite Systems Engineer.

Interview. June. 1997.

Roberts, John. PL/WSAE employee.

Interview. July. 1997.

Rudder, Ralph, Dr. PL/WSAE employee.

Interview. July. 1997.

Shell, Jim, Captain USAF. Chief, Laser Effects Test Facility.

Interview. July. 1997.

**DEVELOPMENT OF ALGORITHMS TO OBJECTIVELY FORECAST
PRESENT WEATHER AND SURFACE VISIBILITY BY MEANS OF A REGIONAL
NUMERICAL MODEL- INDECISIVE APPROACHES**

Joanne Wu

**Newton North High School
360 Lowell Avenue
Newton, MA 02166**

**Final Report for:
High School Apprentice Program
Phillips Laboratory**

**Sponsored by:
Air Force Office of Scientific Research
Bolling Air Force Base, DC**

and

**Phillips Laboratory
Hanscom Air Force Base, MA**

August 1997

**DEVELOPMENT OF ALGORITHMS TO OBJECTIVELY FORECAST
PRESENT WEATHER AND SURFACE VISIBILITY BY MEANS OF A REGIONAL
NUMERICAL MODEL- INDECISIVE APPROACHES**

Joanne Wu

Newton North High School

Abstract

Three distinct statistical approaches to probabilistically weather forecast precipitation were studied: Perfect Prog, Model Output Statistics, and Modified Perfect Prog. Each of their respective advantages and disadvantages were weighed in terms of their effectiveness in the Present Weather/Surface Visibility algorithm development. The results of the study indicated that, although far from perfect, the Modified Prog approach was the most appropriate technique for the given application

**DEVELOPMENT OF ALGORITHMS TO OBJECTIVELY FORECAST
PRESENT WEATHER AND SURFACE VISIBILITY BY MEANS OF A REGIONAL
NUMERICAL MODEL- INDECISIVE APPROACHES**

Joanne Wu

Introduction

One of the principle functions of the United States Air Force (USAF) is to complete missions by means of traveling in the air. Such a job requires the Air Force Global Weather Center (AFGWC) to provide precise forecasts of weather conditions to facilitate smooth missions. Currently, the Air Force lacks accuracy in its forecasts for specific weather elements that could be potential obstacles in any mission. Consequently, due to the implicit nature of current operational numerical models, the Air Force is in need of an improved form of weather diagnosis that is able to predict sensible weather conditions with greater precision. The main objective of the Air Force Global Theater Battle Management (TBM) Program is to provide AFGWC with an enhanced forecasting technique for a wide selection of parameters. This will be accomplished by means of producing algorithms which can use standard numerical model output to make efficient and reliable probabilistic forecasts. The project is currently being carried out in the Atmospheric Sciences Division (ASD) of the Geophysics Department of Phillips Laboratory (PL) at Hanscom Air Force Base, MA. Work done on TBM will be applied on the Theater (Regional) and Global scales. Forecast parameters of interest specified by AFGWC include: Present Weather/Surface Visibility, Clouds (e.g., ceiling height, thickness,) icing, turbulence and thunderstorms. Since each of these parameters presents a unique type of aviation hazard during the course of any flight mission, individual algorithmic research is needed for this project. Each group within the ASD starts out with common goals of successful algorithm development: a) to determine statistical correlation between output from selected models and observed weather parameter values, b) to develop algorithms from established relationships, c) to make forecasts on future parameter values using algorithms, and d) to determine accuracy of the algorithms through testing with an independent data set. With these set objectives in mind, different working groups within the ASD at PL are charged with independent algorithm development for distinct parameters. For instance, the purpose of this paper is to describe the study design of the research headed by Ken Heideman and Capt. Brian P. Newton at PL on Present Weather/Surface Visibility algorithm development. Towards the completion of the TBM Program, the final product will be assembled by linking the work of all the groups and creating a unified set of algorithms that act like a black box; the input of analyzed and observed parameter values will result in forecasts for future respective values at various intervals. However, for now, the overall discussion will be focused on the methodology of and the problems encountered by Heideman and Newton during their ongoing Present Weather/Surface Visibility algorithm development.

Methodology

To begin the research on theater scale algorithm development in Present Weather/Surface Visibility, the continental United States is divided into 12 regions (see Map 1.) The region assignments are based on similar weather characteristics. For example, land along geographic features like the Gulf Coast, the Rockies, the Appalachians, the Great Lakes, the Pacific and the Atlantic Oceans are all grouped independently because their distinct locale subjects these regions to unique weather patterns. Following the region establishments, data of present weather observations are requested at an average of 10 stations (most of which are located at or near Air Force Bases) in each region for the years of 1992-1993 at specified times of 0:00 and 12:00 GMT (Greenwich Mean Time.) Since the Nested Grid Model (NGM) was the chosen model for development, for reasons which will be discussed, the stations located on grid points would be ideal. Unfortunately, stations which satisfy that requirement are sparse (see Map 2.) In order to compensate the error caused by the distances between the actual station and the NGM grid points, the data from each station is interpolated (see Diagram 1.) The results from the calculation through weighted bilinear interpolation are the basic data given to Heideman and Newton to begin Present Weather/Surface Visibility algorithm development.

To understand the use of the given raw data, one must first know the AFGWC requirements of Present Weather/Surface Visibility algorithm development (see Chart 1.) The AFGWC first wants to know which of the two general weather categories present weather conditions fall in: Precipitation or No Precipitation (see Chart 1) Cases where no Precipitation occurs yet is a hindrance to surface visibility, like fog and haze, are placed into the Miscellaneous category. Precipitation events must again be sorted into stratiform (e.g. stable snow, rain) or convective weather (e.g., thunderstorms, showers.) For further specifications, AFGWC requires the Present Weather/Surface Visibility algorithms to probabilistically forecast the exact type of weather or weather combination. The final product would then be an additional Probability of Precipitation (PoP) guidance for meteorologists in forecasting, except with more detail and, hopefully, with greater accuracy.

The raw data from each region is first separated into 2 seasons: warm (April-September) and cold (October-March.) This split is required since weather patterns during the warm season vary dramatically from those of the cold season. Then, development of predictive equations begin with a comparison of potential predictors (the independent variable, x) and the predictands (the dependent variable, y.) Predictors are essential to the development of algorithms. Think of the predictors being clues like sound, pattern, and smell that help one guess what is inside a mysterious black box. Thus, no matter how

insignificant most of them might be, the higher the number of initial predictors, the better the chance of finding solid statistical relationships between some of the predictors and the predictands. However, the total number of the model-generated predictors at the two designated times being used in Present Weather/Surface Visibility algorithm development is limited (see Chart 2). To expand on the number of potential predictors, other parameters such as the dewpoint and divergence at various pressure levels (see Chart 2) are derived from the predictors generated by the model and those given by the observations. Further experimentation on parameters requires slight variations such as combining given and derived parameters through simple mathematical calculations (e.g., multiplication by constants). Thus, the pool of predictors is increased from the original 38 given parameters. However, the number and the type of predictors that the project begin with and eventually end with will not be the same among all 12 regions. For example, most of the current work is being completed on region 6 (the Gulf Coast) and the number of possible predictors stands at around 170. These 170 or so predictors from region 6 will not be identical to those from another region (e.g., region 10, the Great Lakes, for which there are approximately 150). Then, in order to begin algorithm development, observed present weather data is again sorted into specific categories. Initially, all kinds of present weather (e.g., no weather, thunderstorms, rain, snow) are arbitrarily given a number. Then, the data is further categorized in their respective groups: No weather, Miscellaneous, Stratiform, and Convective. Each category assigned a number (0, 10, 20, 30) to prepare the observed and forecasted data for the next phase: Logistic Regression. Statistical Logistic Regression is then applied to the four categories and distinct equations are derived. The result is four equations that produce probability of the corresponding category of weather occurring at the valid times of 0:00 and 12:00 GMT. By observing the calculated Probability of Detection (POD) and False Alarm Rate (FAR), it is determined whether some mathematical variation is needed to increase the accuracy of the derived equations. Other pre-existing algorithms (see Ivens, 1987) and empirically derived algorithms are then used as assistance in determining which specific type of precipitation, if any, has the highest probability of occurring at a specified future time and location. To formally evaluate the Present Weather/Surface Visibility algorithms, a series of testing is done through use of an independent database, which consists of every fourth observation in the two-year database. The observations in the independent database were not included when the forecast equations were first developed.

Types of Approaches

Due to the uncertainty of which specific type of operational regional model would be implemented by AFGWC in 1997, the first task was to determine which regional numerical model would be most feasible to use in developing the Present Weather/Surface Visibility algorithms. Two criteria were essential in

choosing the model: 1.) a long and reliable archived data set must be made available, and 2) the archived data set must contain enough model-generated variables to present a sufficient amount of potential predictors to the developmental database. The final selection of the NGM for development of the algorithms was based largely on the fulfillment of these two criteria. Ideally, the ultimate Present Weather/Surface Visibility algorithms would need not to be dependent on the NGM or any other operational numerical model.

The Model Output Statistics (MOS) approach (Glahn and Lowry, 1972) is a PoP forecasting technique used by many in the field of Meteorology as highly reliable forecast guidance. The MOS approach relates weather observations (predictands) to variables forecast by numerical models (predictors) and calculates a set of equations that fit with the chosen model for development. Typically, separate equations are created for each forecast projection, independent of whether the projection range is short or long. An advantage of the MOS approach is that it takes into account climatic frequencies for particular regions and adjusts the numerical forecast equations so that errors are reduced in future forecasts. Thus, it is not very likely that in longer range forecasts, MOS equations would result in forecasts that deviate dramatically from what that particular region had experienced at the same time in the past. Another advantage is that MOS partially compensates for error bias in the numerical forecasts made by the model it is developed on. However, the constant compensation can also be a disadvantage in situations where no error is present in the numerical forecasts. Thus, any adjustment made by MOS would create a biased forecast. Another disadvantage of this technique is that its accuracy depends on the length of the data archives. Since MOS examines climatic frequencies and takes past observations into account, this approach requires at least two or three years of data sample to be effective. In addition, there must be no changes to the model during the period of development. Equations derived from this approach are only accurate with the chosen model of development. Attempts to apply resulting MOS equations to other operational numerical models could yield undesirable results.

In contrast to the MOS technique, the Perfect Prog approach (Klein et. al., 1959) develops relationships through use of simple regression techniques between predictors and predictands. Equations between numerical model analyses and observations are valid only at designated times of development. In addition, the Perfect Prog approach is based on numerical models such as the NGM and other gridded graphs. The equations are derived by means of plotting numerical data points and drawing the most feasible line to represent the data. The line is drawn such that standard deviation is minimized. Through use of this method, distinct equations are derived for each potential predictor. Only predictors whose relationships with the predictands in both the forecasted and observation data are considered. One advantage of this technique, on the contrary to MOS, is that

equations developed do not completely depend on the operational numerical model chosen. Equations are flexible enough so that they are able to evolve through time. Also, in contrast with MOS, a robust database is not necessary for equation development. However, Perfect Prog is not flawless. A disadvantage of Perfect Prog is that the resulting forecasts are made with an implicit assumption that the numerical model data used as inputs are "perfect." As discussed above, error is almost always embedded in any operational numerical model. Moreover, if a small database is used, rare events such as precipitation (particularly in some regions) will be underrepresented in the development of the equations. Thus, resulting Perfect Prog forecasts will be less accurate.

In addition to MOS and Perfect Prog, a third approach called the Modified Perfect Prog approach has shown effectiveness in producing statistical forecasts. In contrast with the two techniques above, Modified Perfect Prog uses short-ranged numerical forecasts (0:00-12:00 GMT) as predictors as opposed to observations. However, Modified Perfect Prog also bears similarities to certain aspects of MOS and standard Perfect Prog approaches. A common advantage of standard and Modified Perfect Prog is, while still valid at any projection, only one equation needs to be derived for each time of the day. This advantage remains true provided that the obvious changes in the projection of predictors occur similar to standard technique. However, like one disadvantage of Perfect Prog, "Perfection" of the numerical model data used as inputs for Modified Prog statistical analysis is implicitly assumed. Thus, although very short ranged MOS equations are developed in actuality, forecasts with the use of Modified Prog do not account for the potential error in the chosen numerical model like with the use of MOS. Fortunately, as with one advantage of MOS, the Modified Perfect Prog approach does not pose any limitations on the type of variables needed to be used for development. In addition to the observed variables at 0:00 and 12:00 GMT, other variables such as vertical velocity made available by most numerical models, can also be utilized. Overall, due to the fact short-ranged numerical model output has a consistently high reliability and the approach itself is not model-dependent, Modified Perfect Prog is a preferred guidance for most forecasters in making short-ranged forecasts.

Results

After careful scrutiny of MOS, standard and Modified Perfect Prog approaches, it was concluded that the most reasonable technique for Present Weather/Surface Visibility algorithm development is Modified Prog. Given the initial vacillation in model decision-making on the part of the AFGWC, MOS was eliminated because of the lack of available numerical data. If AFGWC had known precisely which operational regional model would be desirable beginning in the year of 1996, a complete 3-5 year archive of the model's output would be available for use of the MOS approach. Algorithm development with the

MOS approach would yield results that would specifically accommodate Air Force needs. Due to the fact that this information was inaccessible, the choice was between standard and Modified Perfect Prog approaches. Advantages to both techniques are that the resulting equations would not be model-dependent and an immense data archive was not needed for development. However, the primary disadvantage is the implicit assumption of the "perfection" in numerical model output. With these facts in mind, the final choice was the Modified Perfect Prog approach by reason of its greater flexibility in choosing potential predictors. Furthermore, Modified Prog allows assistance from pre-existing algorithms in the prediction of the exact type of Precipitation when Precipitation occurs.

Concluding Remarks

Although the objectives of the Theater Battle Management (TBM) at Phillips Lab are the same among all weather application components, each group has to create a study design that is specifically tailored to its respective needs. The above discussion pertains to the ongoing work in Present Weather/Surface Visibility algorithm development. With the Modified Prog approach as the chosen course of action, current algorithm development is being carried out in the Gulf Coast region (see Map 1; Region 6). Given the initial uncertainty of the model chosen by AFGWC, the selection of Modified Perfect Prog approach is most reasonable when compared with the MOS and Perfect Prog techniques. However, even with use of the Modified Perfect Prog approach, it is discovered that the short length of the data archive had a tremendous affect on the resulting equations. Due to the lack of sufficiently frequent observations (0:00 and 12:00 GMT in 1992-1993 only), rare weather events such as precipitation in particular regions are under-represented. Thus, accurate predictions of those events is difficult even with the application of the Modified Perfect Prog approach. In spite of inherent problems and limitations, work on this TBM project reinforces the value of statistical approaches to weather forecasting in supplementing numerical model forecasts.

Acknowledgments

Due to a personal lack of full meteorological understanding, this paper could not have been written without the unyielding support and patience of my mentor, Ken Heideman of PL/GPOF. It was with his aid that I was able to piece together all the basic meteorological concepts to give the work on the Present Weather/Surface Visibility algorithm development that I had accomplished this past summer a more tangible feel. Also, without the constant support and humor of Bob d'Entremont and Captain Brian P. Newton of PL, this paper would not be complete due to the high stress level it occasionally generated.

References

H. R. Glahn, and Lowry, D. A., 1972b: The use of Model Output Statistics (MOS) in objectively weather forecasting. Journal of Applications in Meteorology, 11, pp. 1203-1211

Julian, P.R., and A. H. Murphy, 1972: Probability and statistics in meteorology: A review of some recent developments. Bulletin of the American Meteorological Society, 53, pp 957-965

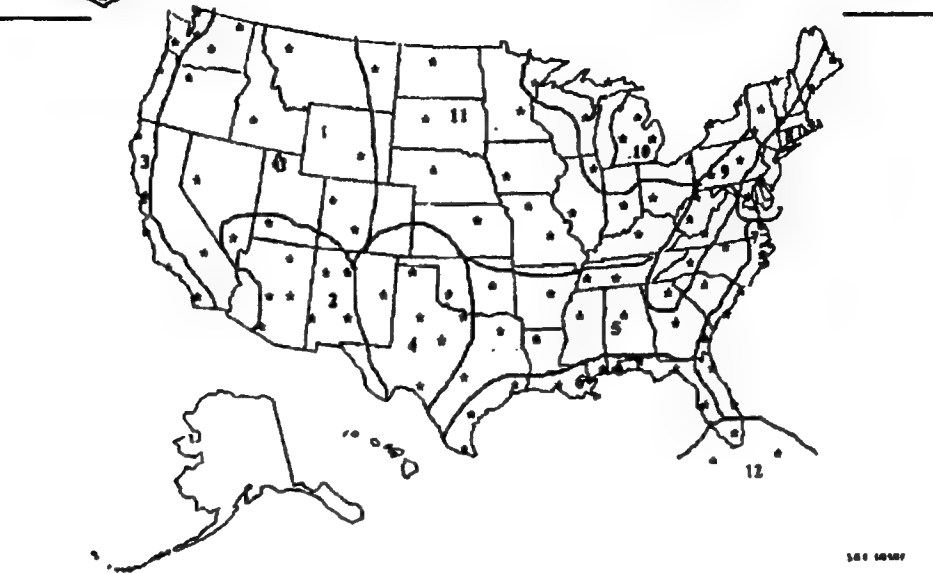
H. R. Glahn, 1969a: An operational method for objectively forecasting probability of precipitation. Abstract in Bulletin of American Meteorological Society, 50, p. 458

H. R Glahn, and Lowry, D. A., 1976: An operational method for forecasting probability of precipitation - PEATMOS PoP. Monthly Weather Review, 104, pp. 221-232

H. R. Glahn and Lowry, D. A., 1969b: Relationships between integrated atmospheric moisture and surface weather. Journal of Applications in Meteorology, 8, pp. 762-768

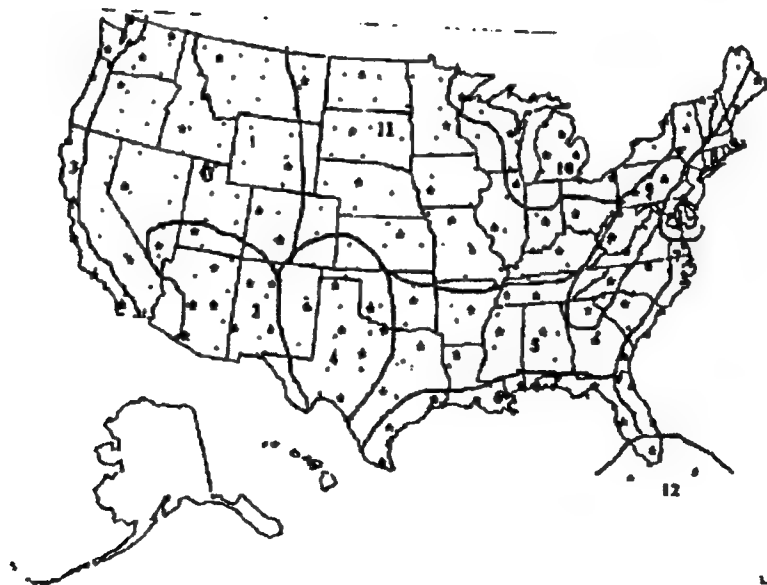
Map 1

Regions Used For Algorithm Development

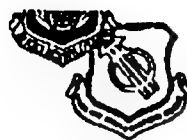


130-1000

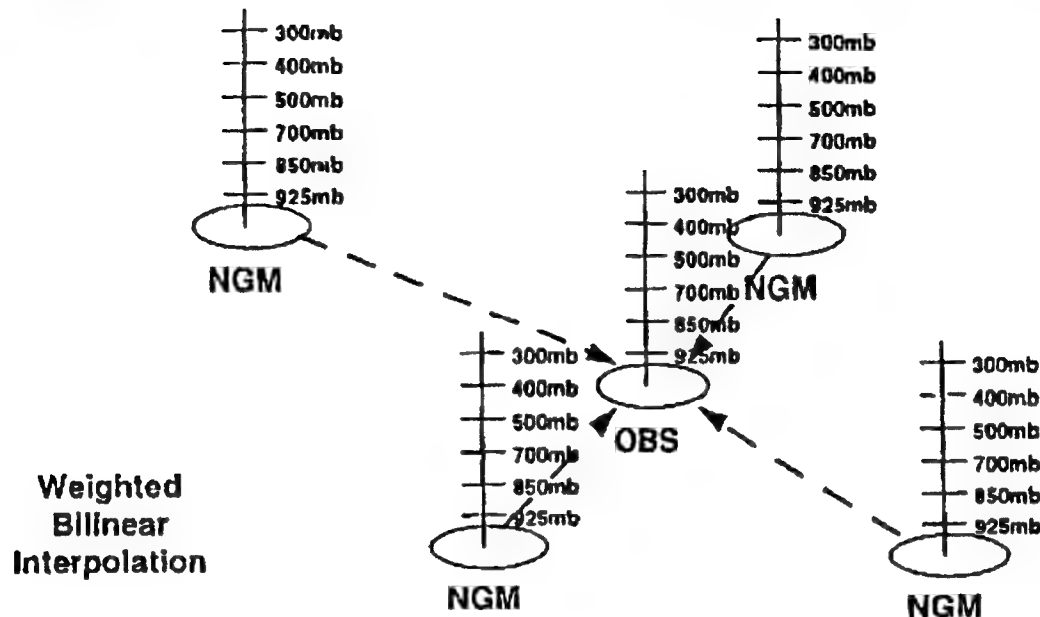
Map 2



130-1000



Horizontal Interpolation



BASIC WEATHER SYMBOLS

Chart I



Present Weather Categories

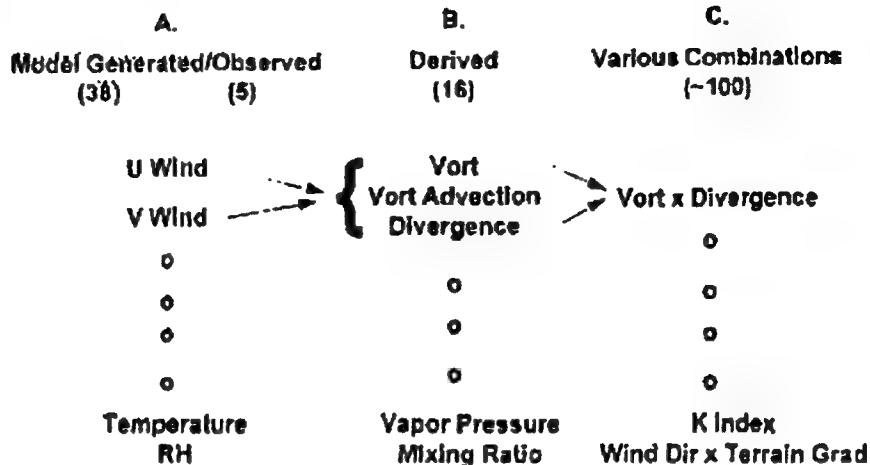


No Weather	Other Haze	Stratiform Freezing Rain (Lgt/Mod/Hvy)	Convective Thunderstorms
Fog		Freezing Drizzle	Rain Showers (Lgt/Mod/Hvy)
Freezing Fog		Ice Pellets	Snow Showers (Lgt/Mod/Hvy)
Sand (Blowing)		Snow (Lgt/Mod/Hvy)	Ice Pellet Showers
Dust (Blowing)		Rain (Lgt/Mod/Hvy)	
Blowing Snow		Drizzle	



Predictors

(~154)



IVENS LEGEND

TWML: Maximum Wet Bulb Temperature in the warm Layer
(>0 C)

TWG: Wet Bulb Temperature at the surface

R: Forecasted amount of Precipitation

RC: Critical Precipitation for Snow

$$= .055 * \text{Vertical Mean Temperature} * \text{Thickness of the Layer}$$

RCM: Critical Precipitation for Melting Snow

$$R1 = 2.42^* R^*.68 + 1.50^* R^*.34 + .23$$

$$RCM = RC - R1$$

IDASS ADDITIONS

Aaron Zimmerman

Sandia High School
7801 Candelaria Road NE
Albuquerque, NM 87110

Final Report For:
High School Apprentice Program
Phillips Laboratory

Sponsored By:
Air Force Office of Scientific Research
Bolling Air Force Base, DC

and

Phillips Laboratory

August 1997

IDASS ADDITIONS

Aaron Zimmerman
Sandia High School

Abstract

To create a user friendly, efficient, and overall more productive program, additions to Phillips Laboratory's Intelligence Data Analysis System for Spacecraft (IDASS) core program are needed. Two additions added during the 1997 summer are the ability to communicate and share data with Satellite Tool Kit (STK), by Analytical Graphics Inc., and the ability to receive data from telescope images of deep space satellites. These two additions allow the user a broader range of choices to complete the task desired. With the two additions to IDASS, the user, who may be in the intelligence field, who may be in charge of satellite development and tracking, or a casual or serious observer, will benefit greatly in productivity and efficiency.

IDASS ADDITIONS

Aaron Zimmerman

Introduction:

With the ever increasing number of satellites being launched in the closing years of this century, it is no surprise that software companies have realized the profits that would accompany satellite tracking programs. Although many companies realize the income potential, some cannot or have not spent the time and money necessary to create a satellite identification and tracking program. One reason for this may be the high graphical and processing power required to render three-dimensional models and perform orbital calculations. This restraint allows only users working on expensive power computers the ability to run these programs. As personal computers are becoming increasingly powerful, at least one company, Analytical Graphics Inc., has created spacecraft tracking software for the PC. Many companies are sure to follow. In the near future, two satellite programs might be in use by interested companies. These companies include the Air Force and any other company dealing with the manufacturing, launching, or tracking of satellites.

Phillips Laboratory wrote a satellite identification program called Intelligence Data Analysis System for Spacecraft (IDASS) , see Figure 1, which allows a user to identify a satellite using a variety of means. Image Comparison (IC) allows a three-dimensional

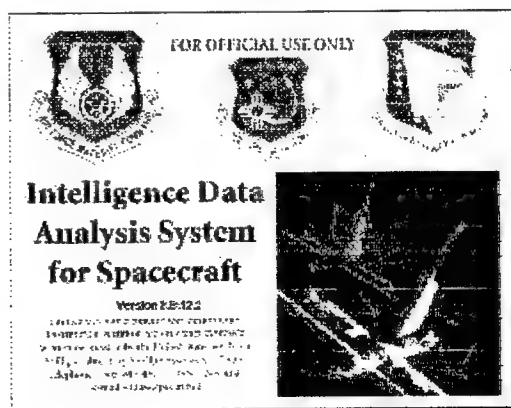


Figure 1. IDASS screen splash

model to be super-imposed over a telescopic photograph of a satellite. The three-dimensional model is created by laboratory workers using Satellite Modeling Tool (SMT) another program written by Phillips Laboratory. Being able to see both a three-dimensional model and a satellite image laid on top of each other allows the user to identify the satellite based on tie points. Tie points are distinct features present on both the satellite model and the satellite image. After identifying the satellite, the user is then able to diagnose the satellites functions. Using Motion Estimation (ME), the user is able to see if a spacecraft is alive and functioning or dead and drifting about in space. Along with an Orbital Visualizer (OV), IDASS is indispensable tool for anyone needing to identify a satellite.

Where IDASS can be used for both identification and visualization of satellites, Analytical Graphic's Satellite Tool Kit (STK), see Figure 2, is primarily used for visualizing spacecraft and their orbits (See Figure 4 and 5 to see a side by side comparison of IDASS and STK user interfaces). STK core program comes with a two-dimensional viewer that allows vehicles, facilities, and sensors to be seen. With the purchase of a

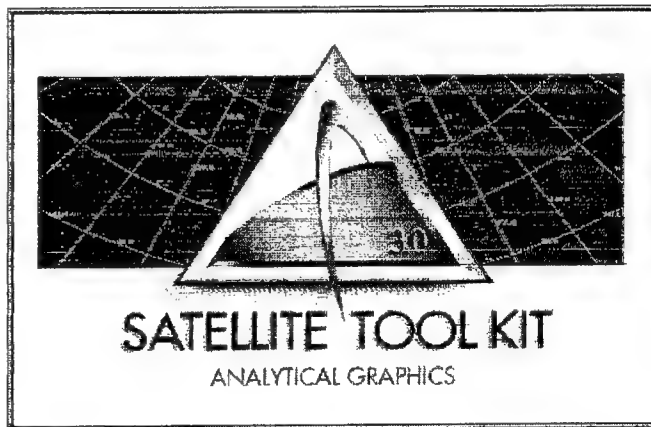


Figure 2. STK screen splash.

Visualization Option Module (VO) the user is able to see the satellites and orbits in a simulated three-dimensional space. The VO Module allows STK to use three-dimensional models much like IDASS does in its Orbital Visualizer (OV) (See Figures 5 and 6 for a comparison of IDASS OV and STK VO). STK also has another add-on module called the Interprocess Module (IPC) which allows STK program commands to

be sent from outside the program. Program commands can be sent from other programs or can be read off a text file. This extends the usability of the program. IDASS implements the IPC Module from within its Orbital Visualizer. These two high-power programs working together create unbeatable interface for anyone dealing with spacecraft.

In addition to the power gained from the IPC Module and the IdaSTKInterface class, IDASS may also receive additional power from another Phillips Laboratory project. The Multi-Spectral project headed by Captain Conrad Poelman and Stephanie Meltzer will allow a deep space satellite to be identified. These satellites are beyond visual range, so IDASS Image Comparison will not work. An idea was introduced that telescopes are still able to receive photons from the satellites, and that if each satellite has a specific photon pattern it can be identified. Using simulated data, a neural network, and patience the results being returned are near one hundred percent correct identification. The ability to correctly identify deep space satellites will be another addition to IDASS impressive identification suite.

With IDASS leading the way in satellite identification and tracking, program code must be written to keep up with new advancements like the multi-spectral project. Code to allow the communication between IDASS and STK was needed as was code to incorporate filter files into the output of the multi-spectral project.

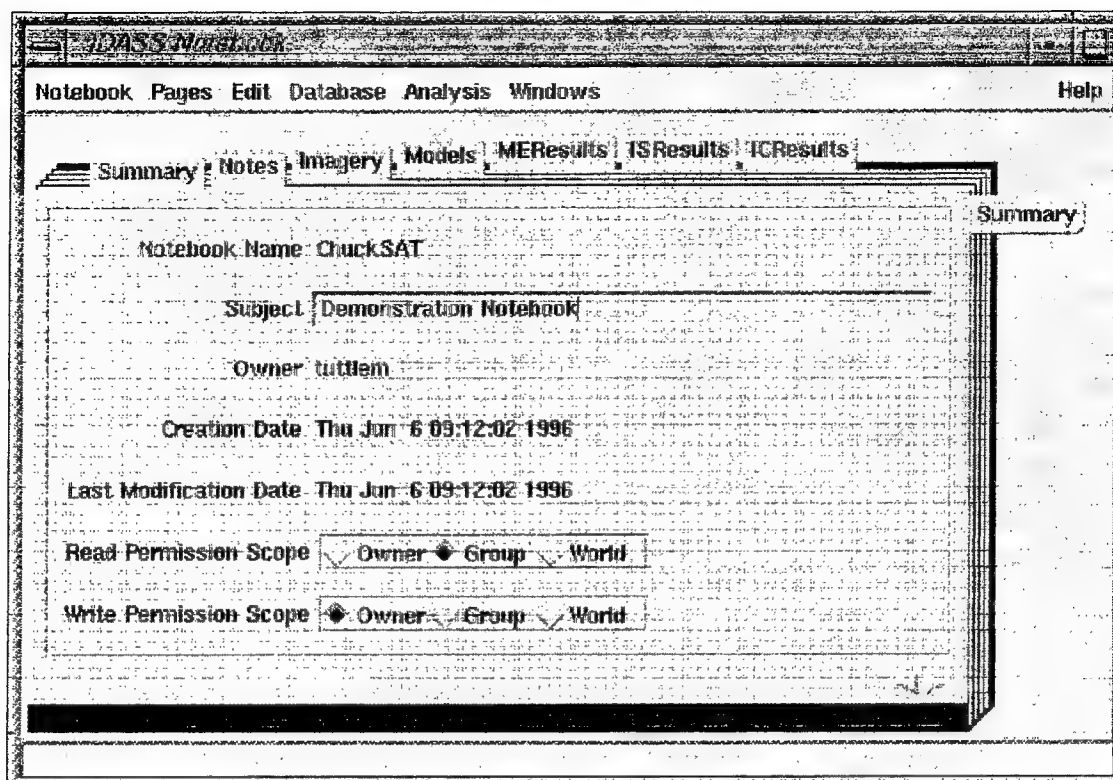
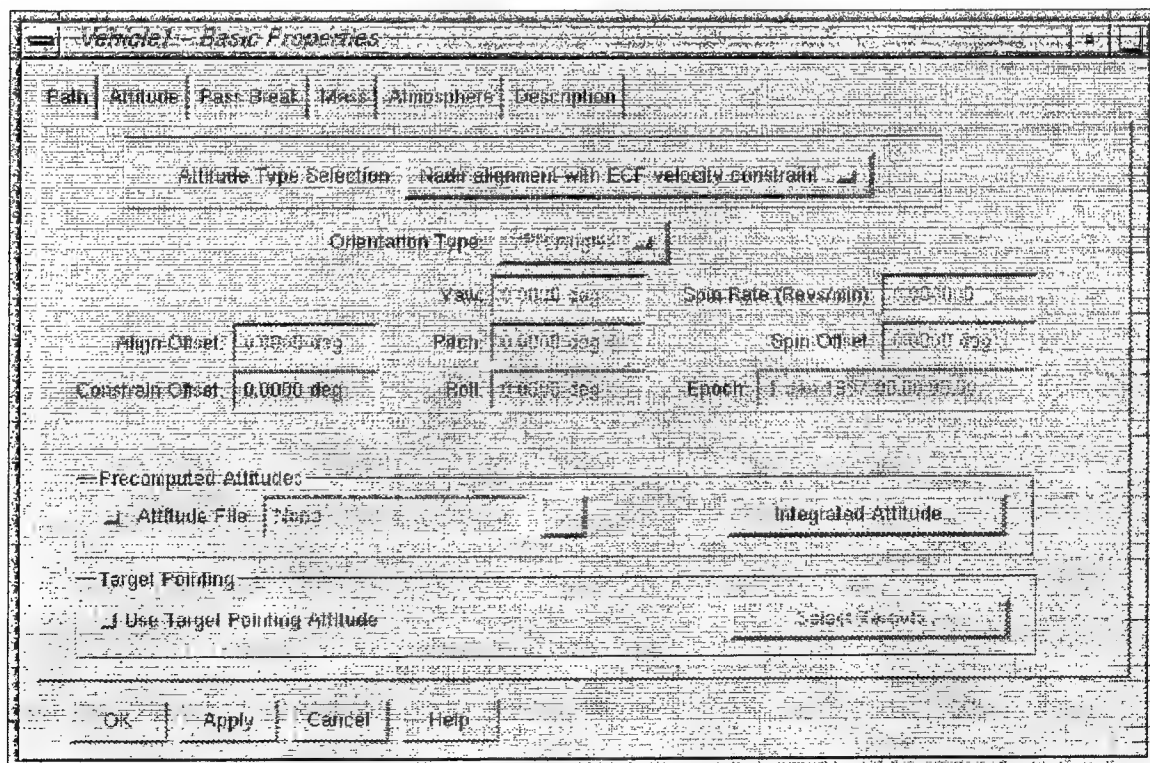


Figure 3 and 4. The IDASS (above) and STK (below) user interfaces.



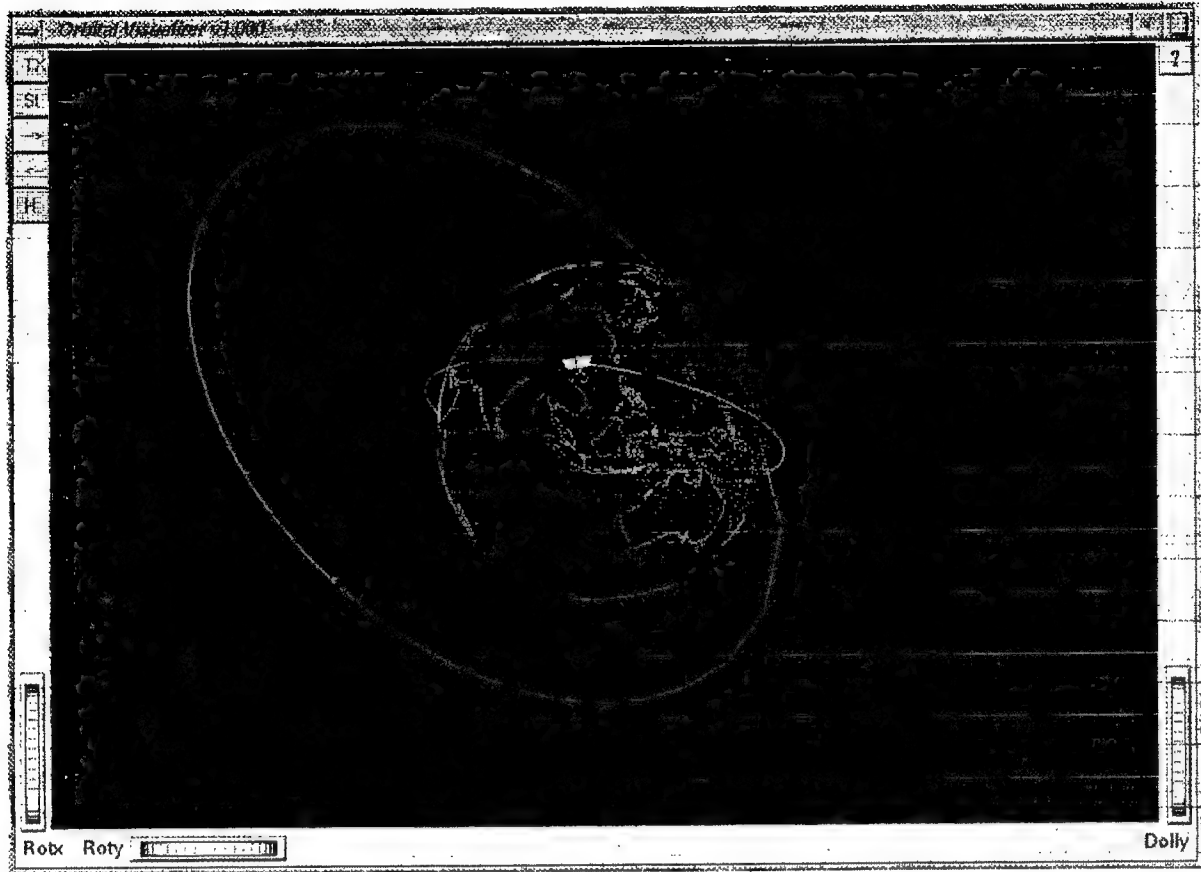
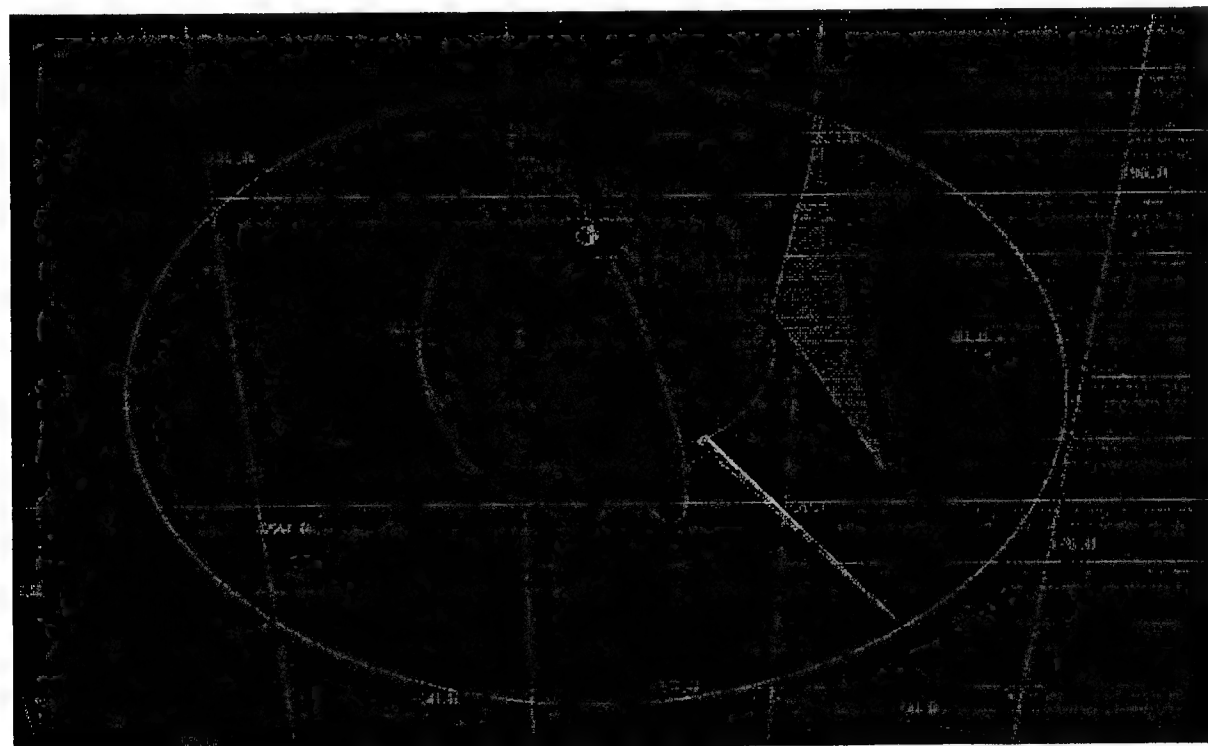


Figure 5 and 6. A side by side comparison of IDASS OV (above) and STK VO (below).



Methodology:

The program written to allow IDASS and STK to communicate is called the IdaSTKInterface. This code is actually just a C++ class that contains a list of public methods that IDASS can call from its OV page. A class was selected due to its efficiency and its ability to be added without rewriting the program. The class contains all the methods required to setup the communication socket, send the data to STK via the IPC Module, handle errors, and disconnect communication from STK. The communication takes place through a UNIX socket. This program was added after IDASS had been written so the class made it easy for the Phillips programmers to implement IdaSTKInterface without disturbing previously written code.

The first step in creating a class was to create the socket and test the ability of both programs to communicate. The test included basic commands that STK would recognize including “New / /Scenario IDASS” which creates a scenario called IDASS. A scenario is the basic building block when dealing with vehicles and facilities. The scenario contains the objects and events that take place during an allotted amount of time. Only one scenario in STK can be loaded at a time. After receiving a success upon receiving the data, communication between the two programs was proven successful.

After proving it is possible to send data between programs, it is necessary to code a method for every command that IDASS will use. The bulk of the IdaSTKInterface program contained these methods. The IPC Module provided an excellent link between the two programs. Some example of commands that would be sent from IDASS to STK are: “New / /Scenario/IDASS/Vehicle NewVehicle”, “Articulation /Scenario/IDASS/Vehicle/NewVehicle 1920 30 Cargo Rotate 0 -160”,

and "Point /Scenario/IDASS/Vehicle/NewVehicle/Sensor/NewSensor Relative 0 -90".

The first example will create a new vehicle (satellite) called "NewVehicle". The second

example will rotate the cargo hatch on

NewVehicle from 0 to -160 degrees,

see Figure 7. The final example will

point NewVehicle's sensor at the

Earth. An example of a sensor can be

seen in Figure 6. The sensor is the

cone going from the satellite to the

Earth. Of course, the user will not

have to type in these commands,

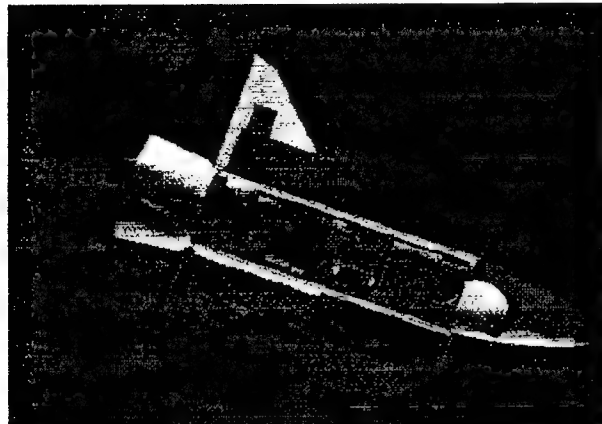


Figure 7. A sample 3-D shuttle model with cargo bay articulation.

rather press an interface button, and IDASS will pass the correct data to

IdaSTKInterface and then IdaSTKInterface will pass the data to the IPC Module.

The third step in creating the IdaSTKInterface program was to test all the commands from IdaSTKInterface. Since the class was not implemented into IDASS yet, a local method called Run() was used to call the public methods simulating calls IDASS would make. Problems in reading information, receiving the wrong data, and typographical errors had to be corrected. This third step will ensure that the user will be able to use IdaSTKInterface without crashing STK and/or IDASS. After testing was completed, the program was left for the Phillips programmers to incorporate it into IDASS.

From within IDASS, the buttons that will send data to STK will probably be located on the Orbital Visualizer page, see Figure 5. It is not definite where they will go since the class has not been implemented yet. The ability to send data to STK will

allow the user another choice in how they may wish to visualize the satellite and its orbit. The combination of IDASS ability to identify spacecraft along with STK ability to display the spacecraft on two-dimensional and three-dimensional planes, will provide the best satellite watching program available. The programs will save both time and man power, precious commodities in any business.

The Phillips Laboratory Multi-Spectral project uses many different programs, some commercial, some written at Phillips, to identify a deep space vehicle. One of these programs needed to be rewritten to allow for filter files to be integrated into the final output. The filter files specifies a set of values that correspond to the wavelengths at which a filter allows light to pass. These filters are placed in a filter wheel and positioned between the object and the instrument used to capture the data. To simulate real life data that the telescope would receive the filter files had to be part of the output. This program that reads in data, changes the data, and prints out the data to a file is called convert.c.

To start the program, the input file format and the output file format had to be determined before any coding could take place. The input files were created by TASAT, and the output files needed to be in the correct format that the PDP++, the neural network, needs.

After deciding on the format, it was necessary to brainstorm the fastest way to

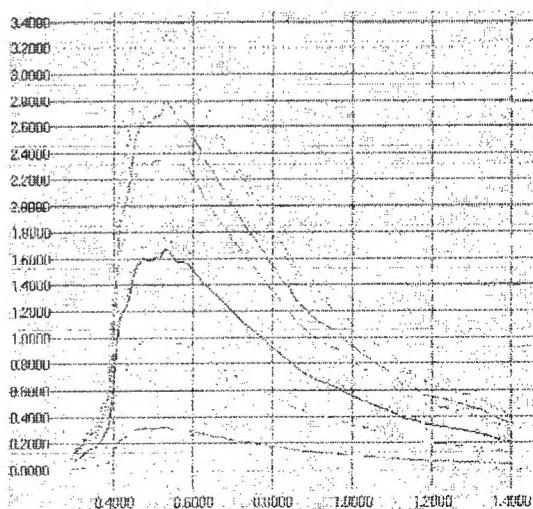


Figure 8. The output in Xgraph before data is run through convert.c.

read in the input file and write the data to the output file. This is accomplished using *for* and *while* loops. Convert.c also creates output files for a graphing program called Xgraph, see Figures 8 and 9. The output files for Xgraph also had to be determined and created.

After planning convert.c, it was time to start coding. The data that needed to be stored in data and the functions to manipulate the data was unclear and messy in the C programming language so another C++ class was implemented for the Xgraph program. The class was not explicitly for the Xgraph program, but for all of convert.c to use. The class will provide an ordered and clearer approach to the use of files. ReadInFile(), WriteToFile(), WriteToScreen(), and Interpolate() are just a few of the methods the class will have. The classes data members will hold two list of numbers, files, and other miscellaneous variables that the class will use.

After testing the output files with previously complied files, error in coding and output had to be corrected. Many times the file was not as expected so the program had to be debugged to find out why the output file was wrong. Many debug sessions later, the program was working, and was given to the project creators to test their data.

At this time using three satellites, the program is showing near one hundred percent correct identification. Being able to identify deep space satellites based solely upon the photons they emit is a great advantage to anyone looking for deep space identification. Testing is still being performed on more satellites at this time. The data

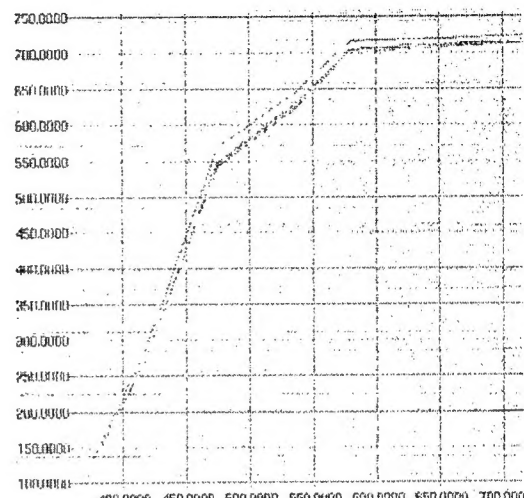


Figure 9. Data in Xgraph format after being run through convert.c.

and input files that are being used are produced by a simulation and are not real data. Real data will be available soon, and real results will be determined soon. Hopefully, the results will be near the simulated data results.

Adding the ability to identify deep space satellites will provide the IDASS user one more way to make their work more productive. Anyone who deals with deep space vehicles will be able to work more efficiently with the Multi-Spectral addition to IDASS.

With the two additional programs added to IDASS, IdaSTKInterface and convert.c, the user will have more methods to get the results desired. Creating these programs took hours of coding and debugging, but the payoff is the increased productivity and efficiency of the IDASS and STK user.

Results:

The results from each program are promising. The IdaSTKInterface program allows the user to successfully give STK commands from within IDASS. These are simulated commands because the IdaSTKInterface class has not been included in the IDASS program. Even with the simulated commands, every call to STK was performed successfully. Results from the multi-spectral project and the convert.c program have also been promising. With the simulated data for three satellites, one hundred percent correct identification was produced. With the real satellite data coming in the future, the results will, hopefully, be one hundred percent also. The ability to identify deep space satellites will be a great addition to IDASS along with the ability to communicate with STK.

Conclusion:

The additions to Phillips Laboratory's Intelligence Data Analysis System for Spacecraft will give IDASS user more power to perform their desired tasks. The IdaSTKInterface class added to IDASS with give users of both IDASS and STK a way to use both IDASS and STK program strengths. For IDASS the strengths are its ability to identify spacecraft, while STK strength is its two-dimensional and three-dimensional viewers. Add to that the ability to identify deep space spacecraft and IDASS becomes an even more powerful satellite identification and tracking program. Convert.c's ability to incorporate filter files and format the files which helps the multi-spectral project to identify deep space satellites correctly and quickly outperforms older methods of identification. After identifying a deep space satellite and predicting its orbit, the information then could be sent to STK, via the IdaSTKInterface class, for further analysis. IDASS and the IdaSTKInterface and the multi-spectral project and convert.c will provide spacecraft manufactures, satellite tracking, and intelligence personnel a productive and efficient method of identifying and tracking both near-earth and deep space satellites.

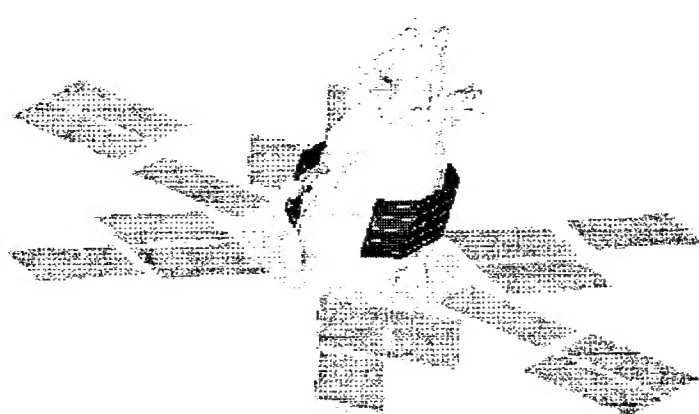


Figure 10. A rendered 3-D model of a satellite whose data was used for testing.